

SANDIA REPORT

SAND2000-2696

Unlimited Release

Printed November 2000

The Consistent Kinetics Porosity (CKP) Model: A Theory for the Mechanical Behavior of Moderately Porous Solids

Rebecca M. Brannon

Prepared by
Sandia National Laboratories
Albuquerque, New Mexico 87185 and Livermore, California 94550

Sandia is a multiprogram laboratory operated by Sandia Corporation,
a Lockheed Martin Company, for the United States Department of
Energy under Contract DE-AC04-94AL85000.

Approved for public release; further dissemination is unlimited.



Sandia National Laboratories

Issued by Sandia National Laboratories, operated for the United States
Department of Energy by Sandia Corporation.

NOTICE: This report was prepared as an account of work sponsored by an agency of the United States Government. Neither the United States Government, nor any agency thereof, nor any of their employees, nor any of their contractors, subcontractors, or their employees, make any warranty, express or implied, or assume any legal liability or responsibility for the accuracy, completeness, or usefulness of any information, apparatus, product, or process disclosed, or represent that its use would not infringe privately owned rights. Reference herein to any specific commercial product, process, or service by trade name, trademark, manufacturer, or otherwise, does not necessarily constitute or imply its endorsement, recommendation, or favoring by the United States Government, any agency thereof, or any of their contractors or subcontractors. The views and opinions expressed herein do not necessarily state or reflect those of the United States Government, any agency thereof, or any of their contractors.

Printed in the United States of America. This report has been reproduced directly from the best available copy.

Available to DOE and DOE contractors from
U.S. Department of Energy
Office of Scientific and Technical Information
P.O. Box 62
Oak Ridge, TN 37831

Telephone: (865)576-8401
Facsimile: (865)576-5728
E-Mail: reports@adonis.osti.gov
Online ordering: <http://www.doe.gov/bridge>

Available to the public from
U.S. Department of Commerce
National Technical Information Service
5285 Port Royal Rd
Springfield, VA 22161

Telephone: (800)553-6847
Facsimile: (703)605-6900
E-Mail: orders@ntis.fedworld.gov
Online order: <http://www.ntis.gov/ordering.htm>



SAND2000-2696
Unlimited Release
Printed November 2000

The Consistent Kinetics Porosity (CKP) Model: A Theory for the Mechanical Behavior of Moderately Porous Solids.

Rebecca M. Brannon
Computational Physics and Simulation Frameworks
Sandia National Laboratories
P.O. Box 5800
Albuquerque, NM 87185-0820

ABSTRACT

A theory is developed for the response of moderately porous solids (no more than ~20% void space) to high-strain-rate deformations. The model is “consistent” because each feature is incorporated in a manner that is mathematically compatible with the other features. Unlike simple p - α models, the onset of pore collapse depends on the amount of shear present. The user-specifiable yield function depends on pressure, effective shear stress, and porosity. The elastic part of the strain rate is linearly related to the stress rate, with nonlinear corrections from changes in the elastic moduli due to pore collapse. Plastically incompressible flow of the matrix material allows pore collapse and an associated macroscopic plastic volume change. The plastic strain rate due to pore collapse/growth is taken normal to the yield surface. If phase transformation and/or pore nucleation are simultaneously occurring, the inelastic strain rate will be non-normal to the yield surface. To permit hardening, the yield stress of matrix material is treated as an internal state variable. Changes in porosity and matrix yield stress naturally cause the yield surface to evolve. The stress, porosity, and all other state variables vary in a consistent manner so that the stress remains on the yield surface throughout any quasistatic interval of plastic deformation. Dynamic loading allows the stress to exceed the yield surface via an overstress ordinary differential equation that is solved in closed form for better numerical accuracy. The part of the stress rate that causes no plastic work (i.e., the part that has a zero inner product with the stress deviator and the identity tensor) is given by the projection of the elastic stress rate orthogonal to the span of the stress deviator and the identity tensor. The model, which has been numerically implemented in MIG format, has been exercised under a wide array of extremal loading and unloading paths. As will be discussed in a companion sequel report, the CKP model is capable of closely matching plate impact measurements for porous materials.

Acknowledgments

I thank Paul Yarrington and Steve Montgomery for allocating time and funding for the development of this consistent kinetics porosity (CKP) model. I am grateful to Randy Weatherby, Josh Robbins, Bruce Tuttle, John Aidun, Stewart Silling, Steve Montgomery, Pat Chavez, and Paul Yarrington for their insightful constructive criticisms of draft versions of this manuscript. Practically every member of the ALEGRA team has helped me at one point or another during the course of this work, but I would especially like to thank Mike Wong for adding the ability to dynamically allocate field variables based on user input and for adding the ability to assign properties to entire “blocks” of finite elements. Sharon Petney and Sue Carrol also deserve kudos for their endless patience in helping me navigate the darker corners of ALEGRA’s framework and development scripts. I am grateful to John Aidun for encouraging me to develop this model and for providing part of the resources and environment necessary to accomplish the tasks. I have also been inspired and guided by ongoing interest in this model from outside researchers such as H.L. Schreyer, A.M. Rajendren, J.K. Dienes, P.J. Maudlin, F.L. Addressio, and M.W. Lewis. The CKP model is essentially a synthesis of numerous theories and ideas that have existed in the literature for quite some time. I learned most of this theory while a graduate student at the University of Wisconsin, Madison, and I therefore thank my former advisor Walter Drugan for his continued influence on my way of thinking.

This work was performed at Sandia National Laboratories. Sandia is a multiprogram laboratory operated by Sandia Corporation, a Lockheed Martin Company, for the United States Department of Energy under Contract DE-ALO4-94AL8500.

Contents

ABSTRACT.....	i
Acknowledgments	ii
Preface.....	vii
1. Introduction.....	1
Purpose	1
Problem.....	2
Scope	4
Limitations.....	5
Overview of main report contents	8
Overview of report appendices.....	11
Notation	12
2. Porous elastic constants.....	13
The ZTW model	13
The exponential approximation	14
3. Isomorphic (projected) decomposition of stress.....	15
Projected or “isomorphic” stress measures	16
Conventional stress measures	18
4. Plastic yield surface	19
The yield surface normal	19
5. Decomposition of the strain rate	22
6. Linear-elastic relations	23
7. Void nucleation	25
8. Trial “elastic” stress rate	26
9. Plastic normality	27
10. Hardening.....	28
11. Plastic consistency	29
Stress remains on/within the yield surface	29
NUMERICAL ISSUE: return algorithms in generality	29
Avoidance of radial and oblique return methods	31
Out-of-plane stress rate.....	32
NUMERICAL ISSUE: Integrating the rate of a unit tensor.....	33
NUMERICAL ISSUE: Third-order stress corrections.....	36
12. Plastically incompressible matrix.....	38
13. Advanced/superposed model features	39
The basic QCKP model is quasistatic	39
An overstress model permits rate dependence	39
Phase transformation strain is handled externally	39
Principle of material frame indifference.....	39
14. Exact solution of the QCKP equations.....	40
15. Limiting Cases	42
Limiting case #1: Conventional p - α model	42
<i>Effect of hardening.....</i>	45
<i>Admissible crush curves.....</i>	45
<i>Existence of stress jumps</i>	47
Limiting case #2: Classical Von Mises plasticity.....	48
16. Two popular yield functions.....	49
The Gurson-Tvergaard yield function	49
The “ p - α ” yield function	50
Comparison of the Gurson and “ p - α ” yield functions.....	51
17. Verification calculations using the QCKP model.....	53

EXAMPLE 1: hydrostatic loading	53
EXAMPLE 2: Pure shear with linear hardening	55
EXAMPLE 3: Uniaxial strain (mixed) loading	56
18. Rate dependence.....	59
19. Default "dearth of data" (D.O.D.) yield function.....	62
The D.O.D. crush curves	67
Verification results	69
Allowing finite crush pressures	72
Measuring a crush curve.....	73
20. Concluding remarks.....	76
REFERENCES.....	77
APPENDIX A: Solution of the governing equations.....	A-1
APPENDIX B: Porosity dependence of the elastic moduli.....	B-1
The ZTW model.	B-1
The exponential model	B-4
User inputs for the elastic constants.	B-6
Newton solver for matrix moduli	B-6
APPENDIX C: Proper application of return algorithms.....	C-1
Return algorithms in generality	C-1
Geometric perils of return operations	C-4
APPENDIX D: The predictor-corrector QCKP algorithm	D-1
APPENDIX E: The CKP coding	E-1
APPENDIX F: Coding for the Gurson yield criterion.....	F-1
APPENDIX G: Manuals for VERSION 001009 of the CKP model	G-1
Instructions for model installers	G-1
User instructions	G-3
APPENDIX H: Nomenclature and Glossary.....	H-1

Figures

1.1	Images of porosity.	2
1.2	Shear-dependence of elastic limit pressure.	3
11.1	Finite difference error in updating unit tensor.	33
11.2	Comparison of finite difference coefficients.	35
11.3	A CKP verification calculation for changes in strain rate direction.	36
11.4	Distinction between trial stress and test stress.	37
15.1	Isotropic loading in the Rendulic plane.	42
15.2	A conventional porosity crush-up model.	44
15.3	Isotropic stress-strain response and the implied Gurson “ $p-\alpha$ ” curves.	44
15.4	Effect of hardening in the isotropic response.	45
15.5	Inadmissibility of TENSILE growth curves.	47
15.6	Purely deviatoric loading in the Rendulic plane.	48
16.1	Gurson’s yield surface compared with a $p-\alpha$ surface.	50
16.2	The $p-\psi$ curve associated with the Gurson model.	51
16.3	The p v.s. ψ^{loaded} curve.	52
17.1	Hydrostatic compression with phase transformation.	53
17.2	Mean stress vs. logarithmic volumetric strain for purely isotropic straining. . .	54
17.3	Simple linear hardening under uniaxial shear.	55
17.4	Uniaxial stress vs. logarithmic strain for uniaxial strain controlled loading. . .	56
17.5	Linear hardening and cyclic unloading.	57
17.6	Steady state response to multiple uniaxial strain cycles.	58
18.1	Overstress rate dependent stress relaxation.	59
18.2	Rate-dependent “apparent” yield stress.	60
18.3	Overstress rate dependence in pure shear with Gurson yield function.	61
18.4	Rate dependence in isotropic loading.	61
19.1	A $p-\psi$ yield surface.	63
19.2	A nominal ellipsoidal yield surface.	63
19.3	Shear-enhanced porosity compaction/dilatation.	64
19.4	Different yield in compression and tension.	64
19.5	$p-\alpha$ curve and stress-strain response.	69
19.6	Effect of changing YSLOPE.	70
19.7	Effect of changing (a) YCURVE, (b) YRATIO, and (c) YSLOPE for uniaxial strain compression followed by tension.	71
19.8	Crush transition model.	72
19.9	Inferring crush data from a hydrostatic stress-strain plot.	73
B.1	Dependence of the relative moduli on the matrix Poisson’s ratio.	B-2
B.2	Effect of porosity on the elastic moduli.	B-3
B.3	The ZTW and exponential models of porosity dependence of elastic moduli. . .	B-4
B.4	Dependence of Young’s modulus on porosity.	B-5
C.1	Oblique projection.	C-3
C.2	Counterintuitive behavior with non-isomorphic stress measures.	C-5
D.1	The effect of predictor-corrector scheme.	D-6

Tables

Table 19.1:	Material parameters defining the evolving yield function.....	68
Table G.1:	Essential USER INPUT	G-4
Table G.2:	Supplemental (advanced) USER INPUT.....	G-5

Preface

I originally became exposed to theories for porous media while studying geomechanical materials at the University of Wisconsin, Madison. At that time, I was interested in learning how modern constitutive research might lead to “non-classical” plasticity features such as non-normality of the plastic strain rate, plastic compressibility, non-symmetric acoustic tensors, etc.

A few years after I came to Sandia National Laboratories in 1993, I became involved in the modelling porous materials whose matrix material is capable of transforming at the same time that pores collapse in compression at high strain rates. Because phase transformation is typically stress-dependent, it became essential to model the effect of porosity on the stress level by a transformation strain that couples back into the stress constitutive model. Transformation of the matrix material is one feature that distinguishes the consistent kinetics porosity (CKP) model from other porosity models in the literature.

Another distinguishing feature of the CKP model is that it treats the porous yield function as a “black box,” ideally to be supplied by the user (though, for completeness and shake-down calculations, the model naturally comes equipped with a default yield function). I felt that it was essential for the yield model to be written in an easily adjusted manner. In this way, as soon as sufficient experimental measurements become available, better yield functions can be seamlessly incorporated into the material model.

The consistent kinetics porosity (CKP) model is written in an abstract purely-academic setting that permits the model to apply equally well to ceramics, porous metals, and (dry) geomaterials. Because of the abstract nature of the concepts, I have purposely refrained from presenting specific applications for specific materials in this report. I am completing a companion sequel report that covers applications for materials of interest to us. By employing different measured or published yield functions for different materials, the reader should be able to simulate the unique stress-strain curves for those materials.

For possible application to rocks, I hope eventually to add the effect of fluids within the pores. I also hope to incorporate deformation-induced anisotropy. For now, the CKP model should be regarded as a general starting framework within which more advanced constitutive features can be consistently incorporated.

Rebecca Brannon
rmbrann@sandia.gov
October 20, 2000 1:56 pm

This page intentionally left blank.

The Consistent Kinetics Porosity (CKP) Model: A Theory for the Mechanical Behavior of Moderately Porous Solids.

Rebecca Brannon

1. Introduction

Purpose

This report describes a constitutive model for moderately porous solids. The model combines many conventional theories for porous materials into a single self-consistent formulation, which is why we call it the “Consistent Kinetics Porosity (CKP) model.” By *consistent*, we mean that each feature of the model is implemented in a manner that is mathematically compatible with the other features. For example, the elastic moduli are permitted to change as a result of phase transformation, so the rate forms of the governing equations contain terms arising from the rate of change of the matrix properties. The figures on pages 53-61 of this report illustrate the stress-strain response predicted by the CKP model for several canonical loading paths.

The CKP model has been implemented and tested in a stand-alone deformation driver code [1] and in Sandia National Laboratories’ parallel arbitrary Lagrangian-Eulerian finite element code, ALEGRA [2, 3]. The numerical implementation follows the MIG model interface guidelines [4], making it ready for implementation in other host codes with minimal modifications.* Readers interested in installing the model into their own code should follow the instructions given in Appendix G. That appendix also contains a brief user’s guide which describes the input keywords. In its most basic form, the CKP model requires only four parameters (See table G.1 in Appendix G):

1. The porosity (volume fraction of void).
2. The shear modulus of the porous material.
3. The bulk modulus of the porous material.
4. The yield stress of the matrix material.

Advanced features of the CKP model (phase transformation, shear-enhanced compaction or dilatation, hardening, etc.) are invoked through the use of additional material parameters (See table G.2 in Appendix G).

The body of this report focuses on the *physical theory* of the CKP model. Details about the numerical implementation are found in the appendices.

* To date, benchmarks for this model have been tested on the following computer platforms: ASCI red T-flop, SGI, HP, Sun Solaris, Microsoft Windows, and Linux.

Problem

We are interested in modelling the mechanical effects of low to moderate levels of porosity (no more than $\sim 20\%$). Experiments [5] reveal marked dependence of the elastic properties on porosity. The CKP model employs published expressions for the shear and bulk moduli that are explicit functions of the porosity. During *elastic* loading, any changes in porosity are recoverable by simply releasing the load. If the load becomes high enough to induce plastic flow of the matrix material, then an irreversible change in the porosity (not recoverable by unloading) occurs. The CKP model presumes that the *unloaded* permanent volume change of the matrix material is negligible, which therefore gives us a connection between the unloaded porosity and the macroscopic volume change of the porous material.

Comparison of hydrostatic stress-strain curves with, say, uniaxial stress curves typically shows that the pressure at pore collapse decreases with increasing shear stress. Furthermore, continued pore collapse generally requires increasing stress magnitudes. Consequently, we take the plastic yield function to depend on pressure, equivalent shear stress, porosity, and other (optional) internal state variables such as the hardening yield stress of the matrix material. *Conventional* decoupled schemes use yield models only for determining the stress deviator, with the pressure being determined by a separate hydrodynamic equation of state equipped with, say, a p - α model [8] for the pore collapse. With our unified approach, the yield surface affects *both* the deviatoric and the isotropic response. If the material is loaded under pure *isotropic* compression, then the response is elastic until the yield surface is reached. This critical stress state has a zero equivalent shear (because the loading is isotropic) and a pressure that corresponds to the elastic limit pressure P_E seen in simple p - α models. As the pressure is further increased, irreversible pore collapse occurs, and the yield surface evolves in shape and size.

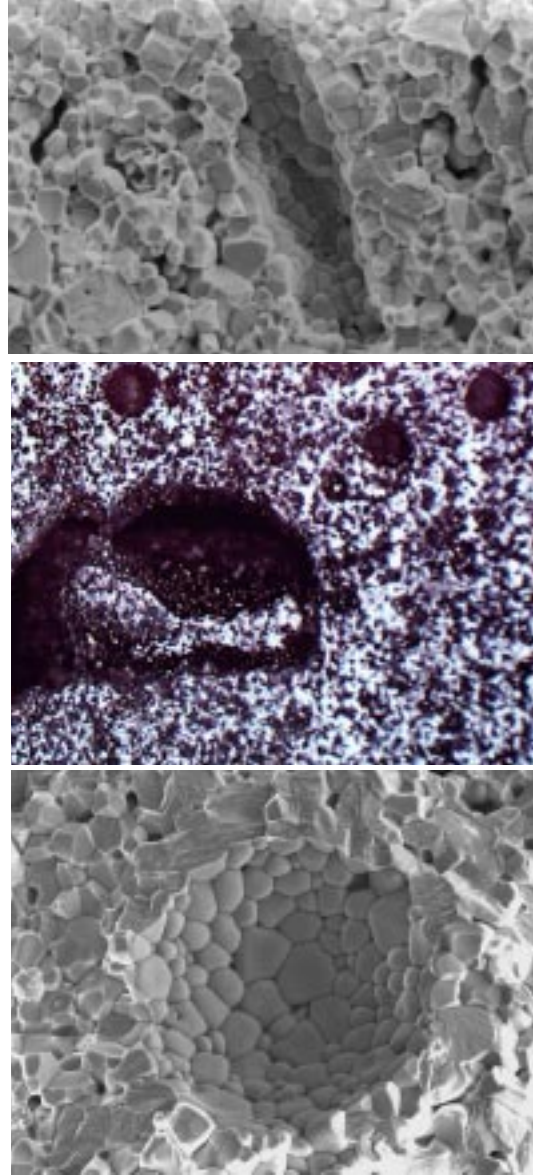


Figure 1.1. *Images of porosity.* These micrographs [6,7] show interstitial porosity between solid grains as well as larger — sometimes odd-shaped — pores that span several grains.

Specifically, the yield surface becomes larger as pores collapse because larger stresses are required to reach yield. In contrast, the yield surface *collapses* as pores grow in *tension* because the critical stress required to induce pore growth becomes *lower* as porosity increases. The evolution of the point on the yield surface where equivalent shear stress is zero corresponds to a curve of yield pressure that increases with decreasing porosity, much like a p - α curve. The importance of evolving the *entire* yield function even during isotropic loading becomes apparent if the direction of the loading is then changed to, say, uniaxial strain. Such loading direction changes are typical in important applications such as plate impact experiments.

In a *very crude* sense, the CKP model is a p - α model in which a *family* of p - α crush curves exists depending on the level of shear stress present, as suggested in Fig. 1.2. The problem with this sort of interpretation is that it does not clearly indicate the direction of subsequent plastic flow. Shear dependence permits pore collapse to commence at a much lower pressure under uniaxial strain than under isotropic compression, a feature not captured by ordinary p - α crush models. For the CKP model, pore collapse commences sooner for uniaxial loading, but the subsequent *amount* of pore collapse is initially lower. A CKP stress-strain curve has a dramatic slope discontinuity under purely-isotropic compression, but a rounded response under uniaxial strain.

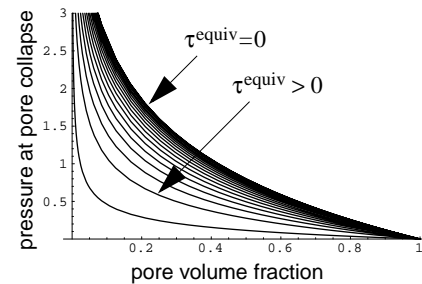


Figure 1.2. *Shear-dependence of elastic limit pressure.* Pressure at the elastic limit (where pores start to collapse) decreases with porosity, but it also decreases with the amount of shear stress present.

The CKP model is a rate-dependent extension of what we call the QCKP model, where “Q” stands for quasistatic. For low (quasistatic) strain rates, the QCKP model imposes a consistency condition for continued pore collapse so that the stress, porosity, and internal state variables evolve in such a manner that the equilibrium stress remains on the yield surface throughout any *quasistatic* interval of plastic deformation. Combining this consistency condition with the other rate forms of the governing equations (strain rate decomposition, elastic response, matrix incompressibility, phase transformation, etc.) leads to explicit *closed-form* expressions for the porosity and stress rates, which may then be integrated to update the *quasistatic* equilibrium state.

To allow strain rate effects, we permit the *actual* stress state to transiently lie outside the yield surface, but it is attracted back towards the quasistatic equilibrium stress (obtained as described above using the QCKP sub-model) at a rate proportional to the distance between them.

Scope

The CKP model includes the material (and numerical) response features and capabilities listed below. Most of these features are “optional” in the sense that their effects may be ignored through the use of appropriate user inputs (see Appendix page G-7).

- Porosity dependence of the elastic moduli.
- Porosity dependence of the onset of yield.
- Straining due to phase transformation of the matrix material.
- Changes in the matrix elastic moduli resulting from phase transformation.
- Hardening of the matrix material.
- Shear dependence of the onset of pore collapse.
- Shear dependence of the rate of pore collapse.
- Void nucleation.
- True plastic normality (with inelastic non-normality permitted by other contributions to the inelastic strain rate).
- Rigorous plastic consistency. During quasistatic plastic loading, the stress remains on the evolving yield surface.
- Overstress model for rate dependence. During rapid loading, the stress is permitted to lie transiently outside the yield surface, but is attracted back towards the equilibrium stress. This approach makes the yield stress appear to increase under high strain rates.
- Exact integration of the part of the stress deviator rate that is perpendicular to the stress deviator itself (i.e., the part that does no plastic work).
- Removal of third-order errors in the stress prediction that result from slight yield surface curvature.
- Closed-form (consistent) solution of the rate equations.
- Reduction to simpler uncoupled models (such as the popular p - α model [8]) under simpler hydrostatic and pure shear loading.
- Capability of matching measured shock loading response curves.
- Satisfaction of the principle of material frame indifference (PMFI).
- Predictor-corrector scheme for numerical integration of rate equations.
- Numerical implementation permitting a user-defined yield function.
- A flexible default yield function (to be used only for preliminary calculations until data become available), which permits:
 - (i) Different yield points in tension and compression.
 - (ii) Shear-enhanced compaction or dilatation.
 - (iii) Adjustable pressure dependence of yield.
 - (iv) Adjustable porosity dependence of yield.
 - (v) Optional Drucker-Prager yield for the matrix.
 - (vi) Optional yield “cap” type behavior.

This report initially develops what we call the “quasistatic consistent kinetics porosity (QCKP)” model, which applies only to slow strain rates without phase transformation. This foundation is then built upon by adding rate dependence, phase transformation, and material frame indifference. Throughout the upcoming theoretical development, the boxed set of equations will eventually form the complete set of QCKP equations that are linear with respect to the unknown rate quantities. The set of boxed equations is solved explicitly and then integrated to update the equilibrium state to the end of the time step. After deriving the governing equations, the basic features of the QCKP model are illustrated for several canonical load/unload paths using two different yield functions. The advanced features of rate dependence, phase transformation, and frame indifference characterize the full CKP model. We have obtained excellent agreement with shock-compression data for porous ceramics, as will be reported in the companion sequel to this report.

The CKP model assumes that the yield function is expressible in terms of the equivalent shear stress, the pressure, the porosity, and optional user-defined internal state variables. The CKP model does not assume any particular form for the yield function — this critical material function is ideally supplied by the user. As a service to our users, we have equipped the numerical implementation with a default yield function which is a generalized variation of the well-known Gurson [9] function. Users are *strongly* encouraged to replace the default CKP yield function with one that is actually measured for their material of interest. Measurement of yield functions can be a very expensive endeavor. Often, limited funding is sufficient to measure only the so-called p - α crush curve that describes the decrease in porosity as a function of applied pressure under purely *hydrostatic* loading. This leaves the effect of shear stress unknown. In the event of incomplete yield surface characterization, our implementation permits the user to specify a measured p - α crush curve, and then our default yield function approximates the effect of shear in a qualitatively reasonable manner that should be far superior to the results obtained from ordinary shear-independent p - α porosity models.

Limitations

Although the CKP model is comparatively sophisticated in that it models many more material behaviors than common porosity models, the present version also has several important limitations:

- This version of the CKP model is purely mechanical. Thermodynamical effects are ignored. Given that we are interested in applying the CKP model in the strong shock regime, this deficiency must be rectified in future versions, especially since local heating from pore collapse can induce tremendous changes in the matrix properties. The work of Haghi and Anand [10] may be useful in this regard.
- The model does not apply to highly porous media such as foams. This model is intended for moderate porosity levels up to $\sim 20\%$. The model

remains robust and *qualitatively* reasonable even at porosities that approach 100%, but the results at such large porosities are *quantitatively* suspect.

- The user should ideally supply a porosity- and pressure- dependent yield function rather than relying on the default function supplied with the model. Changing the yield function has a profound effect on the material response. The CKP model should be regarded as a stable platform on which to test various yield functions. If the CKP model fails to reproduce a measured hydrostatic stress-strain curve, then it is probably *not* the fault of the CKP model — it is likely because the user is employing an inappropriate yield function. As discussed on page 73, it is theoretically possible to construct a yield function such that it will *exactly* match a measured hydrostatic pressure vs. strain curve.
- Our implementation is written such that the calculation will abort whenever negative plastic work is detected. As discussed on page 45 of this report, positivity of plastic work upon the onset of tensile pore *expansion* depends in part on admissibility conditions that must be satisfied by the user-supplied yield function. The user must recognize that any occurrence of negative plastic work is probably caused by a flaw in the user-supplied yield function, not in the CKP model *per se*. Negative plastic work is extremely rare, usually occurring only when exercising the model under exceptionally extreme loading conditions. Our numerical implementation of the CKP model is equipped with a default yield function (Section 19) that satisfies the admissibility constraints needed to avoid negative plastic work.
- The void nucleation model is quite rudimentary. It is included only to ensure *qualitatively* reasonable model predictions under extreme loading conditions. For the applications of interest to us, the material is typically under a significant amount of compression, so the nucleation model is inconsequential. If the CKP model is to perform well in tension, it must be enhanced to include better models (e.g., [12]) for nucleation and coalescence of voids, ultimately leading to fracture.
- The fundamental elastic response is linear (though the moduli can vary as a result of phase transformation and level of porosity). Our linear elastic assumption is one reason why this model is *not* expected to perform well for foams. Though the model certainly exhibits *plastic* hysteresis, it does not include *elastic* hysteresis (For this version of CKP, the elastic loading and unloading curves exactly coincide — except, of course, when rate dependence is invoked).
- To close the system of equations, it is necessary to assume that the matrix material is plastically incompressible. Releasing this assumption would require knowledge of the *plastic* compressibility of the matrix material.
- For convenience, we have adopted the commonly-used assumption of

so-called *plastic* associativity — i.e., the model assumes normality of the plastic strain rate to the yield surface.* If needed in the future, the CKP model could be easily generalized to permit non-associated flow rules. However, Appendix Figure C.2 shows how flow behavior can sometimes misleadingly *appear* to be nonassociative when it is actually associated. Appendix C also demonstrates that an associated (normality) flow rule generally implies that a trial elastic stress must be projected *obliquely* back to the yield surface. When these subtle issues are not appreciated, researchers can sometimes *wrongly* conclude that their material obeys a non-associated flow rule, when a *properly-applied* associated flow rule is actually the appropriate choice.

- The present version of the CKP model depends only on the pore volume fraction, so it doesn't include the effect of pore morphology. The present CKP model does not account for pore size, shape, or orientation. Nor does this CKP version predict the damaging effects of pore interaction and coalescence which can significantly influence material behavior [15, 16, 17, 14]. Pardoen and Hutchinson [18] have recently extended the Gurson model to include the effects of both pore shape and coalescence. Leblond and Perrin [18] discuss the effect of spatial void clustering. To treat microstructures like the one in Fig. 1.1, future versions of the CKP model may also draw upon Tvergaard's analysis of the interaction between large pores and smaller interstitial pores [13].
- In this version of the CKP model, a linear isotropic hardening model is used for the matrix material. Future versions should permit nonlinear hardening and perhaps even kinematic hardening.
- The model assumes that the pores are filled with void. It cannot, therefore, be applied to geomechanical materials having partially or fully saturated pore spaces, though future versions of this model might incorporate the effect of fluid within and flow between the pores [20].
- The model does not account for deformation-induced anisotropy. The CKP model assumes that the material is isotropic *and remains isotropic*. Such an assumption is clearly unsatisfactory under non-hydrostatic loading such as the uniaxial straining that is typical behind explosively-generated shock waves. Future versions of the CKP model will approximate this effect by applying the isotropic CKP model in an anisotropically distorted stress space.
- The model does not account for residual stress that exists in the matrix material in the macroscopically unloaded state.
- Our implementation of the CKP model satisfies the principle of material frame indifference (PMFI) because we apply it in the unrotated

* Throughout this report, the term “plastic strain rate” refers only to the part of the strain rate from classical plastic flow of the matrix material. The *total* inelastic strain rate is non-associated whenever pores are nucleating or when the matrix material is undergoing a phase transformation.

reference frame, which is equivalent to using polar rates in the spatial frame. Satisfying PMFI merely ensures that the model will predict consistent* results under large material *rotations*. Satisfying this principle has no influence on whether or not a model will yield good results for large material *distortions* (where the material element significantly changes shape) or large material *dilatations* (where the material element significantly changes size). The merits of the current formulation of the CKP model under large material distortions and dilatations will probably depend on the underlying matrix material.

Overview of main report contents

This report is organized as follows:

- Section 1, which is this section, provides a motivation for and overview of the model.
- Section 2 presents two theories for the effect of porosity on the elastic constants. Both models are roughly equivalent for the low to moderate porosity range of interest for our applications.
- Section 3 points out that the yield surface is axisymmetric in stress space. The axis of symmetry is parallel to the identity tensor, so the identity tensor plays a role similar to the $\tilde{\mathbf{e}}_z$ axis in cylindrical coordinates. For cylindrical symmetry, a problem can be solved in the z vs. r plane. Section 3 introduces stress measures σ_m and σ_s that are analogous to r and z from cylindrical coordinates.
- Section 4 presents the assumption that the yield function depends only on the pressure, the equivalent shear stress, the porosity, and a user-definable array of internal state variables. The CKP model is constructed such that the precise functional form for the yield function is user-definable. Since the yield function is one of the most important features governing the stress response of a material, it is essential that CKP users employ a good yield function model. Of course, our numerical implementation comes equipped with a default yield function, but we caution that this default yield function should be used only for order-of-magnitude studies. For better results, *measurements of the yield function for the material must be performed!*
- Section 5 briefly introduces the classical decomposition of the strain

* In this context, the term *consistent* refers to comparison between two deformations that differ only by a rigid rotation. Frame indifference requires that the two predictions of the model must be consistent, which usually means that the predictions for spatial quantities such as the Cauchy stress must differ from each other only by the rigid rotation. PMFI does not require the prediction for *either* deformation to be *good* by itself — PMFI merely asserts that the two predictions must be *consistent* with each other. If a model is good under small deformations, then PMFI ensures quality under large deformations *only in the sense of large displacement gradients from rotations*.

rate into elastic plus inelastic parts. The inelastic strain rate includes contributions from plastic flow of the matrix material, phase transformation, and void nucleation.

- Section 6 presents rate forms of the linear elastic constitutive relations with unconventional nonlinear contributions from irreversible changes in the elastic moduli (such as stiffening due to pore collapse or phase transformation).
- Section 7 provides a very simplistic theory for pore nucleation. We are contented with the *ad hoc* nature of the theory because physical applications of interest to us are primarily compressive, so nucleation is not expected to play a swinging role.
- Section 8 discusses the standard computation of the trial elastic stress rate in the new context of isomorphic projected stress measures.
- Section 9 presents the assumption that the plastic part of the strain “rate” is normal to the yield surface in stress space. This direction is determined by the gradient of the yield function with respect to stress, which takes an intuitively-appealing mathematical structure in terms of our isomorphic projected stress measures. The magnitude of the plastic strain rate (which is called the “plastic segment”) remains undetermined at this point in the analysis.
- Section 10 presents the assumption that each internal state variable (whatever it may be) evolves linearly with the rate of plastic deformation, where the linearity coefficient is a user-supplied parameter.
- Section 11 argues that, for consistency, the stress state must remain on the yield surface during any *quasistatic* interval of continued plastic loading. This means that, not only must the yield function equal zero, its *rate* must also be zero. Whenever this assumption is invoked, the model is called the QCKP model, where Q stands for “quasistatic.” Because we have assumed that the yield function depends on pressure and equivalent shear stress, this QCKP consistency condition constrains allowable rates for the pressure and equivalent shear stress. The part of the stress rate that causes no plastic work (i.e., the part of the *deviatoric* stress rate that is perpendicular to the stress itself) is unconstrained by plastic consistency, and is shown equal to the part of the elastic trial stress rate that is perpendicular to the so-called “Rendulic” plane spanned by the identity tensor and the stress deviator.
- Section 12 introduces the very common assumption that permanent volume changes result primarily from pore collapse. In other words, permanent volume changes of the matrix material are neglected. This constraint provides an essential relationship between the rate of porosity and the plastic strain rate tensor.
- Section 13 summarizes the advanced model features (such as rate dependence, phase transformation, and material frame indifference) that are superposed on the QCKP model to obtain what we call the full CKP

model.

- Section 14 provides the culminating *closed-form* solution to all of the QCKP governing rate equations. Again, we note that the QCKP governing equations are highly nonlinear, but they are all proper functions. Consequently, the rate forms of the governing equations are *linear* with respect to rates, which allows the unknown rates to be determined as a closed-form function of the current state and known rates.
- Section 15 explores two limiting cases — pure isotropic loading and pure shear — to verify that the very general solution simplifies to a familiar and intuitively reasonable form under the assumptions that are appropriate for each canonical loading. We describe a new admissibility constraint on the user-supplied yield function needed to ensure positive plastic work under isotropic *tensile expansion*.
- Section 16 discusses the fairly popular Gurson [9] yield function that is based on an analytical upper bound solution for a regular array of spherical voids embedded within a rigid-plastic matrix material. The Gurson yield surface is shaped almost like an ellipse in shear vs. pressure space. This shape is contrasted with the rectangular *implied* yield surface of traditional p - α models.
- Section 17 presents numerous examples of the predictions of the CKP model for extreme straining under canonical loadings using the Gurson yield function. The examples include isotropic compression with phase transformation, pure shear with hardening, uniaxial (combined) strain loading with periodic load reversals, and cyclic loading with and without hardening.
- Section 18 details the theory of rate dependence for the pore model. Rate dependence is allowed by tracking both the *actual* stress, which is permitted to lie outside the yield surface, and the *equilibrium* stress, which must always lie inside or on the yield surface and is governed by the standard QCKP equations developed in earlier sections.
- Section 19 presents a highly heuristic, but very flexible, yield function that a user might wish to employ when only a p - α curve is known. The corresponding yield surface interpolates between an ellipse and a rectangle in such a way that the response will exactly coincide with the (user-specified) p - α response under isotropic loading but will exhibit a qualitatively reasonable shear dependence under mixed loading. This yield function model also includes parameters that allow the user to optionally define different yield in tension and compression, as well as shear-enhanced compaction or dilatation.
- Section 20 concludes the main part of the report by discussing the merits and caveats of the CKP model along with plans for future development.

Overview of report appendices

This presentation of the CKP model is followed by several appendices that provide the following detailed information relating to the main text:

- Appendix A shows how the boxed rate equations are solved in closed form.
- Appendix B provides detailed exploration of the manner in which the elastic moduli are taken to vary with porosity. This appendix also shows how a Newton solver is used to infer the *matrix* elastic moduli, given only the porosity and initial moduli of the macroscopic porous material.
- Appendix C discusses the proper return direction for plastic return algorithms and it provides further motivation for the use of isomorphic projected stress measures by showing that a return to the nearest point on the yield surface does *not* correspond to a nearest point return in the space of shear-stress vs. mean-stress unless isomorphic measures are used.
- Appendix D provides a step-by-step algorithm for the CKP model in which the equations developed in the main part of this report are implemented numerically via a predictor-corrector scheme.
- Appendix E provides the corresponding source code.
- Appendix F shows how the yield function routines should be written if the user elects to use the Gurson yield function. This appendix should serve as a template for implementing other yield functions.
- Appendix G provides brief instructions for how to install the CKP model into a host code. This appendix also provides a brief user's guide.
- Appendix H is a nomenclature list that defines the many symbols used in this report. This appendix also indicates the inputs and outputs of the CKP main subroutine as well as the material constants that are used within that subroutine.

Notation

Throughout this report, scalars are denoted in plain italics (s, r, t). Vectors are typeset with a single under-tilde ($\underline{\mathbf{y}}, \underline{\mathbf{w}}, \underline{\mathbf{x}}$). Second-order tensors are shown with two under-tildes ($\underline{\underline{\sigma}}, \underline{\underline{\mathbf{S}}}, \underline{\underline{\mathbf{T}}}$). Likewise, the order of higher-order tensors is indicated by the number of under-tildes.

Two vectors written side-by-side are multiplied dyadically. For example, $\underline{\mathbf{a}}\underline{\mathbf{b}}$ is a second-order tensor with ij components given by $a_i b_j$. Any second-order tensor $\underline{\underline{\mathbf{T}}}$ may be expanded in terms of basis dyads as $\underline{\underline{\mathbf{T}}} = T_{ij} \underline{\mathbf{e}}_i \underline{\mathbf{e}}_j$. Here (and throughout this report) repeated indices imply summation from 1 to 3.

A single raised dot denotes the vector inner-product defined by

$$\underline{\mathbf{u}} \bullet \underline{\mathbf{v}} = u_1 v_1 + u_2 v_2 + u_3 v_3 = u_k v_k. \quad (1.1)$$

The single raised dot continues to denote the vector inner product even when acting between higher-order tensors. For example,

$$\underline{\underline{\mathbf{A}}} \bullet \underline{\mathbf{x}} = A_{ij} x_j \underline{\mathbf{e}}_i. \quad (1.2)$$

Composition of two tensors is another example:

$$\underline{\underline{\mathbf{A}}} \bullet \underline{\underline{\mathbf{B}}} = A_{ik} B_{kj} \underline{\mathbf{e}}_i \underline{\mathbf{e}}_j. \quad (1.3)$$

The deviatoric part of a tensor is denoted by a “prime.” Hence,

$$\underline{\underline{\mathbf{A}}} \prime \equiv \underline{\underline{\mathbf{A}}} - \frac{1}{3}(\text{tr } \underline{\underline{\mathbf{A}}}) \underline{\underline{\mathbf{I}}}, \quad (1.4)$$

where $\underline{\underline{\mathbf{I}}}$ is the identity tensor and “tr” denotes the trace. Specifically,

$$\text{tr } \underline{\underline{\mathbf{A}}} \equiv A_{11} + A_{22} + A_{33} = A_{kk}. \quad (1.5)$$

The tensor inner product is denoted by “:” and is defined by

$$\underline{\underline{\mathbf{A}}} : \underline{\underline{\mathbf{B}}} = A_{ij} B_{ij}. \quad (1.6)$$

Note that

$$\underline{\underline{\mathbf{A}}} : \underline{\underline{\mathbf{B}}} = \underline{\underline{\mathbf{B}}} : \underline{\underline{\mathbf{A}}}. \quad (1.7)$$

The magnitude of a second-order tensor is defined

$$\|\underline{\underline{\mathbf{A}}}\| \equiv \sqrt{\underline{\underline{\mathbf{A}}} : \underline{\underline{\mathbf{A}}}}. \quad (1.8)$$

The tensor inner product is allowed to operate between any two tensors of *at least* second order. For example, if $\underline{\underline{\underline{\mathbf{E}}}}$ is a fourth-order tensor, then

$$\underline{\underline{\underline{\mathbf{E}}}} : \underline{\underline{\mathbf{A}}} = E_{ijkl} A_{kl} \underline{\mathbf{e}}_i \underline{\mathbf{e}}_j. \quad (1.9)$$

2. Porous elastic constants

The ZTW model

Zhao, Tandon and Weng [21] provide moderately complicated expressions for the macroscopic shear and bulk moduli (G and K) in a porous material. Brannon and Drugan [22] manipulate those expressions into the following much simpler forms:

$$\frac{G}{G_m} = (1 + \gamma_m \psi)^{-1} \quad \text{where} \quad \gamma_m = \frac{5(4G_m + 3K_m)}{8G_m + 9K_m}. \quad (2.1a)$$

$$\frac{K}{K_m} = (1 + \kappa_m \psi)^{-1} \quad \text{where} \quad \kappa_m = \frac{4G_m + 3K_m}{4G_m}. \quad (2.1b)$$

Here, G_m and K_m are the shear and bulk moduli of the matrix material, and ψ is the ratio of the unstressed void volume to the unstressed solid volume. Thus, if f_v denotes the conventional porosity (i.e., the volume fraction of voids) then the pore ratio ψ is related to f_v by

$$\psi = \frac{f_v}{1 - f_v}. \quad \approx f_v \text{ if } f_v \ll 1 \quad (2.2)$$

The pore ratio ψ is approximately equal to the porosity f_v at low porosities. The CKP model requires only the *unstressed* porosity — i.e., the value of porosity after stress is removed. The actual porosity (which is not needed) can change under elastic loading, but the unstressed porosity can change only as a result of plastic flow of the matrix material. The fact that our pore ratio ψ is the unstressed value means that it remains unchanged during any purely elastic interval of deformation.

The pore ratio ψ is related to the distension parameter α from traditional p - α models by

$$\psi = \alpha - 1. \quad (2.3)$$

The distention α is defined to be the theoretical solid density divided by the actual porous density. As pores are crushed out, the distention α approaches 1.0 and the pore ratio ψ approaches zero. If pores grow in tension, the porosity f_v approaches 1.0, while both the pore ratio and the distention approach infinity.

Appendix B elaborates on implications of the above ZTW equations, showing graphically how the elastic moduli vary with porosity. Fig. B.2 in particular shows that Poisson's ratio is unaffected by porosity whenever the matrix material has a Poisson's ratio equal to 0.2. Fortunately, the materials of interest to us have a Poisson's ratio of approximately 0.2, and our experiments (to be discussed in a sequel to this report) validate our prediction of porosity-independence of Poisson's ratio.

The exponential approximation

Appendix B presents an exponential asymptotic expansion of the ZTW equations. Namely, for moderately small values of ψ (less than $\sim 10\%$), Eq. (2.1) is well approximated by

$$\frac{G}{G_m} = e^{-\gamma_m \psi} \quad (2.4a)$$

$$\frac{K}{K_m} = e^{-\kappa_m \psi}. \quad (2.4b)$$

This approximation gives analytically simple expressions for the time rates of the moduli:

$$\frac{\dot{G}}{G} = \dot{\Upsilon} - \gamma_m \dot{\psi} \quad (2.5a)$$

$$\frac{\dot{K}}{K} = \dot{\Upsilon} - \kappa_m \dot{\psi}, \quad (2.5b)$$

Here, the quantity $\dot{\Upsilon}$ accounts for the possibility that the matrix elastic moduli may stiffen as a result of phase transformation within the matrix material. Specifically, $\dot{\Upsilon}$ is defined by

$$\dot{\Upsilon} = \frac{\dot{G}_m}{G_m} = \frac{\dot{K}_m}{K_m}. \quad (2.6)$$

We have taken the *relative* rates of the matrix moduli to be the same for both the shear and bulk modulus because that is the case for the transforming materials of interest to us. The implication of this assumption is that the Poisson's ratio of the matrix material is unchanged from phase transformation. The quantity $\dot{\Upsilon}$ is supplied as a known input to the CKP subroutines. It is zero if the matrix material has constant elastic moduli. A formula for $\dot{\Upsilon}$ can be derived if one assumes a simple "mixing" rule for the bulk modulus:

$$K_m = K_m^{(0)}(1 - \phi) + K_m^{(1)}\phi, \quad (2.7)$$

where ϕ is the extent of transformation; $K_m^{(0)}$ and $K_m^{(1)}$ are the moduli before and after transformation, respectively. Differentiating gives

$$\dot{\Upsilon} = \frac{\dot{K}_m}{K_m} = \frac{[K_m^{(1)} - K_m^{(0)}]\dot{\phi}}{K_m^{(0)}(1 - \phi) + K_m^{(1)}\phi}. \quad (2.8)$$

Thus, $\dot{\Upsilon}$ can be readily approximated if the transformation rate $\dot{\phi}$ is known.

3. Isomorphic (projected) decomposition of stress*

The stress tensor $\underline{\underline{\sigma}}$ is *conventionally* decomposed into isotropic and deviatoric parts:

$$\underline{\underline{\sigma}} = -p\underline{\underline{I}} + \underline{\underline{S}}, \quad (3.1)$$

where $\underline{\underline{I}}$ is the identity tensor, p is the compressive mechanical pressure and $\underline{\underline{S}}$ is the stress deviator, defined respectively by

$$p \equiv -\frac{1}{3}\text{tr}\underline{\underline{\sigma}} \quad \text{and} \quad (3.2a)$$

$$\underline{\underline{S}} = \underline{\underline{\sigma}} - \frac{1}{3}\text{tr}\underline{\underline{\sigma}}\underline{\underline{I}} = \underline{\underline{\sigma}} + p\underline{\underline{I}}. \quad (3.2b)$$

Equation (3.1) breaks the stress $\underline{\underline{\sigma}}$ into a traceless part $\underline{\underline{S}}$ plus a part that is proportional to the identity tensor $\underline{\underline{I}}$. Being a symmetric tensor, the stress may be viewed as a member of a six-dimensional vector space. In the next section, we will introduce a yield surface that is axisymmetric about an axis parallel to the identity tensor $\underline{\underline{I}}$. The quantity $-p\underline{\underline{I}}$ is the part of the stress tensor that is aligned with this symmetry axis and $\underline{\underline{S}}$ is the part of the stress tensor that is perpendicular to the axis. The identity tensor $\underline{\underline{I}}$ plays a role similar to that of the \underline{e}_z base vector for problems symmetric about the z -axis. Unlike the *unit* vector \underline{e}_z , the identity tensor has a magnitude $\sqrt{\underline{\underline{I}}:\underline{\underline{I}}}$ equal to $\sqrt{3}$, which is a key that will lead us to replace pressure with our alternative measure of mean stress.

The decomposition in Eq. (3.1) defines a two-dimensional linear subspace (herein called **the Rendulic plane**) embedded within 6D symmetric tensor space. Specifically, the Rendulic plane is the plane spanned[†] by the identity tensor $\underline{\underline{I}}$ and the stress deviator $\underline{\underline{S}}$. The Rendulic plane is analogous to the z vs. r plane that is spanned by the unit base vector \underline{e}_z for cylindrical coordinates and the position vector \underline{x} .

* To permit large material rotations, the host code calls the CKP model using exclusively arguments for which material rotation has been removed. Therefore quantities such as stress and strain “rate” should be regarded as those in the unrotated reference configuration. Since CKP uses the (unrotated) symmetric part of the velocity gradient, the reader can regard our strain measure to be (unrotated) logarithmic strain and our stress measure to be the (unrotated) Cauchy stress.

† The **span** of a set of vectors, $Y = \{\mathbf{v}_1, \mathbf{v}_2, \dots, \mathbf{v}_N\}$, is simply the set of all vectors that can be written as a linear combination of the vectors in Y . The set Y may permissibly contain more vectors than needed to define a basis for $\text{span}[Y]$. For example, the span of $\{\mathbf{v}_1 = \underline{e}_1, \mathbf{v}_2 = \underline{e}_2, \mathbf{v}_3 = \underline{e}_1 + \underline{e}_2\}$ is the 1-2 plane. The span of a set of *tensors* is defined analogously; therefore, the span of $\underline{\underline{S}}$ and $\underline{\underline{I}}$ is the set of all tensors expressible in the form $\alpha\underline{\underline{S}} + \beta\underline{\underline{I}}$ for some scalars α and β .

Below we will modify the above decomposition by introducing *unit* base tensors $\hat{\underline{\underline{\mathbf{I}}}}$ and $\hat{\underline{\underline{\mathbf{S}}}}$ that are simply $\underline{\underline{\mathbf{I}}}$ and $\underline{\underline{\mathbf{S}}}$ divided by their own respective magnitudes. The unit tensors $\hat{\underline{\underline{\mathbf{I}}}}$ and $\hat{\underline{\underline{\mathbf{S}}}}$ are analogous to the unit cylindrical base vectors $\underline{\underline{\mathbf{e}}}_z$ and $\underline{\underline{\mathbf{e}}}_r$.

The stress tensor belongs to a six-dimensional tensor space, but we seek to graphically depict it on the two dimensional surface where this report is physically printed (or electronically displayed). The *conventional* method for doing this is by simply plotting $\|\underline{\underline{\mathbf{S}}}\|$ versus the mean stress, $-p$. However, this conventional choice is actually a *distortion* of stress space that does not depict, for example, an accurate picture of stress magnitude nor the angle that the stress tensor forms with the axis of isotropic tensors.

Projected or “isomorphic” stress measures

We employ a modified version of the deviatoric-isotropic stress decomposition that is analogous to writing a position vector as $\underline{\underline{\mathbf{x}}} = z\underline{\underline{\mathbf{e}}}_z + r\underline{\underline{\mathbf{e}}}_r$ for cylindrical coordinates. Specifically, we use a “projected” or “isomorphic” stress decomposition:*

$$\underline{\underline{\mathbf{\sigma}}} = \sigma_m \hat{\underline{\underline{\mathbf{I}}}} + \sigma_s \hat{\underline{\underline{\mathbf{S}}}}, \quad (3.3)$$

where

$$\sigma_m \equiv \frac{1}{\sqrt{3}} \text{tr} \underline{\underline{\mathbf{\sigma}}} = -\sqrt{3} p \quad \text{and} \quad (3.4a)$$

$$\sigma_s = \|\underline{\underline{\mathbf{S}}}\| = \sqrt{S_{ij} S_{ij}}. \quad (3.4b)$$

Here, the tensor $\hat{\underline{\underline{\mathbf{I}}}}$ is merely the identity tensor divided by its own magnitude[†] and $\hat{\underline{\underline{\mathbf{S}}}}$ is the stress deviator divided by its own magnitude (if the stress is isotropic, we can define $\hat{\underline{\underline{\mathbf{S}}}}$ for convenience without loss). Thus,

* A mapping is “isomorphic” if and only if it preserves algebraic and geometric properties such as length and angle. Principal stress space is one example of an isomorphic mapping from stress space to 3D space where the stress is represented by a 3-component vector containing the principal stresses: $\underline{\underline{\mathbf{\sigma}}} = \{\sigma_1, \sigma_2, \sigma_3\}$. Under this isomorphic mapping, length is properly preserved (e.g., $\underline{\underline{\mathbf{\sigma}}}: \underline{\underline{\mathbf{\sigma}}}$ can be computed by $\underline{\underline{\mathbf{\sigma}}} \bullet \underline{\underline{\mathbf{\sigma}}} = \sigma_1^2 + \sigma_2^2 + \sigma_3^2$). In principal stress space, the isotropic axis is parallel to a *unit* vector $\underline{\underline{\mathbf{m}}} = \{1, 1, 1\}/\sqrt{3}$. The component of the stress “vector” in the direction of this unit vector is *not* the pressure — it is instead $\sigma_m = \underline{\underline{\mathbf{\sigma}}} \bullet \underline{\underline{\mathbf{m}}} = (\sigma_1 + \sigma_2 + \sigma_3)/\sqrt{3} = -\sqrt{3} p$. The *isomorphic* Rendulic mapping is heuristically equivalent to shifting your view in principal stress space until the isotropic axis points directly to your right and the stress deviator points straight up. If you do this, then the stress “vector” has components σ_m and σ_s . Under the isomorphic Rendulic mapping, lengths and angles are preserved (for example, $\underline{\underline{\mathbf{\sigma}}}: \underline{\underline{\mathbf{\sigma}}}$ may be computed by $\sigma_m^2 + \sigma_s^2$, and the normal to the yield surface in stress space maps to the normal to the yield surface in σ_s vs. σ_m space — hence preserving the 90° angle between the yield surface and its normal).

† Namely, $\|\hat{\underline{\underline{\mathbf{I}}}}\| = \sqrt{\underline{\underline{\mathbf{I}}}: \underline{\underline{\mathbf{I}}}} = \sqrt{\delta_{ij} \delta_{ij}} = \sqrt{\delta_{ii}} = \sqrt{\text{tr} \underline{\underline{\mathbf{I}}}} = \sqrt{3}$. In principal stress space, $\underline{\underline{\mathbf{I}}}$ is the $\{1, 1, 1\}$ vector and $\hat{\underline{\underline{\mathbf{I}}}}$ is $\{1, 1, 1\}/\sqrt{3}$, which was called $\underline{\underline{\mathbf{m}}}$ in the preceding footnote.

$$\hat{\underline{\underline{\mathbf{I}}}} \equiv \frac{\underline{\underline{\mathbf{I}}}}{\|\underline{\underline{\mathbf{I}}}\|} = \frac{\underline{\underline{\mathbf{I}}}}{\sqrt{3}} \quad \text{and} \quad (3.5a)$$

$$\hat{\underline{\underline{\mathbf{S}}}} = \begin{cases} \underline{\underline{\mathbf{S}}}/\|\underline{\underline{\mathbf{S}}}\| & \text{if } \|\underline{\underline{\mathbf{S}}}\| \neq 0 \\ \text{arbitrary} & \text{if } \|\underline{\underline{\mathbf{S}}}\| = 0 \end{cases} \quad (3.5b)$$

The fact that $\hat{\underline{\underline{\mathbf{S}}}}$ is arbitrary when $\|\underline{\underline{\mathbf{S}}}\| = 0$ should be no more disturbing than the fact that, for cylindrical coordinates, $\underline{\underline{\mathbf{e}}}_r$ is arbitrary when $r=0$. The quantity σ_s is the magnitude of the stress deviator. In our implementation, if $\sigma_s=0$, then we align $\hat{\underline{\underline{\mathbf{S}}}}$ with the *impending* direction of $\underline{\underline{\mathbf{S}}}$, as determined by the direction of the deviatoric strain rate.

If an observer could be oriented to view the six-dimensional stress state in a plane containing $\underline{\underline{\mathbf{S}}}$ and $\underline{\underline{\mathbf{I}}}$, then the components of the stress in that plane would be σ_s and σ_m . Consequently, lengths and angles in the tensor-space Rendulic plane will equal the corresponding lengths and angles measured in our isomorphic σ_s vs. σ_m depiction of the Rendulic plane. These advantages become more apparent in Eq. (4.11) where the normal to the yield surface in 6D stress space is isomorphically related to the normal to the yield surface in the 2D σ_s vs. σ_m Rendulic plane. By using an isomorphic stress projection, normality of the stress to the yield surface in 6D symmetric tensor space will correspond to normality of the projected stress to the yield surface in the 2D Rendulic plane. As illustrated in Fig. C.2 of Appendix C, the conventional decomposition of Eq. (3.1) does not have this property.

The unit tensors $\hat{\underline{\underline{\mathbf{I}}}}$ and $\hat{\underline{\underline{\mathbf{S}}}}$ may be viewed as *orthonormal* base vectors in the Rendulic stress plane. The scalars σ_m and σ_s are *Cartesian* components of the stress in this plane.* Just as the operation $v_k = \underline{\mathbf{v}} \bullet \underline{\mathbf{e}}_k$ gives *Cartesian* the component of a vector $\underline{\mathbf{v}}$ in the direction of a *unit* base vector $\underline{\mathbf{e}}_k$, we note that σ_m and σ_s are given by analogous tensor operations:

$$\sigma_m = \underline{\underline{\sigma}} : \hat{\underline{\underline{\mathbf{I}}}} \quad \text{and} \quad \sigma_s = \underline{\underline{\sigma}} : \hat{\underline{\underline{\mathbf{S}}}}, \quad (3.6)$$

The “double dot” operation is the tensor inner product defined in Eq. (1.6). For future reference, we note that

$$\hat{\underline{\underline{\mathbf{I}}}} : \hat{\underline{\underline{\mathbf{I}}}} = 1, \quad \hat{\underline{\underline{\mathbf{S}}}} : \hat{\underline{\underline{\mathbf{S}}}} = 1, \quad \hat{\underline{\underline{\mathbf{I}}}} : \hat{\underline{\underline{\mathbf{S}}}} = 0. \quad (3.7)$$

These equations are analogous to the properties of cylindrical base vectors:

$$\underline{\underline{\mathbf{e}}}_z \bullet \underline{\underline{\mathbf{e}}}_z = 1, \quad \underline{\underline{\mathbf{e}}}_r \bullet \underline{\underline{\mathbf{e}}}_r = 1, \quad \underline{\underline{\mathbf{e}}}_z \bullet \underline{\underline{\mathbf{e}}}_r = 0. \quad (3.8)$$

* In fairness, we should note that the tensors $\underline{\underline{\mathbf{I}}}$ and $\underline{\underline{\mathbf{S}}}$ in Eq. (3.1) may also be viewed as base tensors for the Rendulic plane, but they are *non-normalized*, so the coefficient $-p$ would have to be regarded as a *contravariant* (non-Cartesian) component.

The rate of a deviatoric tensor is itself a deviatoric tensor. Furthermore, any unit tensor is always geometrically perpendicular to its own rate. Hence, we note for future reference that

$$\hat{\underline{\underline{I}}}:\hat{\underline{\underline{S}}}=0 \quad \text{and} \quad \hat{\underline{\underline{S}}}:\hat{\underline{\underline{S}}}=0, \quad (3.9)$$

This shows that $\hat{\underline{\underline{S}}}$ is perpendicular to the span of $\hat{\underline{\underline{I}}}$ and $\hat{\underline{\underline{S}}}$.

Eq. (3.9) is analogous to similar properties of cylindrical base vectors:

$$\underline{\underline{e}}_z \cdot \dot{\underline{\underline{e}}}_r = 0 \quad \text{and} \quad \underline{\underline{e}}_r \cdot \dot{\underline{\underline{e}}}_r = 0, \quad (3.10)$$

showing that $\dot{\underline{\underline{e}}}_r$ is perpendicular to the plane containing $\underline{\underline{e}}_z$ and $\underline{\underline{e}}_r$.

Conventional stress measures

The CKP model works internally with the projected stress measures σ_s and σ_m . However, it would be unfair to ask *users* to work with these non-conventional stress measures. Hence, once a numerical pore collapse/expansion simulation is complete, a connection naturally must be made between the projected stress measures and other more common stress measures used in the literature. As mentioned earlier, the projected mean stress is related to pressure p by

$$p = -\sigma_m / \sqrt{3}. \quad (3.11)$$

The Von Mises equivalent stress is

$$\sigma^{VM} \equiv \sqrt{\frac{3}{2} \underline{\underline{S}}_{ij} \underline{\underline{S}}_{ij}} = \sqrt{\frac{3}{2}} \sigma_s. \quad (3.12)$$

The equivalent shear stress is

$$\tau^{\text{equiv}} \equiv \sqrt{\frac{1}{2} \underline{\underline{S}}_{ij} \underline{\underline{S}}_{ij}} = \sqrt{\frac{1}{2}} \sigma_s. \quad (3.13)$$

The isomorphic projected shear stress is related to the above stresses by

$$\sigma_s = \sqrt{\frac{2}{3}} \sigma^{VM} = \sqrt{2} \tau^{\text{equiv}}. \quad (3.14)$$

4. Plastic yield surface

The onset of permanent deformation is assumed to occur when the stress becomes sufficiently large, as defined by a yield function $F(\underline{\sigma})$ becoming zero. The yield function might additionally depend on internal state variables. In particular, for an isotropic porous material, we will assume that the yield function depends on four scalars: the projected mean stress σ_m , the isomorphic shear stress σ_s , the pore ratio ψ , and some other unspecified state variable(s) ζ . A given stress state is considered “below yield” and therefore “elastic” if and only if

$$F(\sigma_m, \sigma_s, \psi, \zeta) < 0. \quad (4.1)$$

A stress is “above yield” if and only if

$$F(\sigma_m, \sigma_s, \psi, \zeta) > 0. \quad (4.2)$$

Under quasistatic loading the stress is never permitted to be above yield. A stress is “at yield” if and only if it lies on the “yield surface,” which is the boundary of the set of elastic stresses. Hence, the yield surface is defined by the set of stresses for which

$$F(\sigma_m, \sigma_s, \psi, \zeta) = 0. \quad (4.3)$$

Two popular choices for the yield function (namely the Gurson function and the “ p - α ” function) are discussed on page 49. For now, the yield function is considered to be a known user-specified function.

For future reference, we will assign the following symbols for the derivatives of this yield function:

$$F_m \equiv \frac{\partial F(\sigma_m, \sigma_s, \psi, \zeta)}{\partial \sigma_m} \quad (4.4a)$$

$$F_s \equiv \frac{\partial F(\sigma_m, \sigma_s, \psi, \zeta)}{\partial \sigma_s} \quad (4.4b)$$

$$F_\psi \equiv \frac{\partial F(\sigma_m, \sigma_s, \psi, \zeta)}{\partial \psi} \quad (4.4c)$$

$$F_\zeta \equiv \frac{\partial F(\sigma_m, \sigma_s, \psi, \zeta)}{\partial \zeta}. \quad (4.4d)$$

The yield surface normal

We have already mentioned that our pore ratio ψ is computed using the *unstressed* porosity. Hence, it is unchanged during any interval of elastic loading. The unstressed reference porosity can change only via plastic flow of the matrix material (or void nucleation). We will also presume that the innominate internal state variable ζ is unchanged during elastic deformations. Recognizing these restrictions is essential when defining the yield surface normal. The key implication is that the yield surface itself does not move during elas-

tic loading. If, for example, we had permitted the yield function to depend on the *actual* porosity rather than the unloaded porosity, then the yield surface would expand or contract as we approach it elastically. If the yield function were dependent on the *actual* porosity, then the normal to the yield surface would require knowledge of the derivative of porosity with respect to stress. Because we use the *unstressed* porosity, this information is not needed. Likewise, because we assume that the innominate internal state variable ζ does not change under elastic loading, it must be independent of the stress level just like ψ . Consequently,

$$\frac{d\psi}{d\underset{\approx}{\boldsymbol{\sigma}}} = \underset{\approx}{\mathbf{0}} \text{ for all elastic stress states } \underset{\approx}{\boldsymbol{\sigma}} \text{ (i.e. those below yield)}. \quad (4.5)$$

$$\frac{d\zeta}{d\underset{\approx}{\boldsymbol{\sigma}}} = \underset{\approx}{\mathbf{0}} \text{ for all elastic stress states } \underset{\approx}{\boldsymbol{\sigma}} \text{ (i.e. those below yield)}. \quad (4.6)$$

The yield surface in the two-dimensional Rendulic (σ_s vs. σ_m) plane is defined by $F(\sigma_m, \sigma_s, \psi, \zeta)=0$. Of the four independent variables ($\sigma_m, \sigma_s, \psi, \zeta$), only two of them — σ_m and σ_s — are proper functions of the stress. Hence, the yield surface in *six*-dimensional symmetric tensor space is defined by $F^*(\underset{\approx}{\boldsymbol{\sigma}})=0$, where

$$F^*(\underset{\approx}{\boldsymbol{\sigma}}) \equiv F(\sigma_m(\underset{\approx}{\boldsymbol{\sigma}}), \sigma_s(\underset{\approx}{\boldsymbol{\sigma}}), \psi, \zeta). \quad (4.7)$$

Here, we have emphasized that σ_s and σ_m are proper functions of stress. Specifically, recalling Eq. (3.6) and (3.4b),

$$\sigma_m = \hat{\underset{\approx}{\mathbf{I}}}: \underset{\approx}{\boldsymbol{\sigma}} \quad \text{and} \quad \sigma_s = \sqrt{\underset{\approx}{\mathbf{S}}:\underset{\approx}{\mathbf{S}}}, \quad (4.8)$$

from which it follows that

$$\frac{d\sigma_m}{d\underset{\approx}{\boldsymbol{\sigma}}} = \hat{\underset{\approx}{\mathbf{I}}} \quad \text{and} \quad \frac{d\sigma_s}{d\underset{\approx}{\boldsymbol{\sigma}}} = \hat{\underset{\approx}{\mathbf{S}}}. \quad (4.9)$$

The yield surface is the boundary of elastic stress states, and it is a surface of constant $F^*(\underset{\approx}{\boldsymbol{\sigma}})$. Thus, for a given level of porosity and a given value for the state variable ζ , the outward unit normal to the yield surface must be proportional to the gradient of $F^*(\underset{\approx}{\boldsymbol{\sigma}})$ with respect to $\underset{\approx}{\boldsymbol{\sigma}}$. Applying the chain rule to Eq. (4.7), and recalling from Eq. (4.4) the definitions of F_m and F_s , we conclude that the stress gradient of the yield function is

$$\frac{\partial F}{\partial \underset{\approx}{\boldsymbol{\sigma}}} = F_m \hat{\underset{\approx}{\mathbf{I}}} + F_s \hat{\underset{\approx}{\mathbf{S}}}. \quad (4.10)$$

Thus, the outward *unit* normal to the yield surface is

$$\underset{\approx}{\mathbf{M}} = \frac{1}{\xi} [F_m \hat{\underset{\approx}{\mathbf{I}}} + F_s \hat{\underset{\approx}{\mathbf{S}}}], \quad (4.11)$$

where the proportionality constant ξ must be defined to ensure that $\underset{\approx}{\mathbf{M}}$ is a unit tensor; i.e.,

$$M_{ij}M_{ij} = 1. \quad (4.12)$$

Namely, ξ is just the magnitude of the yield function gradient:

$$\xi = \sqrt{F_m^2 + F_s^2}. \quad (4.13)$$

The simplicity of Eq. (4.10) is another motivation for favoring the isomorphic projected stress decomposition (Eq. 3.3) over the conventional decomposition in (Eq. 3.1). The projected decomposition is *isomorphic* to stress space, and the normal to the yield surface is therefore given by a simple (familiar looking) gradient expression. If the yield function had been phrased in terms of conventional pressure p and Von Mises stress σ^{VM} , then the normal to the yield surface in stress space would *not* be geometrically normal to the yield surface when drawn in σ^{VM} vs. p space. Using p and σ^{VM} would be like printing the σ_s vs. σ_m yield function (and its normal) on a rubber sheet and then stretching the sheet in one direction more than in the other — the yield surface would distort to a shape that's not isomorphic to stress space. Furthermore, the vector normal to the yield surface would distort such that it would no longer be normal to the yield surface in σ^{VM} vs. p space. Using p and σ^{VM} would entail adding awkward correction factors (metric coefficients) to account for this distortion. It's much easier to use σ_s and σ_m during the analysis, and then to simply convert the *final result* to the more conventional stress measures, p and σ^{VM} . See the end of Appendix C for further discussion on this topic.

5. Decomposition of the strain rate

The so-called “rate” of deformation $\underline{\underline{D}}$ is the symmetric part of the velocity gradient. That is,

$$D_{ij} = \frac{1}{2} \left(\frac{\partial v_i}{\partial x_j} + \frac{\partial v_j}{\partial x_i} \right), \quad (5.1)$$

where \underline{v} is the material velocity and \underline{x} is the spatial position vector. For small deformations, the rate of deformation is approximately equal to the logarithmic strain rate.*

The rate of deformation can be decomposed into an elastic part $\underline{\underline{d}}^e$, plus a plastic part $\underline{\underline{d}}^p$ attributable to plastic flow of the matrix material, plus a part $\underline{\underline{d}}^n$ from void nucleation, plus a part $\underline{\underline{d}}^t$ due to phase transformation:

$$\underline{\underline{D}} = \underline{\underline{d}}^e + \underline{\underline{d}}^p + \underline{\underline{d}}^n + \underline{\underline{d}}^t. \quad (5.2)$$

In our numerical implementation, we send an estimate for the local stress in the matrix material to an independent phase transformation utility that interrogates the phase diagram of the solid matrix material to compute the rate of transformation. Knowing the rate of transformation and the strain associated with transformation, we can then construct the transformation strain rate $\underline{\underline{d}}^t$. This task is performed *a priori* before ever calling the CKP model. We compute an *effective* strain rate tensor $\underline{\underline{d}}$ by

$$\underline{\underline{d}} \equiv \underline{\underline{D}} - \underline{\underline{d}}^t. \quad (5.3)$$

This effective strain rate may be regarded as the part of the strain rate that is not caused by phase transformation. Since $\underline{\underline{d}}^t$ can be computed in an uncoupled manner, the tensor $\underline{\underline{d}}$ henceforth will be treated *as though it were the total strain rate*.

* For arbitrarily large material distortions, the symmetric part of the velocity gradient can *not* be written as the material rate of *any* deformation-dependent tensor. Deformation “rate” is therefore a misnomer. (For this reason, Dienes [23] and others call it the “stretching,” though such a term fails to capture its rate-*like* behavior.) For problems involving large material rotations, we replace $\underline{\underline{D}}$ (and all other spatial tensors) by their unrotated counterparts in the polar reference configuration. For small material distortions, the unrotated $\underline{\underline{D}}$ is approximately equal to the unrotated logarithmic strain rate.

6. Linear-elastic relations

This section describes how the elastic strain rate $\underline{\underline{d}}^e$ is related to the stress rate. If pores have collapsed, then the current specific volume is *not* equal to the initial specific volume even if the pressure is zero. Elastic constitutive relations always refer to the stress-free state, not the initial state. Let v_z denote the (theoretical) specific volume that the material would return to if the stress were released everywhere in a small representative sample. In the absence of plastic dilatation, v_z would be simply the initial specific volume v_0 . However, permanent volume change results from phase transformation, pore collapse and/or nucleation. Thus, the unstressed reference volume v_z must be determined by integrating the inelastic part of the strain rate:

$$\frac{\dot{v}_z}{v_z} = \text{tr}(\underline{\underline{d}} - \underline{\underline{d}}^e). \quad (6.1)$$

The *total* specific volume is related to the total strain rate $\underline{\underline{d}}$ by the well-known kinematical equation [24]:

$$\frac{\dot{v}}{v} = \text{tr}\underline{\underline{d}}. \quad (6.2)$$

Keep in mind that we are now speaking of $\underline{\underline{d}}$ as if it were the total strain rate. If the material is simultaneously undergoing phase transformation, Eq. (6.2) actually represents the part of the volumetric strain rate *in excess* of any contributions from phase change. Similarly, Eq. (6.1) is the volumetric strain rate in excess of contributions from elastic deformation as well as from phase change. In other words, Eq. (6.1) represents the part of the volumetric strain rate due to irreversible void growth/collapse and from void nucleation.*

Recall that v_z is the specific volume in the zero-stress (zero-transformation) reference configuration. This configuration is the reference configuration for determining the stress. The conventional linear-elastic[†] constitutive law for pressure is:

$$p = -K \ln \frac{v}{v_z}. \quad (6.3)$$

In rate form, this linear-elastic relationship becomes

$$\dot{p} = -K \left(\frac{\dot{v}}{v} - \frac{\dot{v}_z}{v_z} \right) - \dot{K} \ln \frac{v}{v_z} = -K \left(\frac{\dot{v}}{v} - \frac{\dot{v}_z}{v_z} \right) + \frac{\dot{K}}{K} p, \quad (6.4)$$

* The volumetric strain rate from *reversible* void growth is contained implicitly within $\text{tr}\underline{\underline{d}}^e$, but this contribution is not computed in practice — from a modelling standpoint, only the irreversible void growth has an explicit effect on the stress calculation.

† This equation is obviously nonlinear with respect to v , but it is linear with respect to the logarithmic volumetric strain, $\ln(v/v_z)$.

or, using Eqs. (2.5b), (6.2), (6.1), and (5.2),

$$\dot{p} = -K \text{tr} \underline{\underline{\mathbf{d}}}^e - \kappa_m p \dot{\psi} + \dot{\Upsilon} p. \quad (6.5)$$

Phrasing the elasticity equation this way (such that v_z is removed) relieves us from having to actually solve Eq. (6.1) for the unstressed reference volume v_z .

Similarly, the rate of the stress deviator $\underline{\underline{\mathbf{S}}}$ may be written*

$$\dot{\underline{\underline{\mathbf{S}}}} = 2G \underline{\underline{\mathbf{d}}}^{e'} - \gamma_m \underline{\underline{\mathbf{S}}} \dot{\psi} + \dot{\Upsilon} \underline{\underline{\mathbf{S}}}. \quad (6.6)$$

Where $\underline{\underline{\mathbf{d}}}^{e'}$ is the deviatoric part of $\underline{\underline{\mathbf{d}}}^e$. The *total* stress rate is given by $\dot{\underline{\underline{\sigma}}} = -\dot{p} \underline{\underline{\mathbf{I}}} + \dot{\underline{\underline{\mathbf{S}}}}$. Thus,

$$\dot{\underline{\underline{\sigma}}} = (K \text{tr} \underline{\underline{\mathbf{d}}}^e + \kappa_m p \dot{\psi} - \dot{\Upsilon} p) \underline{\underline{\mathbf{I}}} + 2G \underline{\underline{\mathbf{d}}}^{e'} - \gamma_m \underline{\underline{\mathbf{S}}} \dot{\psi} + \dot{\Upsilon} \underline{\underline{\mathbf{S}}} \quad (6.7)$$

In terms of our alternative isomorphic projected stress decomposition defined in Eq. (3.3), the above elastic stress-strain relation may be written

$$\dot{\underline{\underline{\sigma}}} = \dot{\sigma}_m \hat{\underline{\underline{\mathbf{I}}}} + \dot{\sigma}_s \hat{\underline{\underline{\mathbf{S}}}} + \sigma_s \hat{\underline{\underline{\mathbf{S}}}}, \quad (6.8)$$

where

$$\dot{\sigma}_m = 3K \hat{\underline{\underline{\mathbf{I}}}} : \underline{\underline{\mathbf{d}}}^e - \kappa_m \sigma_m \dot{\psi} + \dot{\Upsilon} \sigma_m \quad (6.9a)$$

$$\dot{\sigma}_s = 2G \hat{\underline{\underline{\mathbf{S}}}} : \underline{\underline{\mathbf{d}}}^e - \gamma_m \sigma_s \dot{\psi} + \dot{\Upsilon} \sigma_s, \quad (6.9b)$$

and

$$\sigma_s \hat{\underline{\underline{\mathbf{S}}}} = 2G [\underline{\underline{\mathbf{d}}}^{e'} - \hat{\underline{\underline{\mathbf{S}}}} (\hat{\underline{\underline{\mathbf{S}}}} : \underline{\underline{\mathbf{d}}}^{e'})]. \quad (6.10)$$

By construction, Eq. (3.3) states that the stress $\underline{\underline{\sigma}}$ itself must lie in the Rendulic plane defined by the span of $\hat{\underline{\underline{\mathbf{I}}}}$ and $\hat{\underline{\underline{\mathbf{S}}}}$. However, the stress *rate* may contain a component that is perpendicular to the Rendulic plane. The first two terms in Eq. (6.8) lie in the Rendulic plane. However, by virtue of Eq. (3.9), the last term in Eq. (6.8) is the part of the stress rate that is perpendicular to the Rendulic plane. Geometrically, the operation in the brackets on the right-hand side of Eq. (6.10) projects the elastic strain rate deviator to its direction that is perpendicular to $\hat{\underline{\underline{\mathbf{S}}}}$.

* The apparent sign differences between Eqs. (6.5) and (6.6) are attributable to the fact that p is positive in compression whereas $\underline{\underline{\mathbf{S}}}$ is positive in tension. If p in Eq. (6.5) were replaced by the tensile mean stress $\bar{p} \equiv -p$, then there would be no structural difference between the signs.

7. Void nucleation

The applications of interest to us occur primarily in the compressive regime, so we do not *require* a void nucleation model. However, in anticipation of exceptional situations in which small regions of material are subjected to large tensile stress, we feel it is important to at least include some means for the material to lose strength by reintroducing porosity under high tensile loads. Furthermore, having a rudimentary nucleation model allows us to generate more reasonable stress strain curves when testing the CKP model under extreme strains. A much more acceptable modification (especially given that this model is being designed for application to ceramics as well as metals) would be to incorporate a fracture model. This activity is left to future work.

The rate of pore nucleation is assumed to be proportional to the amount by which the mean stress in the matrix material exceeds some user specified critical tensile value. The strain rate resulting from pore nucleation is assumed purely isotropic, so it must be expressible in the form

$$\underline{\underline{d}}^n = \dot{\delta}^n \hat{\underline{\underline{I}}} = \dot{\delta}^n \frac{\underline{\underline{I}}}{\sqrt{3}}, \quad (7.1)$$

where an approximation for $\dot{\delta}^n$ (which is the magnitude of $\underline{\underline{d}}^n$) is given below.

The hydrostatic stress in the matrix material is approximated by the macroscopic stress σ_m divided by the volume fraction $1 - f_v$ of the matrix material, $1 - f_v = 1/(1 + \psi)$. Hence, a very crude order-of-magnitude approximation of the hydrostatic elastic strain in the matrix material is

$$\varepsilon_m \approx \frac{\sigma_m(1 + \psi)}{K_m} \quad (7.2)$$

The volumetric strain “rate” $\dot{\varepsilon}^n \equiv \text{tr} \underline{\underline{d}}^n = \sqrt{3} \dot{\delta}^n$ due to void nucleation is taken to be zero until the matrix strain reaches a critical value ε_m^n . Thereafter, void nucleation is assumed to occur at a rate that is proportional to the amount by which the matrix strain exceeds the critical strain for nucleation:

$$\dot{\delta}^n = \dot{\alpha}^n \left[\text{MAX} \left(0, \frac{\varepsilon_m}{\varepsilon_m^n} - 1 \right) \right]. \quad (7.3)$$

The proportionality constant $\dot{\alpha}^n$ and the critical nucleation strain ε_m^n are treated as material constants. The “MAX” operation allows void nucleation only when the mean stress is tensile.

8. Trial “elastic” stress rate

The numerical implementation of our model does not use a conventional radial or oblique return algorithm. Nonetheless, our implementation *does* compute a trial stress rate in which we *tentatively* assume that the plastic part of the strain rate is zero. The tentative elastic strain rate is given by

$$\underline{\underline{\mathbf{d}}}^{e, \text{trial}} = \underline{\underline{\mathbf{d}}} - \underline{\underline{\mathbf{d}}}^n. \quad (8.1)$$

In this case, Eqs. (6.8) through (6.10) become

$$\dot{\underline{\underline{\sigma}}}^{\text{trial}} = \dot{\underline{\underline{\sigma}}}_m^{\text{trial}} \hat{\underline{\underline{\mathbf{I}}}} + \dot{\underline{\underline{\sigma}}}_s^{\text{trial}} \hat{\underline{\underline{\mathbf{S}}}} + \underline{\underline{\sigma}}_s \hat{\underline{\underline{\mathbf{S}}}}^{\text{trial}}, \quad (8.2)$$

where

$$\dot{\underline{\underline{\sigma}}}_m^{\text{trial}} = 3K \hat{\underline{\underline{\mathbf{I}}}} : \underline{\underline{\mathbf{d}}}^{e, \text{trial}} - \kappa_m \sigma_m \dot{\psi}^n + \dot{\Upsilon} \sigma_m \quad (8.3a)$$

$$\dot{\underline{\underline{\sigma}}}_s^{\text{trial}} = 2G \hat{\underline{\underline{\mathbf{S}}}} : \underline{\underline{\mathbf{d}}}^{e, \text{trial}} - \gamma_m \sigma_s \dot{\psi}^n + \dot{\Upsilon} \sigma_s, \quad (8.3b)$$

and

$$\underline{\underline{\sigma}}_s \hat{\underline{\underline{\mathbf{S}}}}^{\text{trial}} = 2G [\underline{\underline{\mathbf{d}}}^{e, \text{trial}} - \hat{\underline{\underline{\mathbf{S}}}}(\hat{\underline{\underline{\mathbf{S}}}} : \underline{\underline{\mathbf{d}}}^{e, \text{trial}})]. \quad (8.4)$$

Above, we have again noted that the unstressed reference porosity ψ remains unchanged when the plastic strain rate is zero (i.e., when the stress state is below yield), except for a possible contribution $\dot{\psi}^n$ from void nucleation. The tentative trial stress rate $\dot{\underline{\underline{\sigma}}}^{\text{trial}}$ is integrated to the end of the computational time step to obtain the trial stress $\underline{\underline{\sigma}}^{\text{trial}}$. If the trial stress does not fall outside the yield surface, then we know that the tentative assumption of elastic response was correct and $\underline{\underline{\sigma}}^{\text{trial}}$ must therefore be the *actual* updated stress. If $\underline{\underline{\sigma}}^{\text{trial}}$ is found to lie outside the yield surface, then we know that the tentative assumption of zero plastic flow was false and the full plasticity equations defined in the subsequent sections must be enforced. In our implementation, we check to see if the time step is actually an elastic interval followed by plastic response. The stress reaches the yield surface at

$$\underline{\underline{\sigma}}^{\text{yield}} = \underline{\underline{\sigma}}^{\text{old}} + \Delta t^e \dot{\underline{\underline{\sigma}}}^{\text{trial}}, \quad (8.5)$$

where Δt^e is the elastic part of the time step. Requiring that $\underline{\underline{\sigma}}^{\text{yield}}$ must be on the yield surface, we may write

$$F(\underline{\underline{\sigma}}^{\text{old}} + \Delta t^e \dot{\underline{\underline{\sigma}}}^{\text{trial}}, \psi^{\text{old}}, \zeta^{\text{old}}) = 0. \quad (8.6)$$

In our implementation, we use an iterative Newton scheme to solve the above equation for Δt^e (For more details, see “step 4” in Appendix D). We apply the full plasticity equations only after updating the state to the end of the elastic time step.

9. Plastic normality

Recall that $\underline{\underline{\mathbf{d}}}^p$ is the plastic strain rate resulting from ordinary plastic flow of the matrix material. Following conventional plasticity theory [25,11,26], the direction of the *plastic part* of the strain rate $\underline{\underline{\mathbf{d}}}^p$ is assumed to be given by a known plastic potential $\Lambda(\underline{\underline{\boldsymbol{\sigma}}}, \dots)$ such that

$$\underline{\underline{\mathbf{d}}}^p \propto \frac{\partial \Lambda}{\partial \underline{\underline{\boldsymbol{\sigma}}}} \quad (9.1)$$

For simplicity, this present version of the CKP model takes the plastic potential function to be identical to the yield function: $\Lambda = F$. Therefore, this version of the CKP model uses the plastic “associativity” assumption that the *plastic part* of the inelastic strain rate $\underline{\underline{\mathbf{d}}}^p$ is proportional to the yield surface normal $\underline{\underline{\mathbf{M}}}$ defined in Eq. (4.11). That is,

$$\underline{\underline{\mathbf{d}}}^p = \dot{\lambda} [F_m \hat{\underline{\underline{\mathbf{I}}}} + F_s \hat{\underline{\underline{\mathbf{S}}}}], \quad (9.2)$$

The proportionality constant $\dot{\lambda}$ is called the “plastic segment.” The plastic segment is not a true rate,* but it is nonetheless routinely written as a rate because it behaves in “rate-like” manner. As mentioned earlier, it is important that our innominate internal state variable(s) ζ and our porosity measure ψ be defined such that they are constant during elastic deformation. Otherwise, the outward normal would also contain contributions from F_ψ and F_ζ .

The plastic segment $\dot{\lambda}$ will be determined below by requiring that the stress state remain on the yield surface during any quasistatic interval of continued plastic deformation. Positivity of plastic work (*i.e.*, $\underline{\underline{\boldsymbol{\sigma}}}: \underline{\underline{\mathbf{d}}}^p > 0$) in combination with convexity of the yield surface demands that $\dot{\lambda}$ should be nonnegative. We will later show that this restriction has implications on admissible ways that the yield surface may evolve with plastic deformation.

Recall from Eq. (4.3) that the *magnitude* of the yield function gradient is $\xi \equiv \sqrt{F_m^2 + F_s^2}$. This intuitively appealing Euclidean expression for magnitude applies because of our isomorphic projection decomposition of the stress, in which $\hat{\underline{\underline{\mathbf{I}}}}$ and $\hat{\underline{\underline{\mathbf{S}}}}$ are *unit* base tensors. In terms of the outward *unit* normal to the yield surface, Eq. (9.2) may be written

$$\underline{\underline{\mathbf{d}}}^p = \xi \dot{\lambda} \underline{\underline{\mathbf{M}}}. \quad (9.3)$$

Since $\underline{\underline{\mathbf{M}}}$ is a unit tensor, we note for future reference that

$$\xi \dot{\lambda} = \underline{\underline{\mathbf{M}}}: \underline{\underline{\mathbf{d}}}^p. \quad (9.4)$$

* *i.e.*, there exists no path-independent state variable whose rate is $\dot{\lambda}$.

10. Hardening

Experimental observations of real material behavior often suggest that certain internal state variables evolve with the so-called equivalent plastic strain:*

$$\varepsilon_p^{\text{equiv}} \equiv \int_0^t \sqrt{\frac{2}{3} \underline{\underline{\mathbf{d}}}_p : \underline{\underline{\mathbf{d}}}_p} dt = \sqrt{\frac{2}{3}} \int_0^t \dot{\lambda} \xi dt . \quad (10.1)$$

For the present analysis, we will allow the rates of our (as yet) user-defined internal state variable(s) ζ to evolve *linearly* with the plastic strain. In other words, for each internal state variable ζ , we assume that there exists a second-order tensor $\underline{\underline{\mathbf{G}}}$ such that

$$\dot{\zeta} = \underline{\underline{\mathbf{G}}} : \underline{\underline{\mathbf{d}}}_p , \quad (10.2)$$

where $\underline{\underline{\mathbf{G}}}$ is a tensor constructed from physical arguments appropriate to the nature of the internal state variable.

Applying Eq. (9.3), the evolution equation of Eq. (10.2) may be written in the following equivalent form:

$$\dot{\zeta} = h \xi \dot{\lambda} , \quad \text{where } h \equiv \underline{\underline{\mathbf{G}}} : \underline{\underline{\mathbf{M}}} . \quad (10.3)$$

Later on, an evolution law of this form will be used to permit simple plastic hardening of the matrix material. For linear hardening, h would be a material constant. Power law hardening has been explored by Duva and Hutchinson [27].

One way to incorporate rate dependence is to allow the parameter ζ to *also* depend on the stress or strain rate, but this approach would make Eq. (10.2) nonlinear with respect to strain rates. Instead of adopting such an approach, we assume that the linear Eq. (10.2) holds for *quasistatic* loading, and we shall later use a straightforward overstress model (described on page 59) to superimpose strain rate dependence.

* Note that our definition of equivalent plastic strain uses the total plastic strain rate, not just its deviatoric part. Thus, our equivalent plastic strain includes contributions from the isotropic part of $\underline{\underline{\mathbf{d}}}_p$, as it should since that part corresponds to irreversible pore collapse from plastic flow of the matrix material.

11. Plastic consistency

Stress remains on/within the yield surface

Throughout any quasistatic interval of continued yielding, the stress must be on the yield surface *and remain on the yield surface*. Thus

$$F(\sigma_m, \sigma_s, \psi, \zeta) = 0 \quad \text{at yield, and} \quad (11.1a)$$

$$\boxed{F_m \dot{\sigma}_m + F_s \dot{\sigma}_s + F_\psi \dot{\psi} + F_\zeta \dot{\zeta} = 0} \quad \text{for continued yield.} \quad (11.1b)$$

Assuming that the yield function depends on only the pressure and shear stress invariants is inappropriate whenever the loading is significantly non-hydrostatic. *Realistically*, pore collapse in the presence of shear would cause a change in cavity shape from spherical to ellipsoidal, and the yield function would need to become anisotropic, depending on the actual stress components, not just the isotropic stress invariants. Including such behavior would tremendously complicate the present model. Future extensions of this model will address this very important issue of deformation-induced anisotropy.

Equation (11.1b) constrains $\dot{\sigma}_m$ and $\dot{\sigma}_s$, but it does not constrain the part of the stress rate that is perpendicular to the Rendulic plane. Consistency constrains only the *part* of the stress rate that lies in the same plane as the identity tensor and the stress itself. The rest of this section shows that the out-of-plane stress rate equals the out-of-plane part of the elastic trial stress rate.

NUMERICAL ISSUE: return algorithms in generality

The CKP model developed in this report falls under the general framework of hardening/softening plasticity, for which the governing equations (during intervals of continued inelastic deformation) are given in Appendix equations (C.1) through (C.4). Namely,

$$\underline{\underline{\mathbf{B}}}: \underline{\underline{\dot{\sigma}}} + \underline{\underline{\mathbf{G}}}: \underline{\underline{\mathbf{d}}}^i = 0 \quad (11.2)$$

$$\underline{\underline{\mathbf{D}}} = \underline{\underline{\mathbf{d}}}^e + \underline{\underline{\mathbf{d}}}^i \quad (11.3)$$

$$\underline{\underline{\mathbf{d}}}^i = \dot{\Gamma} \underline{\underline{\mathbf{m}}} \quad (11.4)$$

$$\underline{\underline{\dot{\sigma}}} = \underline{\underline{\mathbf{E}}}: \underline{\underline{\mathbf{d}}}^e, \quad (11.5)$$

In these equations, the following quantities are *usually* known:

$\underline{\underline{\mathbf{B}}}$, gradient of the yield function at the current state ($B_{ij} = \partial F / \partial \sigma_{ij}$), which is therefore normal to the yield surface.

$\underline{\underline{\mathbf{G}}}$, an internal state tensor that accounts for a change in the yield function. For the porous model, this tensor depends on the pore ratio and the hardening modulus of the matrix material.

$\underline{\underline{\mathbf{D}}}$, the total strain “rate.”

$\underline{\underline{\mathbf{E}}}$, the fourth-order elastic tangent stiffness tensor.

$\underline{\underline{\mathbf{m}}}$, the unit tensor in the direction of the $\underline{\underline{\mathbf{d}}^i}$ inelastic strain rate^{*}

The following quantities are unknown:

$\underline{\underline{\dot{\sigma}}}$, the rate of stress.

$\underline{\underline{\mathbf{d}}^e}$, the elastic part of the strain rate.

$\underline{\underline{\mathbf{d}}^i}$, the inelastic part of the strain rate.

(for the CKP model, $\underline{\underline{\mathbf{d}}^i} = \underline{\underline{\mathbf{d}}^p} + \underline{\underline{\mathbf{d}}^n} + \underline{\underline{\mathbf{d}}^t}$).

$\dot{\Gamma}$, the magnitude of the inelastic part of the strain rate.

The plastic consistency restriction of Eq. (11.2) says that the stress state must remain on the yield surface. Of course, the stress can move tangentially across the yield surface. For continued plastic yielding, the normal component of the stress rate must “keep up” with the expansion or contraction speed of the evolving yield surface.

Given the nature of our porous yield function, the normal to our yield surface — and therefore the tensor $\underline{\underline{\mathbf{B}}}$ — are in the Rendulic plane (i.e. the linear tensor subspace spanned by $\hat{\underline{\underline{\mathbf{I}}}}$ and $\hat{\underline{\underline{\mathbf{S}}}}$). Of course the stress tensor itself is also in this plane, but the stress *rate* might have a component out of this plane. The inner product $\underline{\underline{\mathbf{B}}}: \underline{\underline{\dot{\sigma}}}$ is independent of this out-of-plane component. Consequently, *the out-of-plane part of the stress rate is not restricted by the plastic consistency condition*. The out-of-plane stress rate is determined solely by the *elastic* trial stress rate, as we will now show in generality.

Substitution of Eqs. (11.3) and (11.4) into Eq. (11.5) reveals that

$$\underline{\underline{\dot{\sigma}}} = \underline{\underline{\mathbf{E}}}: \underline{\underline{\mathbf{D}}} - \dot{\Gamma} \underline{\underline{\mathbf{E}}}: \underline{\underline{\mathbf{m}}}. \quad (11.6)$$

Appendix C (or Ref. [28]) shows that the above equations may be solved by projecting the trial elastic stress rate back to the yield surface, where the projection direction must be parallel to $\underline{\underline{\mathbf{E}}}: \underline{\underline{\mathbf{m}}}$. This approach is especially appealing since it is numerically valid to second order even if part of the time step is purely elastic [29].

* For this general discussion, the inelastic strain rate is not necessarily restricted to be normal to the yield surface. We only require that its direction be *known*.

Avoidance of radial and oblique return methods

We elect to spurn the classical “return” method that computes a trial elastic stress and then (if it lies outside the yield surface) projects it back to the yield surface to obtain the updated stress. *Properly applied*, a return algorithm is a perfectly legitimate means of solving the governing equations of plasticity. Return methods are especially appealing because they remain second-order accurate even if the computational interval is partially elastic. However, the more esoteric features of our porosity model make determination of the *proper return direction* prohibitively complicated.

To be properly applied, the trial stress must be obliquely projected back to the yield surface along a direction parallel to $\underline{\underline{E}}:\underline{\underline{m}}$, where $\underline{\underline{m}}$ is a unit tensor in the direction of the inelastic strain rate $\underline{\underline{d}}^i$. One complicating factor for our porosity model is that the direction $\underline{\underline{m}}$ is *not* known *a priori*. The inelastic strain rate $\underline{\underline{d}}^i$ is a superposition of the plastic strain rate $\underline{\underline{d}}^p$ from plastic flow of the matrix material plus the nucleation strain rate $\underline{\underline{d}}^n$ plus the transformation strain rate $\underline{\underline{d}}^t$. From Eqs. (9.3) and (7.1), we do know the *individual* directions of $\underline{\underline{d}}^p$, $\underline{\underline{d}}^n$, and $\underline{\underline{d}}^t$. However, *we do not know the direction $\underline{\underline{m}}$ of their sum*. This situation precludes the use of a traditional radial or oblique return algorithm to solve the governing equations.

Even though we cannot use a traditional return algorithm for our model, the general structure of the governing equations is still revealing. For the present porosity model, we assume plastic normality. Therefore we know that $\underline{\underline{M}}$ lies in the Rendulic plane spanned by $\hat{\underline{\underline{I}}}$ and $\hat{\underline{\underline{S}}}$. Likewise, if we subtract away transformation strain rate before calling the CKP model, then we do know that $\underline{\underline{m}}$ also lies in the Rendulic plane. We also assume isotropic elasticity, making the second term on the right-hand-side of Eq. (11.6) in the Rendulic plane. The strain rate $\underline{\underline{D}}$ might have a component that is perpendicular to the Rendulic plane. Consequently, the part of the stress rate that is perpendicular to the Rendulic plane must equal the part of the trial *elastic* stress rate $\underline{\underline{E}}:\underline{\underline{D}}$ that is perpendicular to the plane. This result is re-derived below in the specific context of the porous model.

Out-of-plane stress rate

Plastic consistency demands that stress deviator *magnitude* and the pressure must be constrained to remain on or within the yield surface during any interval of quasistatic plastic loading. This condition alone leaves the change in the stress deviator *direction* $\hat{\underline{\underline{S}}}$ unconstrained. We reiterate in this section that, even though $\dot{\underline{\underline{S}}} \neq \dot{\underline{\underline{S}}}^{\text{trial}}$, it does turn out that $\dot{\underline{\underline{S}}} = \dot{\underline{\underline{S}}}^{\text{trial}}$. In other words, the part of the stress rate that is perpendicular to the Rendulic plane must be identical to the part of the *trial elastic stress rate* that is perpendicular to the Rendulic plane defined by the span of $\hat{\underline{\underline{I}}}$ and $\hat{\underline{\underline{S}}}$. The rate $\dot{\underline{\underline{S}}}$ has a zero inner product with both $\hat{\underline{\underline{I}}}$ and $\hat{\underline{\underline{S}}}$.

Note from Eq. (9.2) that $\underline{\underline{d}}^p$ is a linear combination of $\hat{\underline{\underline{I}}}$ and $\hat{\underline{\underline{S}}}$. Therefore $\underline{\underline{d}}^{p'}$ must be parallel to $\hat{\underline{\underline{S}}}$. Hence, the part of $\underline{\underline{d}}^{p'}$ that is perpendicular to $\hat{\underline{\underline{S}}}$ must be zero. Stated mathematically,

$$\underline{\underline{d}}^{p'} - \hat{\underline{\underline{S}}}(\hat{\underline{\underline{S}}}:\underline{\underline{d}}^{p'}) = \underline{\underline{0}}, \quad (11.7)$$

Recall that $\underline{\underline{d}}^e = \underline{\underline{d}} - \underline{\underline{d}}^n - \underline{\underline{d}}^p$, or

$$\underline{\underline{d}}^e = \underline{\underline{d}}^{e, \text{trial}} - \underline{\underline{d}}^p. \quad (11.8)$$

Using Eq. (11.7) we note that

$$\underline{\underline{d}}^{e'} - \hat{\underline{\underline{S}}}(\hat{\underline{\underline{S}}}:\underline{\underline{d}}^{e'}) = \underline{\underline{d}}^{e', \text{trial}} - \hat{\underline{\underline{S}}}(\hat{\underline{\underline{S}}}:\underline{\underline{d}}^{e', \text{trial}}). \quad (11.9)$$

Thus, Eq. (6.10) becomes

$$\boxed{\sigma_s \dot{\underline{\underline{S}}} = \sigma_s \dot{\underline{\underline{S}}}^{\text{trial}}}. \quad (11.10)$$

This is the expression for the out-of-plane stress rate. Namely, the part of the actual stress rate that is perpendicular to both $\hat{\underline{\underline{I}}}$ and $\hat{\underline{\underline{S}}}$ is given by the part of the *elastic trial stress rate* that is perpendicular to both $\hat{\underline{\underline{I}}}$ and $\hat{\underline{\underline{S}}}$. This result is intuitively appealing since this part of the stress rate does no plastic work.

Thus, through slightly different arguments, we again arrive at the conclusion of Eq. (6.8). Namely,

$$\dot{\underline{\underline{\sigma}}} = \dot{\sigma}_m \hat{\underline{\underline{I}}} + \dot{\sigma}_s \hat{\underline{\underline{S}}} + \sigma_s \dot{\underline{\underline{S}}}, \quad (11.11)$$

where, recalling Eqs. (6.9) and (6.10)

$$\dot{\sigma}_m = 3K \underline{\underline{d}}^e : \hat{\underline{\underline{I}}} - \kappa_m \sigma_m \dot{\psi} + \dot{\Upsilon} \sigma_m \quad (11.12a)$$

$$\dot{\sigma}_s = 2G \underline{\underline{d}}^e : \hat{\underline{\underline{S}}} - \gamma_m \sigma_s \dot{\psi} + \dot{\Upsilon} \sigma_s \quad (11.12b)$$

$$\sigma_s \dot{\hat{\mathbf{S}}} = \sigma_s \dot{\hat{\mathbf{S}}}^{\text{trial}} = 2G[\hat{\mathbf{d}}^{e\text{trial}} - \hat{\mathbf{S}}(\hat{\mathbf{S}}:\hat{\mathbf{d}}^{e\text{trial}})]. \quad (11.12c)$$

Recall that $\hat{\mathbf{d}}^e = \hat{\mathbf{d}} - \hat{\mathbf{d}}^p - \hat{\mathbf{d}}^n$. Equation (9.2) shows that $\hat{\mathbf{d}}^p:\hat{\mathbf{I}} = F_m \hat{\lambda}$ and $\hat{\mathbf{d}}^p:\hat{\mathbf{S}} = F_s \hat{\lambda}$. Furthermore, Equation (7.1) shows that $\hat{\mathbf{d}}^n:\hat{\mathbf{I}} = \hat{\delta}^n$ and $\hat{\mathbf{d}}^n:\hat{\mathbf{S}} = 0$. Hence Eqs. (11.12) become:

$$\dot{\sigma}_m = 3K(\hat{\mathbf{d}}:\hat{\mathbf{I}} - F_m \hat{\lambda} - \hat{\delta}^n) - \kappa_m \sigma_m \dot{\psi} + \dot{\Upsilon} \sigma_m \quad (11.13a)$$

$$\dot{\sigma}_s = 2G(\hat{\mathbf{d}}:\hat{\mathbf{S}} - F_s \hat{\lambda}) - \gamma_m \sigma_s \dot{\psi} + \dot{\Upsilon} \sigma_s. \quad (11.13b)$$

$$\sigma_s \dot{\hat{\mathbf{S}}} = 2G[\hat{\mathbf{d}}' - \hat{\mathbf{S}}(\hat{\mathbf{S}}:\hat{\mathbf{d}}')]. \quad (11.13c)$$

The above boxed equations are our two key equations governing the isomorphic stress rates and the rate of the stress that is perpendicular to the Rendulic plane. For the last of these equations, we have noted that Eq. (7.1) shows that the deviatoric part of $\hat{\mathbf{d}}^n$ is zero and therefore, from Eq. (8.1), we note that $\hat{\mathbf{d}}^{e\text{trial}} = \hat{\mathbf{d}}'$. The operation in brackets in Eq. (11.13c) extracts the part of the strain rate that is perpendicular to both $\hat{\mathbf{S}}$ and $\hat{\mathbf{I}}$.

NUMERICAL ISSUE: Integrating the rate of a unit tensor

The reader may skip this section without loss in continuity of later sections. Equation (11.13c) gives the time rate of the unit tensor $\hat{\mathbf{S}}$. As illustrated in Fig. 11.1, a first-order finite difference integration, $\hat{\mathbf{S}}^{\text{new}} = \hat{\mathbf{S}}^{\text{old}} + \hat{\mathbf{S}} \Delta t$, will not result in a unit tensor for $\hat{\mathbf{S}}^{\text{new}}$.

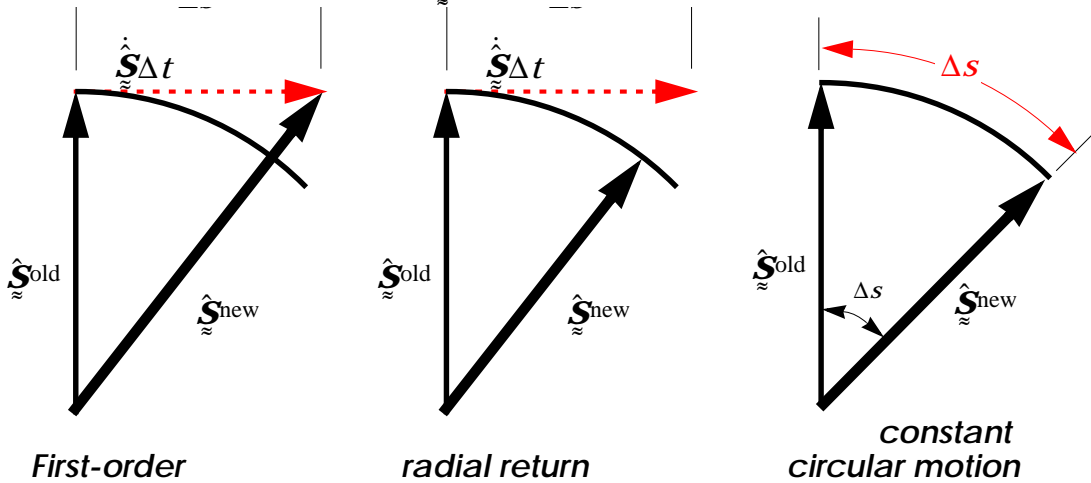


Figure 11.1. Finite difference error in updating unit tensor. First-order results in a non-unit tensor. The radial return solution merely reduces the magnitude of the first-order solution to obtain a unit tensor. The solution for a constant angular speed is shown at the far right. The angle equals the arc length Δs because the circle is of unit radius.

Conventional radial return algorithms automatically compensate for this unacceptable first-order error by simply scaling down the magnitude of the forward difference solution to obtain:

$$\hat{\underline{\underline{\mathbf{S}}}}^{\text{new}} = \alpha[\hat{\underline{\underline{\mathbf{S}}}}^{\text{old}} + \hat{\underline{\underline{\mathbf{S}}}}\Delta t], \quad \leftarrow \text{radial return} \quad (11.14)$$

where the coefficient α is set to ensure that $\hat{\underline{\underline{\mathbf{S}}}}^{\text{new}}$ is a unit tensor. Specifically,

$$\alpha = \frac{1}{\sqrt{1 + (\Delta s)^2}}, \text{ where } \Delta s \equiv \left\| \hat{\underline{\underline{\mathbf{S}}}}\Delta t \right\|. \quad (11.15)$$

The order of accuracy of this approach cannot be assessed unless the exact solution is known. For constant strain rates, Wilkens [29] demonstrated that radial return is a second-order accurate method for numerically solving *classical* nonhardening von Mises plasticity equations, which is a situation that is structurally equivalent to our task of integrating the rate of a unit tensor. If the strain rate is constant, then the angular speed of $\hat{\underline{\underline{\mathbf{S}}}}$ decreases with time. Knowledge of the angular speed of $\hat{\underline{\underline{\mathbf{S}}}}$ is necessary to evaluate the order of accuracy of the finite difference solution for $\hat{\underline{\underline{\mathbf{S}}}}^{\text{new}}$. All three of the finite difference solutions sketched in Fig. 11.1 are expressible in the following form:

$$\hat{\underline{\underline{\mathbf{S}}}}^{\text{new}} = a\hat{\underline{\underline{\mathbf{S}}}}^{\text{old}} + b\hat{\underline{\underline{\mathbf{S}}}}\Delta t. \quad \leftarrow \text{constant angular speed} \quad (11.16)$$

The coefficients a and b are selected according to the preferred finite difference rule. Specifically,

$$a = b = 1 \text{ for first-order (left side of Fig. 11.1)} \quad (11.17)$$

$$a = b = \frac{1}{\sqrt{1 + (\Delta s)^2}} \text{ for radial return (middle of Fig. 11.1)} \quad (11.18)$$

$$a = \cos(\Delta s) \quad \text{and} \quad b = \frac{\sin(\Delta s)}{\Delta s} \text{ for constant angular speed}^* \quad (11.19)$$

(this solution is shown on the far right side of Fig. 11.1)

As mentioned earlier, engineering codes typically seek an updated stress under the assumption that the applied strain rate is constant over the time step. Naturally, if the strain rate is constant, then the angular speed of $\hat{\underline{\underline{\mathbf{S}}}}$ decreases with time, so Eq. (11.19) would be an unwise choice. In the limit of extremely long time steps, or extremely fast strain rates, the angular location of $\hat{\underline{\underline{\mathbf{S}}}}$ should never spin around by any more than 90° under constant strain

* These coefficients are determined by the restrictions $\hat{\underline{\underline{\mathbf{S}}}}^{\text{new}} \cdot \hat{\underline{\underline{\mathbf{S}}}}^{\text{new}} = 1$ and $\hat{\underline{\underline{\mathbf{S}}}}^{\text{old}} \cdot \hat{\underline{\underline{\mathbf{S}}}}^{\text{new}} = \cos(\Delta s)$.

rate conditions (contrast this with constant angular rate conditions, where the angle of rotation can be arbitrarily large). Suppose that the rate $\dot{\hat{\mathbf{S}}}^{\text{old}}$ at the beginning of the step is regarded as a constant strain rate. Since the stress rate must move tangentially along the yield surface, we can then approximate the motion of $\hat{\mathbf{S}}$ by the following differential equation:

$$\begin{aligned} \dot{\hat{\mathbf{S}}} &= \hat{\mathbf{C}} - \hat{\mathbf{S}}(\hat{\mathbf{S}}:\hat{\mathbf{C}}) \text{ subject to } \hat{\mathbf{S}} = \hat{\mathbf{S}}^{\text{old}} \text{ when } t = t^{\text{old}}, \\ \text{where } \hat{\mathbf{C}} &\text{ is a constant tensor such that } \hat{\mathbf{C}}:\hat{\mathbf{S}}^{\text{old}} = 0, \\ \text{and therefore } \hat{\mathbf{C}} &= \dot{\hat{\mathbf{S}}}^{\text{old}} \end{aligned} \quad (11.20)$$

The exact solution to the above equation, evaluated at $t^{\text{new}} = t^{\text{old}} + \Delta t$ is

$$\begin{aligned} \hat{\mathbf{S}}^{\text{new}} &= a\hat{\mathbf{S}}^{\text{old}} + b\dot{\hat{\mathbf{S}}}\Delta t, \\ \text{where } a &= \frac{1}{\cosh(\Delta s)}, \text{ and } b = \frac{\tanh(\Delta s)}{\Delta s} \\ \text{for "constant strain rate"} \end{aligned} \quad (11.21)$$

Similar to Eq. (11.14), these alternative coefficients prevent the new deviator direction from differing from the old one by any more than 90° . Comparisons of the $\{a, b\}$ coefficients for different presumed exact solutions are shown in Fig. 11.2. Again we emphasize that the order of accuracy of the difference method cannot be assessed unless the exact solution is known. If the angular speed is constant, then Eq. (11.19) will be exactly correct. However, if the applied strain rate is constant, then Eq. (11.18) or Eq. (11.21) will give a much higher-order accurate result.

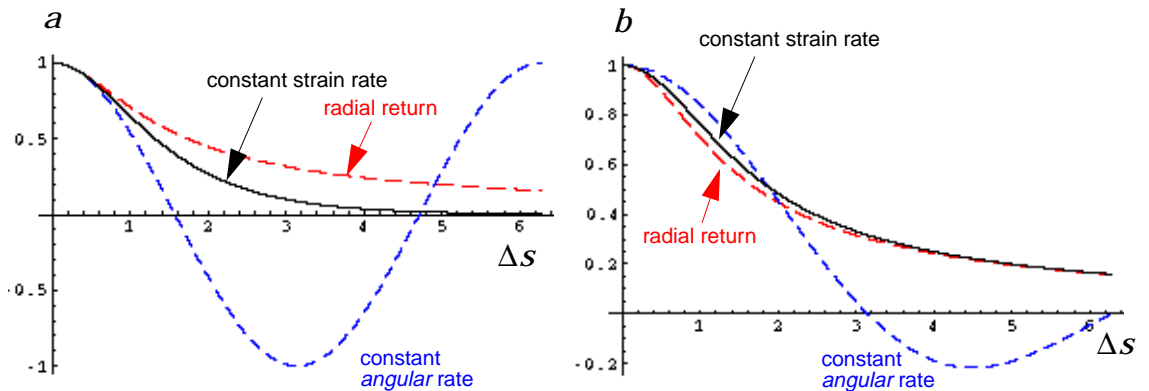


Figure 11.2. Comparison of finite difference coefficients. The “best” choices for the $\{a, b\}$ coefficients depends on the exact solution. These plots show the appropriate choices for three different assumed exact solutions. The choices coincide in the limit of small time steps.

Even though we have not yet finished the derivation of the complete set of governing equations for the CKP model, now is an appropriate time to show a verification calculation that was performed using the completed numerical implementation of the CKP model. This verification problem was designed to test if the CKP algorithm would properly follow along the yield surface in deviatoric space even for grossly large time steps. Using zero porosity and zero hardening, Fig. 11.3 shows the CKP model's prediction under two significant changes in straining directions. The model performs in the desired manner.

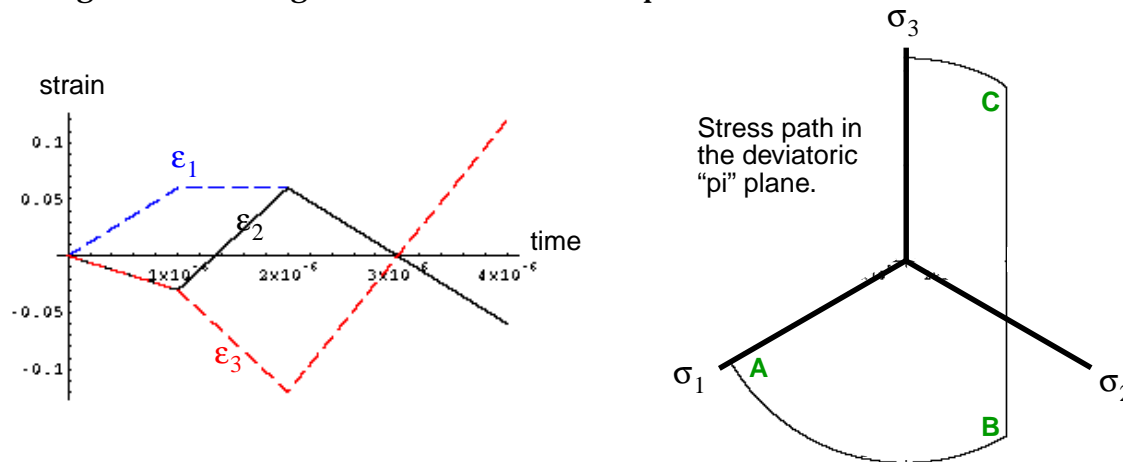


Figure 11.3. A CKP verification calculation for changes in strain rate direction. This zero porosity test first applied a strain rate proportional to $\text{DIAG}[1, -1/2, -1/2]$, so the stress satisfied $\sigma_2 = \sigma_3$, eventually inducing continued yield at point **A**. Then the strain rate was changed to become proportional to $\text{DIAG}[0, 1, -1]$, which was perpendicular to the initial strain rate and therefore caused the stress to travel tangentially along the yield surface. Holding this strain rate long enough forced the stress state at point **B** to eventually become perpendicular to the stress state at point **A**. The strain rate was then made proportional to $\text{DIAG}[-1/2, -1/2, 1]$, which caused the stress to move elastically within the interior of the yield surface until eventually yielding at point **B**. Continued strain in the same direction caused the stress to move along the yield surface toward the point where $\sigma_1 = \sigma_2$.

NUMERICAL ISSUE: Third-order stress corrections.

In the limit of an infinitely small time step, the CKP plasticity equations always give a stress state at or below yield. However, for numerical implementations, a finite time step might allow the predicted stress state to lie *very* slightly outside the yield surface. Left uncorrected, we *originally* felt that this situation might lead to cumulative errors in the predictions because the material response for a state at yield is significantly different from a state slightly below yield. Since the present model uses only the first-order yield function derivatives, we were concerned that slight errors in placing the stress on the yield surface might accumulate unless corrected. We explain our return method here for completeness, even though numerical experiments revealed that improvements in the results were virtually unnoticeable.

The *test* stress $\underline{\underline{\sigma}}^T$ is the stress found by breaking the time step into two phases: the elastic phase that takes the stress to the yield surface, and then the plastic phase that moves the stress along the yield surface. In contrast to the trial stress $\underline{\underline{\sigma}}^{\text{trial}}$, the test stress is always very close to the yield surface. For classical return methods, the stress which is projected back to the yield surface is the *elastic trial stress* $\underline{\underline{\sigma}}^{\text{trial}}$, which might lie extremely far outside the yield surface, making the return direction crucial. In our situation, we have already integrated the plastic governing equations to obtain a second-order accurate *test* solution $\underline{\underline{\sigma}}^T$ for the *actual final stress*. Hence, our test stress $\{\sigma_m^T, \sigma_s^T\}$ is already extremely close to the yield surface. Small finite difference errors (caused by yield surface curvature) might cause this test state to lie slightly outside the yield surface, so we simply reduce this third-order error by adjusting the final stress state according to the following normal projection:

$$\sigma_m^{\hat{\underline{\underline{\sigma}}}} + \sigma_s^{\hat{\underline{\underline{\sigma}}}} = \sigma_m^T \hat{\underline{\underline{\mathbf{I}}}} + \sigma_s^T \hat{\underline{\underline{\mathbf{S}}}} - \mu \underline{\underline{\mathbf{M}}}, \quad (11.22)$$

where $\underline{\underline{\mathbf{M}}}$ is the yield surface normal defined in Eq. (4.11) and μ is selected to make $\{\sigma_m^{\hat{\underline{\underline{\sigma}}}}, \sigma_s^{\hat{\underline{\underline{\sigma}}}}\}$ lie exactly on the yield surface. That is, μ is selected so that

$$F\left(\sigma_m^T - \mu \frac{F_m}{\xi}, \sigma_s^T - \mu \frac{F_s}{\xi}, \psi, \varsigma\right) = 0. \quad (11.23)$$

The appropriate value of μ may be found via Newton-Raphson iteration. Recalling Eq. (4.13), and taking $\mu = 0$ as a first guess, an improved estimate for μ is given via a Newton-Raphson iteration as

$$\mu = \frac{F(\sigma_m^T, \sigma_s^T, \psi, \varsigma)}{\xi}. \quad (11.24)$$

Thus, improved estimates for the actual mean and shear stresses are

$$\sigma_m = \sigma_m^T - \left[\frac{F^T}{\xi^2}\right] F_m^T \quad \text{and} \quad \sigma_s = \sigma_s^T - \left[\frac{F^T}{\xi^2}\right] F_s^T, \quad (11.25)$$

where the superscript ‘‘T’’ indicates that the functions are to be evaluated at the test state. These expressions may be used to iteratively place the final stress state on the yield surface.

Numerical experiments have revealed that bothering to place the stress exactly on the yield surface leads to no perceptible difference in the final results because our plastic stress is already extremely close to the yield surface. The procedure does, however, improve the convergence rate of the iterations that determine what fraction of the time step is elastic.

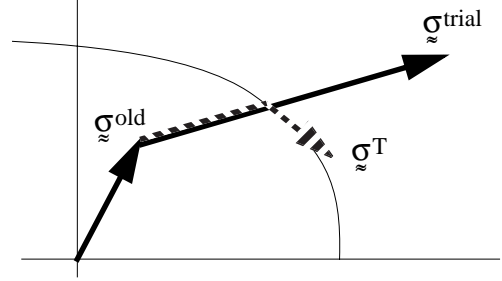


Figure 11.4. Distinction between trial stress and test stress. The trial stress generally falls far outside the yield surface, whereas the test stress is always quite close to the yield surface.

12. Plastically incompressible matrix

Recall that the yield function depends on porosity. Thus, there is a family of different yield surfaces, depending on the current value of porosity. In this sense, porosity is an internal state variable. In this section, we derive the exact evolution law governing the porosity under the assumption of a *plastically incompressible matrix material*.

We will assume that *permanent* dilatation of the matrix material is zero. Then permanent volume change must be attributable exclusively to changes in porosity. It can be shown [30, 22] that the rate of the pore volume fraction f_v must therefore be related to the inelastic strain rate by

$$\dot{f}_v = (1 - f_v)\text{tr}(\underline{\underline{\mathbf{d}}}^p + \underline{\underline{\mathbf{d}}}^n). \quad (12.1)$$

Recalling that $f_v = \psi/(1 + \psi)$, this may be written

$$\dot{\psi} = (1 + \psi)\text{tr}(\underline{\underline{\mathbf{d}}}^p + \underline{\underline{\mathbf{d}}}^n) = \sqrt{3}(1 + \psi)\hat{\underline{\underline{\mathbf{I}}}}:(\underline{\underline{\mathbf{d}}}^p + \underline{\underline{\mathbf{d}}}^n), \quad (12.2)$$

or, using Eqs. (9.2), (7.1), and (7.3),

$$\dot{\psi} = \dot{\psi}^p + \dot{\psi}^n,$$

where $\dot{\psi}^p \equiv \sqrt{3}(1 + \psi)F_m\dot{\lambda}$

$$\text{and } \dot{\psi}^n = \sqrt{3}(1 + \psi)\dot{\delta}^n = \text{MAX}\left[0, \sqrt{3}(1 + \psi)\dot{\alpha}^n\left(\frac{\sigma_m(1 + \psi)}{\varepsilon_m^n K_m} - 1\right)\right] \quad (12.3)$$

Physically, $\dot{\psi}^p$ is the rate of the pore ratio due to plastic flow of the matrix material and the concomitant collapse or growth of existing voids; $\dot{\psi}^n$ is the rate of the pore ratio due to pore nucleation.

Recalling that $\dot{\lambda}$ is positive, $\dot{\psi}^p$ shares the same sign as F_m . The derivative F_m typically shares the same sign with σ_m . Thus, existing pores will grow under tension and collapse under compression, as expected intuitively.

Equation (9.2) shows that $F_m\dot{\lambda} = \hat{\underline{\underline{\mathbf{I}}}}:\underline{\underline{\mathbf{d}}}^p$, permitting the expression for $\dot{\psi}^p$ in Eq. (12.3) to be written $\dot{\psi}^p = \underline{\underline{\mathbf{G}}}\cdot\underline{\underline{\mathbf{d}}}^p$, where $\underline{\underline{\mathbf{G}}} \equiv \sqrt{3}(1 + \psi)\hat{\underline{\underline{\mathbf{I}}}}$. Consequently, in the absence of nucleation, the pore ratio is an internal state variable of the generalized class discussed in Section 10.

13. Advanced/superposed model features

The basic QCKP model is quasistatic

The equations presented thus far form what we call the QCKP model, where the “Q” stands for quasistatic. The model is called “consistent” because consistency of the yield condition is rigorously enforced — an interval of continued yielding corresponds to a stress state that is both on the yield surface ($F=0$) and remains on the yield surface ($\dot{F}=0$). The resulting rate forms of the governing equations are *linear* in the rates and may therefore be solved analytically, which is the purpose of next section. Once the rates of all the state variables are known, they may be integrated via finite difference to update the equilibrium state to the end of a numerical time step.

An overstress model permits rate dependence

Linearity of the governing equations essentially implies that the QCKP equations are rate independent. Our actual implementation of the CKP model includes additional advanced features that are incorporated “on top” of QCKP. To allow for rate dependence, our implementation includes an overstress model (described on page 59) in which the actual stress state is permitted to lie off the yield surface. The stress state is attracted back to an “equilibrium” stress state at a rate that is proportional to the distance between them. The “equilibrium” stress is computed using QCKP. Details of the rate-dependent overstress model are given later in Section 18.

Phase transformation strain is handled externally

Our implementation of the CKP model includes phase transformation as discussed on page 22. In the presence of transformation strain, the strain rate $\underline{\underline{d}}$ sent to the QCKP subroutines is actually the total strain rate *minus* the contribution from transformation. This computation of the effective strain rate is performed by the host code before calling the CKP routines, so it is properly regarded as a superposed feature.

Principle of material frame indifference

Finally, our implementation of the CKP model is guaranteed to be frame indifferent by solving the governing equations in the unrotated reference frame. Instead of sending the stress $\underline{\underline{\sigma}}$ when we call the CKP model, we actually send the unrotated stress $\underline{\underline{R}}^T \cdot \underline{\underline{\sigma}} \cdot \underline{\underline{R}}$. Likewise, the rate of deformation $\underline{\underline{d}}$ (i.e., the symmetric part of the velocity gradient) is actually the *unrotated* rate of deformation $\underline{\underline{R}}^T \cdot \underline{\underline{d}} \cdot \underline{\underline{R}}$. Upon return from the CKP subroutines, the updated state is rotated back to the spatial configuration. This approach merely ensures frame indifference; small distortions are still assumed [31].

14. Exact solution of the QCKP equations

The boxed equations of the preceding sections are all in rate form. For our numerical implementation, we assume that the material state variables (i.e., the non-rate quantities) are known at the beginning of a time step. We wish to solve the QCKP rate equations to obtain the rate of change of the (equilibrium) material state so that it may be updated to the end of the step.

For our numerical implementation, we assume that the following quantities or functions are *known* or can be readily computed at the beginning of the time step (see the nomenclature Appendix H for definitions of the symbols):

- The effective total strain rate $\underline{\underline{d}}$ obtained within the host code by subtracting the (presumably known) transformation strain rate $\underline{\underline{d}}^t$ from the actual strain rate $\underline{\underline{D}}$. That is, $\underline{\underline{d}} = \underline{\underline{D}} - \underline{\underline{d}}^t$.
- The quantity $\dot{\gamma}$ that equals the normalized rate of the *matrix* moduli. Namely, $\dot{\gamma} = \dot{K}_m/K_m = \dot{G}_m/G_m$. This assumes that $\dot{v}_m=0$.
- The current value of the pore ratio ψ .
- The bulk modulus K and shear modulus G , obtained by applying Eq. (2.1) using the current porosity at the beginning of the step.
- The yield function F and its derivatives, (F_m , F_s , F_ψ and F_ζ) evaluated at the current state as defined in Eqs. (4.1) and (4.4). Ideally, these functions are written by the user. However, a default yield function is supplied with the CKP model, as discussed in Sections 16 and 19.
- The magnitude of the yield function gradient ξ computed using Eq. (4.13).
- The pore nucleation rate $\dot{\psi}^n$ computed by applying Eq. (12.3) at the beginning of the step.
- The hardening modulus h of Eq. (10.3), which is a user input constant.

The following rate quantities are the unknowns:

- $\dot{\sigma}_m$, the rate of the isomorphic projected mean stress.
- $\dot{\sigma}_s$, the rate of the isomorphic projected effective shear stress.
- $\dot{\psi}$, the rate of the pore ratio.
- $\dot{\lambda}$, the plastic segment defined in Eq. (9.2).
- $\dot{\zeta}$, the rate of the internal state variable(s).

Eqs. (10.3), (12.3), (11.1b), (11.13a), and (11.13b) form a set of five equations for five unknowns, $\{\dot{\sigma}_m, \dot{\sigma}_s, \dot{\psi}, \dot{\lambda}, \dot{\zeta}\}$. Appendix A gives details on how these equations may be solved for $\dot{\lambda}$ to obtain the key result:

$$\dot{\lambda} = \frac{\sqrt{3}KF_m \text{tr} \underline{\underline{d}}^{\text{ep}} + 2GF_s \underline{\underline{d}} : \underline{\underline{S}} + \dot{\psi}^n (F_\psi - \kappa_m \sigma_m F_m - \gamma_m \sigma_s F_s) + \dot{\gamma} (F_m \sigma_m + F_s \sigma_s)}{3KF_m^2 + 2GF_s^2 + \sqrt{3}(1+\psi)F_m(\kappa_m \sigma_m F_m + \gamma_m \sigma_s F_s - F_\psi) - h\xi F_\zeta}, \quad (14.1)$$

where

$$\underline{\underline{d}}^{\text{ep}} \equiv \underline{\underline{d}} - \underline{\underline{d}}^n = \underline{\underline{d}} - \dot{\delta}^n \underline{\underline{I}}. \quad (14.2)$$

Once $\dot{\lambda}$ is known, the innominate internal state variable ζ (which is the matrix yield stress in our implementation) is updated by integrating

$$\dot{\zeta} = h\xi\dot{\lambda}. \quad (14.3)$$

Eq. (12.3) gives the rate of the pore ratio ψ as

$$\begin{aligned} \dot{\psi} &= \sqrt{3}(1 + \psi)F_m\dot{\lambda} + \dot{\psi}^n, \\ \text{where } \dot{\psi}^n &= \sqrt{3}(1 + \psi)\dot{\delta}^n = \alpha^N \left[\text{MAX} \left(0, \frac{\sigma_m}{\varepsilon^N K_m} - (1 + \psi) \right) \right]. \end{aligned} \quad (14.4)$$

Then Eqs. (11.13) may be used to compute the stress rate as follows:

$$\dot{\sigma}_m = 3K(\underline{\underline{\mathbf{d}}}: \hat{\underline{\underline{\mathbf{I}}}} - F_m\dot{\lambda} - \dot{\delta}^n) - \kappa_m\sigma_m\dot{\psi} + \dot{\gamma}\sigma_m \quad (14.5)$$

$$\dot{\sigma}_s = 2G(\underline{\underline{\mathbf{d}}}: \hat{\underline{\underline{\mathbf{S}}}} - F_s\dot{\lambda}) - \gamma_m\sigma_s\dot{\psi} + \dot{\gamma}\sigma_s. \quad (14.6)$$

The updated value of $\hat{\underline{\underline{\mathbf{S}}}}$ is found by applying the methods described on page 33 to integrate $\hat{\underline{\underline{\mathbf{S}}}}^{\text{trial}}$, which is given in Eq. (11.13c) as*

$$\sigma_s \hat{\underline{\underline{\mathbf{S}}}} = 2G[\underline{\underline{\mathbf{d}}}^{\text{ep}'} - \hat{\underline{\underline{\mathbf{S}}}}(\hat{\underline{\underline{\mathbf{S}}}}: \underline{\underline{\mathbf{d}}}^{\text{ep}'})], \quad (14.7)$$

where we have noted from Eq. (14.2) that $\underline{\underline{\mathbf{d}}}^{\text{ep}'} = \underline{\underline{\mathbf{d}}}'$.

The updated stress tensor is constructed by applying Eq. (3.3):

$$\underline{\underline{\sigma}} = \sigma_m \hat{\underline{\underline{\mathbf{I}}}} + \sigma_s \hat{\underline{\underline{\mathbf{S}}}}. \quad (14.8)$$

A step-by-step algorithm for the solution of the QCKP equations is provided in Appendix D.

* If $\sigma_s^{\text{old}}=0$, then $\hat{\underline{\underline{\mathbf{S}}}}^{\text{old}}$ is arbitrary, so we take it to be in the same direction as the *impending* stress deviator, as determined by the direction of the strain rate. If the strain rate is zero, then $\hat{\underline{\underline{\mathbf{S}}}}^{\text{trial}}$ may be taken to be zero without loss. This is true because, no matter what value we assign to the updated $\hat{\underline{\underline{\mathbf{S}}}}$, the product $\sigma_s \hat{\underline{\underline{\mathbf{S}}}}$ in Eq. (14.8) will be zero.

15. Limiting Cases

Whenever a complicated model like QCKP is developed in extreme generality, it makes sense to examine the model under specialized canonical situations to verify that it reduces to expected results known for simpler models. Limiting case #1 demonstrates that the above general model reduces to a classical p - α type model when the deformation is purely isotropic. Limiting case #2 on page 48 shows that the QCKP model gives Von-Mises type yield behavior under simple shear with a pressure-independent yield surface.

Limiting case #1: Conventional p - α model

Early research [8] on porous media assumed the existence of a p - α curve, where p was the pressure and α was the so-called distention, which is related to our pore ratio by $\alpha = \psi + 1$. In this early work, pore collapse was thought to commence at a critical pressure p^{crit} . As pores crushed out, the value of this critical pressure would increase. The p - α curve was just a plot of this critical pressure versus the distention. Our model generalizes these ideas because, instead of a p - α function, we have a yield function. Our model permits shear stress to accelerate the onset of pore collapse. Naturally, however, if we apply our model under the special case of purely isotropic (shear-free) loading, then it predicts a response that is identical to that of a simple p - α model.

Suppose the loading path is purely isotropic. Then the deviatoric part of the stress is zero — and hence $\sigma_s = 0$. Thus the stress in the Rendulic (σ_s vs. σ_m) plane moves strictly along the σ_m axis. Yield commences when the stress reaches the point where the yield surface intersects the σ_m axis. This intersection point depends on the level of porosity. As plastic flow occurs, the porosity changes and the *entire* yield surface evolves as sketched in Fig. 15.1.

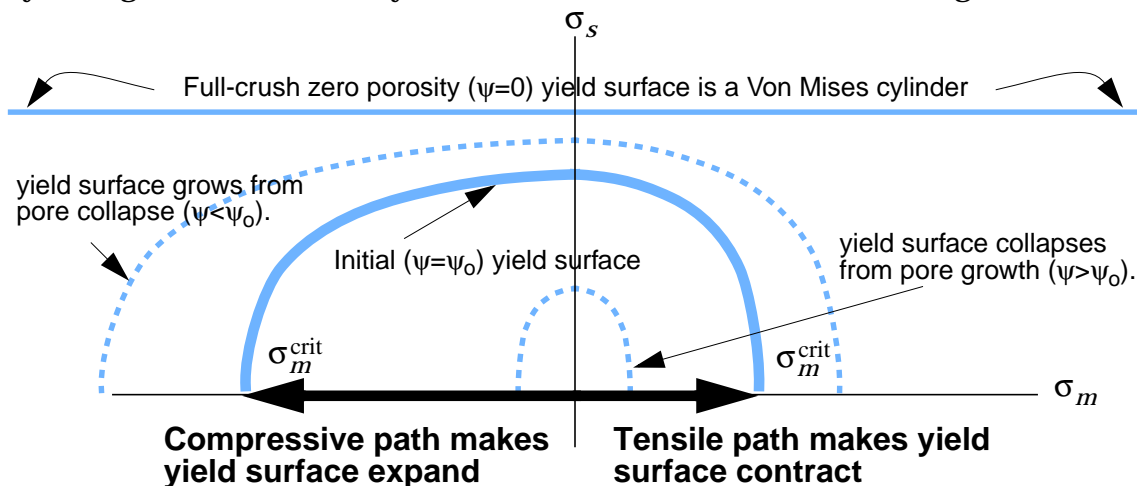


Figure 15.1. *Isotropic loading in the Rendulic plane.* The figure shows a qualitatively reasonable family of yield surfaces corresponding to different levels of porosity ψ . (The actual shapes of these curves are dictated by the user-supplied porosity-dependent yield function). Under *purely isotropic loading*, the stress follows a path through this space that is always along the horizontal ($\sigma_s=0$) axis.

The user-supplied yield function describes a porosity dependent yield surface that is axisymmetric about the isotropic axis in stress space. This means that a purely isotropic stress state (at yield) will always lie at a point on the yield surface where $F_s=0$, which is why the yield surfaces shown in Fig. 15.1 intersect the σ_m axis at right angles.*

We wish to demonstrate that our general solution of Eqs. (14.1) through (14.8) reduces to a familiar p - α form under isotropic loading. For this purpose, we will suppose there is no hardening ($h = 0$), no void nucleation ($\dot{\delta}^n = 0$), no variation of elastic properties with porosity ($\kappa_m = 0$), and no variation of the matrix moduli $\dot{\Upsilon}=0$. The governing equations become

$$\dot{\sigma}_m = 3K(\mathbf{d}:\hat{\mathbf{I}} - F_m\dot{\lambda}) \quad (15.1)$$

$$\dot{\psi} = \sqrt{3}(1 + \psi)F_m\dot{\lambda} \quad (15.2)$$

$$F_m\dot{\sigma}_m + F_\psi\dot{\psi} = 0, \quad (15.3)$$

and the solution for the plastic segment, Eq. (14.1), becomes

$$\dot{\lambda} = \frac{3K\mathbf{d}:\hat{\mathbf{I}}}{3KF_m - \sqrt{3}(1 + \psi)F_\psi}. \quad (15.4)$$

Under isotropic loading, recall that yield commences when σ_m reaches the yield surface intercept σ_m^{crit} , the value of which might be different in tension and compression. For simplicity, consider compression only. Then $\sigma_m = -\sqrt{3}p$ where the conventional pressure p is positive for compression. The critical yield stress σ_m^{crit} varies with the porosity level. Thus, we may imagine the existence of plot of σ_m^{crit} versus pore ratio ψ . Hence, there exists a curve of $p^{\text{crit}} \equiv -\sigma_m^{\text{crit}}/\sqrt{3}$ versus distension $\alpha \equiv \psi + 1$. This curve is the *implied* p - α curve for the material. Keep in mind that such a curve makes sense only for isotropic loading — for general loading, the yield function itself is the generalization of the p - α curve.

The pore rate becomes

$$\dot{\psi} = \frac{3K\mathbf{d}:\hat{\mathbf{I}}}{\frac{\sqrt{3}K}{(1 + \psi)} + h'}, \quad (15.5)$$

where

$$h' \equiv -\frac{F_\psi}{F_m} = \left(\frac{\partial \sigma_m}{\partial \psi} \right)_{\sigma_s, \bar{\sigma}_s}. \quad (15.6)$$

* Some readers may be worrying about a Drucker-Prager type yield surface (which is like an axisymmetric Mohr-Coulomb surface) that intersects the σ_m axis at an acute angle, rather than being perpendicular to the σ_m axis. In stress space, this type of yield surface is like the tip of a pointed cone, so the outward normal to the cone tip may be taken to be directed along the cone axis: $F_s=0$.

In more conventional notation, Eq. (15.5) would be written

$$\dot{\psi} = \frac{K \text{tr} \underline{\underline{d}}}{\frac{K}{(1+\psi)} - \left(\frac{dp}{d\psi}\right)}. \tag{15.7}$$

The function $p(\psi)$ may be interpreted as the conventional p - ψ curve. Recall from elementary continuum mechanics [24] that $\text{tr} \underline{\underline{d}} = \dot{\epsilon}$ where $\epsilon = \ln(\rho_o/\rho)$. Also recalling that Eq. (2.1) gives K as an explicit function of ψ , Eq. (15.7) could be considered a separable ordinary differential equation that may be explicitly integrated to give ψ as a function of ϵ . Unfortunately, this approach is valid only in the limiting case of pure isotropic loading, so we cannot adopt it in general implementations.

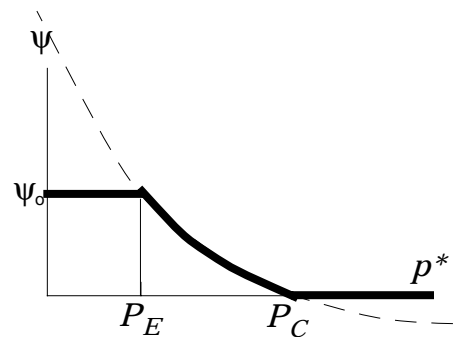


Figure 15.2. A conventional porosity crush-up model. Strictly speaking, such a model is not sensible in the presence of shear stresses.

Figure 15.3 shows a verification calculation of normalized mean stress vs. volumetric strain under isotropic loading for a test calculation run under prescribed isotropic strain using the Gurson yield function. The initial slope at (A) matches the initial bulk modulus K . Pore collapse commences (B) and continues until pores compress out (C), beyond which the slope equals the matrix bulk modulus. Plasticity terminates at “C” for isotropic loading [contrast this behavior with the similar calculation under uniaxial strain presented later in Fig. 17.4]. Release (D) is elastic until eventually enough tension builds to nucleate pores (F), which grow (G), allowing the stress drop. At recompression (H) the elastic modulus is smaller due to increased porosity. Pore collapse commences anew (I), leaving residual stress (J). The growth/crush curves shown in Fig. 15.3 exist only for isotropic loading. The graph of porosity vs. mean stress space is different for different paths.

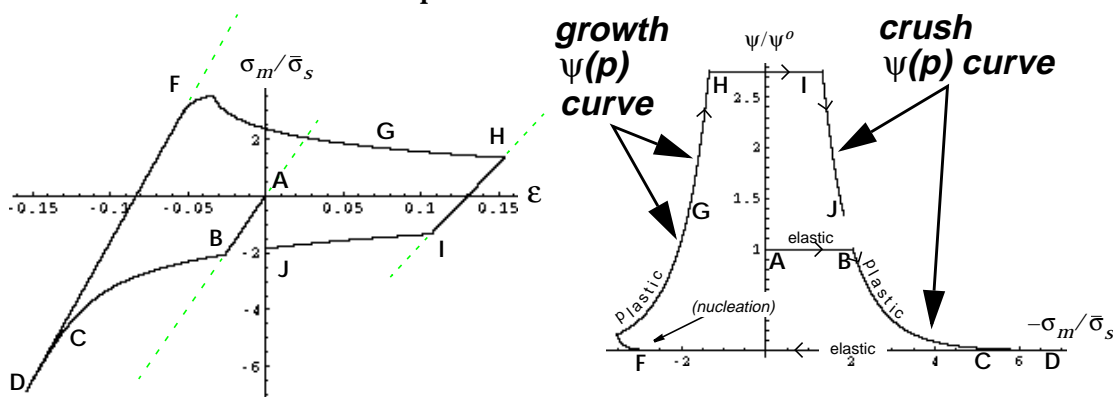


Figure 15.3. Isotropic stress-strain response and the implied Gurson “ p - α ” curves. The (A-J) labels on the stress-strain curve correspond to those on the parametric plot of normalized pore ratio vs. normalized pressure. Note that σ_m is proportional to the negative of pressure, and σ_m/σ_s is the mean stress normalized by the matrix yield stress.

Effect of hardening. Figure 15.4 compares the isotropic response curves with and without hardening.

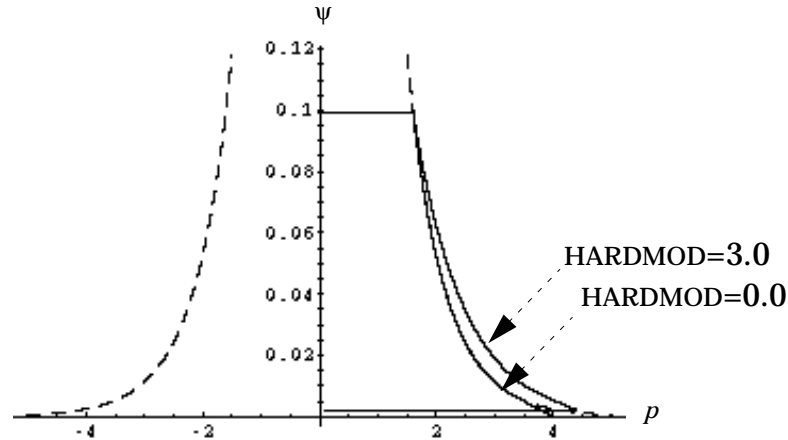


Figure 15.4. *Effect of hardening in the isotropic response.* The dashed line is a plot of the zero shear pressure intercept of the nonhardening yield surface as a function of porosity. The user input HARDMOD is the hardening modulus h divided by the matrix yield in shear (SBY). When hardening is invoked, the yield point gradually expands as desired.

Admissible crush curves. Inspection of Eq. (14.1) shows that some terms are subtracted, suggesting the possibility that $\dot{\lambda}$ might turn out to be negative (in violation of the principal of positive plastic dissipation). We here explore this situation in detail under the simplifying assumption of isotropic loading. We will find that anomalous negative plastic dissipation is indeed possible even in this very simple isotropic context. We do not interpret this result as a flaw in our model; instead we regard it as a new admissibility constraint on the user-defined yield function (in addition to usual constraints such as convexity of the yield surface). In the case of isotropic loading, we shall demonstrate that the plot of ψ vs. p must be sufficiently steep in the *tensile* regime — it is not allowed to asymptote to zero as it may permissibly do on the compressive side. An implication is that any yield function that is symmetric with respect to pressure is potentially inadmissible under tension. Alternatively, some other physical mechanism (such as the pore nucleation seen in the tensile side of Fig. 15.3) must engage before the offensively shallow tensile growth curve is ever reached.*

The dashed p - ψ curve in Fig. 15.2 is sometimes called a crush curve. The p - ψ curve should *not* be regarded as a material function because the path traced in ψ vs. p space depends on the amount of shear stress present. Crush and growth curves are well defined only for purely isotropic loading. As seen in our verification calculation of Fig. 15.3, increasing compressive pressure p

* The derivation of this result also appears in Ref. [32], where more conventional notation is used.

causes a decrease in porosity. When the material is subjected to tension, the parametric plot of the pore ratio ψ vs. the tensile pressure can be called the “growth” curve, as illustrated in Fig. 15.3. Under tension, ψ increases as pores grow under increasing tensile *strain*, and (as indicated in Fig. 15.3), the *stress* therefore decreases in magnitude due to material softening.

Suppose the material is subjected an isotropic monotonically increasing volume. Then the strain rate has a positive trace. In other words, $\underline{\underline{d}}:\hat{\underline{\underline{I}}}>0$, and the first term in Eq. (15.1) is positive. Recall that we have assumed that the matrix material is plastically incompressible. Therefore, under isotropic expansion, permanent volume changes must correspond to an increase in porosity ψ , and Eq. (15.2) implies that the quantity $F_m \dot{\lambda}$ must positive. Under expanding strain, the mean stress σ_m is itself positive, but in the absence of hardening, we expect the tensile mean stress σ_m to decrease as porosity increases. Hence, not only must the quantity $F_m \dot{\lambda}$ be positive, it must be large enough to make $\dot{\sigma}_m < 0$ in Eq. (15.1). Recalling that we demand $\dot{\lambda} > 0$, this implies that $F_m > 0$. Combining Eqs. (15.4) and (15.6) shows that

$$F_m \dot{\lambda} = \frac{\underline{\underline{d}}:\hat{\underline{\underline{I}}}}{1 + \frac{(1 + \psi)}{\sqrt{3}} h'}. \quad (15.8)$$

In tension, the stress is positive. We expect the stress to decrease as pores grow in tension. Thus, we want the stress rate to be negative when $\underline{\underline{d}}:\hat{\underline{\underline{I}}}>0$, so requiring that $\underline{\underline{d}}:\hat{\underline{\underline{I}}} - F_m \dot{\lambda} < 0$ gives the following restriction:

$$h' < 0. \quad (15.9)$$

The requirement that $\dot{\lambda} > 0$ provides another bound. In short, h' must be negative, but not excessively negative.

$$\frac{-\sqrt{3} K}{(1 + \psi)} < h' < 0. \quad (15.10)$$

This restriction must hold for all values of porosity. Hence, it must hold when the porosity is zero. Thus,

$$-\sqrt{3} K < h' < 0. \quad (15.11)$$

The slope of the tensile σ_m vs. ψ growth curve must be negative, but not too large in magnitude. Physically, there must be a yield “cap” at low porosities. In other words, the slope of the σ_m vs. ψ growth curve must not be too steep. Equivalently, the slope of the inverse ψ vs. σ_m growth curve must not be too shallow. If, for example, the porosity has been nearly all crushed out, yield upon a tensile load reversal *must* initiate again at a finite pressure. Fig. 15.5 shows qualitatively why this issue is important only when the starting porosity is extremely low.

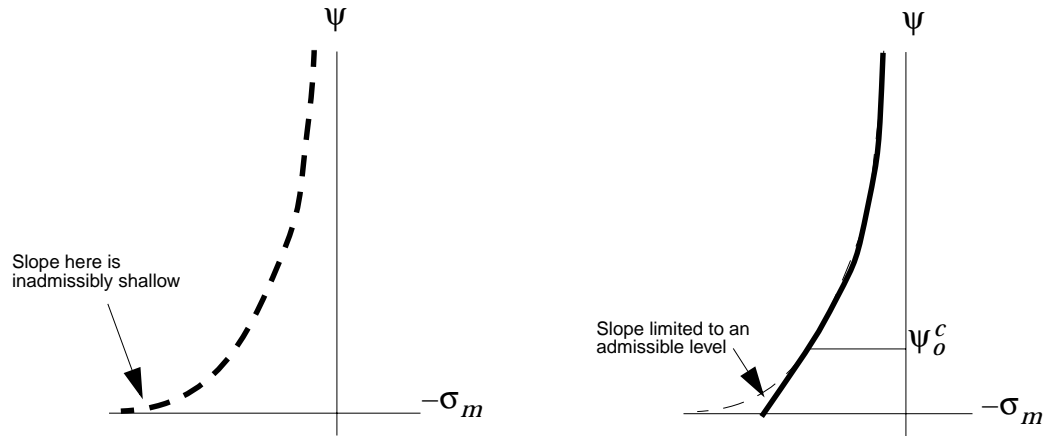


Figure 15.5. Inadmissibility of TENSILE growth curves. The tensile growth curve on the left is inadmissible because, at low porosities, the slope is too shallow. This curve could be replaced with the one on the right by simply using a tangent extrapolation to the original growth curve whenever the porosity is below the critical porosity ψ_o^c . Since porosity *increases* upon *tensile* yielding, there is no difference between the two curves whenever the starting porosity is large enough!

To summarize, the presence of F_ψ in the denominator of Eq. (15.4) means the growth curve can't be completely arbitrary. The growth curve must be such that the plasticity parameter $\dot{\lambda}$ will never be negative. In our numerical applications, the growth curve is a user-specified function. Quite often, measurements do not provide the nature of the growth curve at extremely small porosities, so it is difficult for users to satisfy the slope limitation. Furthermore, it is likely that the growth curve at small porosities is unmeasurable because fracture and/or pore nucleation is likely to occur well before yielding. As a matter of fact, the onset of an inadmissible slope might be useful as a possible *criterion* for pore nucleation.

In our numerical implementation, we artificially introduce void nucleation whenever the slope of the user-specified growth curve exceeds an admissible value. This is done strictly to achieve robustness. Preferably, the user would supply a sensible growth curve and/or preemptive nucleation parameters in the first place.

Existence of stress jumps. The fact that the yield surface contracts in tension has implication on the existence of moving surfaces of stress discontinuity that are sometimes proposed to exist in asymptotic solutions for the stress field near a growing crack tip. Brannon and Drugan [22] showed that such discontinuities are impossible whenever the current yield surface encloses all prior yield loci. The fact that this condition does not hold when there is tensile pore growth means that stress jumps *might* indeed exist near a moving crack tip, so long as porosity is higher on the “shocked” side of the jump.

Limiting case #2: Classical Von Mises plasticity

Consider a yield function (such as that of Gurson [9]) where $F_m=0$ when $\sigma_m=0$. In other words, when stress is purely deviatoric, then the outward normal to the yield surface is itself purely deviatoric and parallel to the stress. Such a point should give simple shear response identical to conventional Von Mises plasticity. When $F_m = 0$, Eqs. (14.1) and (12.3) become

$$\dot{\lambda} = \frac{2GF_s \underline{\underline{\mathbf{d}}}: \hat{\underline{\underline{\mathbf{S}}}}}{2GF_s^2 - h\xi F_\zeta} \text{ and } \dot{\psi} = 0, \quad (15.12)$$

and Eqs (11.13) become

$$\dot{\sigma}_m = 3K(\underline{\underline{\mathbf{d}}}: \hat{\underline{\underline{\mathbf{I}}}}) \quad (15.13a)$$

$$\dot{\sigma}_s = 2G(\underline{\underline{\mathbf{d}}}: \hat{\underline{\underline{\mathbf{S}}}}) \left(\frac{u}{u-1} \right) \text{ where } u \equiv \frac{h\xi F_\zeta}{2GF_s^2}. \quad (15.13b)$$

The mean stress is entirely elastic and depends only on the bulk modulus and the volumetric strain rate ($\text{tr} \underline{\underline{\mathbf{d}}}$). The isomorphic shear stress σ_s responds as it would for a classical Von Mises plasticity model. In the limit of a nonhardening matrix material (*i.e.*, $h = 0$), the magnitude of the stress deviator remains constant and its direction may be computed by a simple radial return of the trial elastic stress. In the absence of hardening, ψ and ζ remain constant, and the yield surface remains stationary in the Rendulic plane; this classical Von-Mises-like response occurs only for purely deviatoric loading in conjunction with a yield function having the property that $F_m=0$ whenever $\sigma_m=0$.

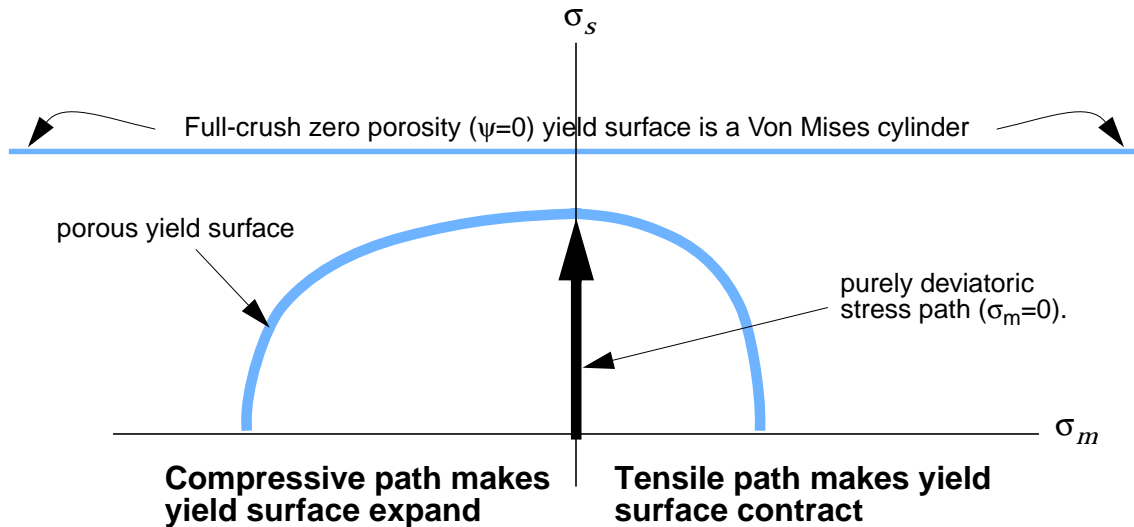


Figure 15.6. Purely deviatoric loading in the Rendulic plane. The onset of yield in pure shear is affected by the porosity level. However, if the slope of the yield curve is zero (*i.e.*, if the outward normal has no isotropic part), then the plastic strain rate will be purely deviatoric, and plastic flow in pure shear will *not* change the porosity level. Thus, the yield surface can evolve only via matrix hardening. Shear-enhanced compaction/expansion will occur only if the user-supplied yield curve has a nonzero slope at points where $\sigma_m=0$.

16. Two popular yield functions.

For the purpose of illustration, this section provides the porous yield functions for the two most common porosity models: The Gurson-Tvergaard model and the p - α model. Other yield models have been recently reviewed by Ragab and Saleh [33].

The Gurson-Tvergaard yield function

In the foregoing analysis, the yield function $F(\sigma_{mp}, \sigma_s, \psi, \zeta)$ has been assumed known. Gurson and Rice [9] derived such a yield function for hexagonal distributions of spherical voids embedded in an elastic-perfectly plastic von Mises matrix material. In terms of *conventional* stress measures, the Gurson-Tvergaard yield function is

$$F = \left(\frac{\sigma^{VM}}{Y} \right)^2 - \left[q_3 f_v^2 + 1 - 2 f_v q_1 \cosh \left(\frac{q_2 \text{tr} \underline{\sigma}}{2Y} \right) \right] \quad (16.1)$$

where σ^{VM} is the von Mises equivalent stress [defined in Eq. (3.14)] and Y is the von Mises yield stress of the matrix material. Also recall that f_v is the void volume fraction, which is related to the pore-solid ratio ψ by

$$f_v = \frac{\psi}{1 + \psi}. \quad (16.2)$$

The parameters $\{q_1, q_2, q_3\}$ were introduced by Tvergaard [34, 35] to empirically match numerical simulations for porous metals that included the effect of pore interaction. For illustration purposes, will henceforth take the $\{q_1, q_2, q_3\}$ parameters to all equal unity. Incidentally, Fig. 1.2 on page 3 was generated by setting $F=0$ in Eq. (16.1), and solving for $\text{tr} \underline{\sigma}$ (which equals $-3p$) as a function of porosity f_v at various values of the equivalent shear stress $\tau^{\text{equiv}} = \sigma^{VM} / \sqrt{3}$.

To re-cast the Gurson yield function in terms of our isomorphic stresses, we recall that $\sigma_s = \sqrt{\frac{2}{3}} \sigma^{VM}$, and we define an isomorphic yield stress $\bar{\sigma}_s \equiv \sqrt{\frac{2}{3}} Y$. Then the isomorphic expression of the Gurson yield function is

$$F(\sigma_{mp}, \sigma_s, f_v, \bar{\sigma}_s) = \frac{\sigma_s^2}{\bar{\sigma}_s^2} - \left[f_v^2 + 1 - 2 f_v \cosh \left(\frac{\sigma_m}{\sqrt{2} \bar{\sigma}_s} \right) \right], \quad (16.3)$$

The isomorphic yield stress $\bar{\sigma}_s$ is a material constant (equal to $\sqrt{2/3}$ times the von Mises yield stress of the matrix material, which is equal to $\sqrt{2}$ times the shear strength of the matrix material) and f_v is the void volume fraction, which is related to the pore ratio ψ by

The Gurson-Tvergaard yield surface is sketched in Fig. (16.1) for various values of the void volume fraction f_v .

The “ p - α ” yield function

Another popular treatment of void collapse is the so-called “ p - α ” model where void collapse is assumed to occur at a critical value of pressure, *independent of the shear stress*. The critical void collapse pressure is taken to depend only on the distention α , which equals $\psi + 1$ and is usually defined as the solid mass density divided by the macroscopic porous density. Usually p - α models are used in combination with a traditional Von Mises yield model in which yield occurs at a critical shear stress *that is independent of the pressure*. Thus plastic flow will commence when the stress reaches the Von Mises yield cylinder or the p - α crush/growth curve — whichever comes first. If the stress reaches the Von Mises cylinder first, no pore collapse will occur until the pressure becomes high enough to reach the critical pressure defined by the p - α function. In the present QCKP lexicon, the “ p - α ” yield surface is therefore a *rectangular box* in isomorphic Rendulic $\{\sigma_m, \sigma_s\}$ space.

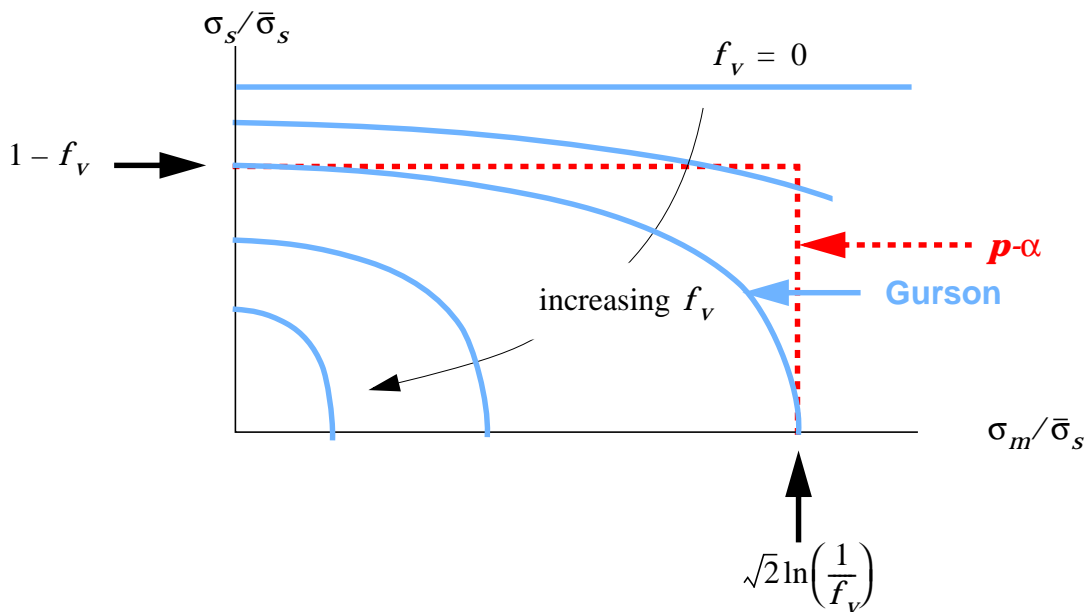


Figure 16.1. Gurson's yield surface compared with a p - α surface. The parameter f_v is the void volume fraction (see Eq. 16.2). Gurson's surface is a well-behaved differentiable function of both shear and pressure whereas the p - α surface is rectangular. The Gurson surface intersects the pressure axis at a stress that depends only on porosity (and the matrix yield stress). Hence, this intersection point implicitly defines a p - α curve (shown by the dashed line in Fig. 15.4) that would be observed whenever a Gurson-type material is subjected to hydrostatic loading. The above figure shows the p - α yield surface that would need to be used in order to obtain identical results in pure shear or pure hydrostatic loading.

Comparison of the Gurson and “ p - α ” yield functions

Fig. (16.1) shows that the Gurson model and the p - α model are capable of predicting identical results when run in either pure shear or pure isotropic compression — the distinction between the models becomes apparent for mixed loading paths such as uniaxial strain.

For the Gurson yield function, we identify the innominate internal state variable ζ to be the parameter $\bar{\sigma}_s$. Figures 17.2 and 17.4 assume this parameter is a material constant (which means the matrix material is nonhardening).

The derivatives of the Gurson yield function are

$$F_m = \frac{\sqrt{2} f_v}{\bar{\sigma}_s} \sinh\left(\frac{\sigma_m}{\sqrt{2} \bar{\sigma}_s}\right) \quad (16.4)$$

$$F_s = \frac{2\sigma_s}{\bar{\sigma}_s^2} \quad (16.5)$$

$$F_\psi = \frac{\partial F(\sigma_m, \sigma_s, f_v)}{\partial f_v} \left(\frac{\partial f_v}{\partial \psi}\right) = \dots = 2(1 - f_v)^2 \left[\cosh\left(\frac{\sigma_m}{\sqrt{2} \bar{\sigma}_s}\right) - f_v \right] \quad (16.6)$$

$$F_\zeta = \frac{-1}{\bar{\sigma}_s^2} \left\{ \frac{2\sigma_s^2}{\bar{\sigma}_s} + \sqrt{2} f_v \sigma_m \sinh\left(\frac{\sigma_m}{\sqrt{2} \bar{\sigma}_s}\right) \right\}. \quad (16.7)$$

Coding for these equations is provided in Appendix F.

Fig. 16.1 shows that the yield surface intercepts the horizontal pressure axis at

$$\frac{\sigma_m}{\bar{\sigma}_s} = \pm \sqrt{2} \ln\left(\frac{1}{f_v}\right). \quad (16.8)$$

By using Eq. (3.11), this relationship gives the *effective* p - ψ curve illustrated in Fig. 16.2. The dashed line in Fig. 15.4 is a plot of the Gurson implied p - ψ curve, and that demonstration calculation shows that the parametric plot of ψ vs. p follows this crush curve during intervals of nonhardening plastic pore collapse/expansion.

In more conventional notation, Eqs. (16.2) and (16.8) may be solved for ψ as a function of the compressive pressure p and the Von Mises yield stress for the matrix material ($\bar{\sigma}^{VM} \equiv \bar{\sigma}_s \sqrt{3/2}$). Namely,

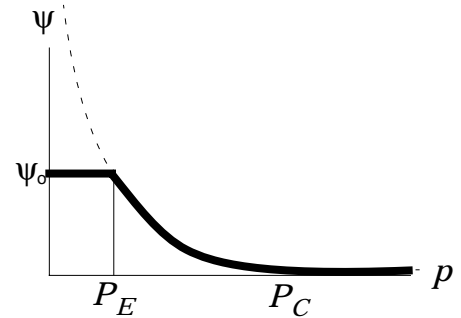


Figure 16.2. The p - ψ curve associated with the Gurson model. This model does not have a crush pressure *per se*; rather, the curve approaches zero so rapidly that a crush pressure might appear to exist in experiments.

Two popular yield functions.

$$\psi = \frac{1}{e^{3p/2\bar{\sigma}^{\text{VM}}} - 1}. \quad (16.9)$$

For the Gurson model, there is no distinct full-crush pressure P_C . However, the approach of ψ to zero is exponential so, from an experimental point of view, full crushing might appear to be achieved. An experimentally measured p - α curve may be used to determine the parameter $\bar{\sigma}^{\text{VM}}$. Namely

$$\bar{\sigma}^{\text{VM}} = \frac{-3P_E}{2\ln f_v^0}. \quad (16.10)$$

We reiterate that our porosity measure ψ is the ratio of the pore volume to the solid volume *when the material is in an unstressed state*. Consequently, as seen in Fig. 16.2, this porosity measure remains constant until the yield surface is reached. As shown in Fig. 16.3, the actual *loaded* porosity decreases with increasing compressive pressure. Our model is *not* neglecting this effect. The fact that we use the unloaded porosity to describe the yield surface does not mean that the actual porosity does not change. Although rarely recognized in the literature, Eq. (12.2) is valid only if the *unloaded* porosity is used.

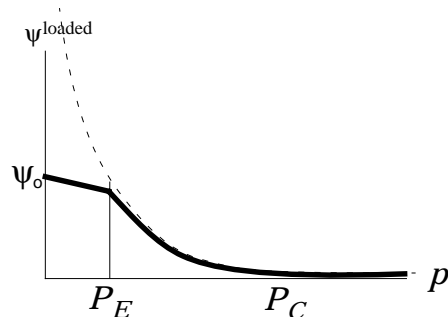


Figure 16.3. The p v.s. ψ^{loaded} curve. Comparison with Fig 16.2 shows that actual loaded porosity decreases with pressure even during the elastic loading phase. This behavior is implicit in the CKP model.

The expressions for the elastic moduli should properly use the loaded porosity. However, the initial slope of ψ^{loaded} vs. p is on the order of $3/(4G_m)$, where G_m is the shear modulus of the matrix material [36]. This slope is so shallow that it would result in only a negligible correction to Eq. (6.5), so it is not worth pursuing.

We now show the results of the present theory when used in conjunction with the Gurson yield criterion. We again emphasize that the Gurson surface is being used only for illustration purposes.

Subroutines that implement the Gurson model are provided in Appendix F. These routines were used as the user-defined yield function for most of the sample calculations presented in this report. However, the present numerical version of the CKP model comes with a different (more flexible) default yield function described in Section 19.

Keep in mind that the numerical implementation of this model permits and encourages the user to define their own yield function. The sample calculations presented in this report can change dramatically when a different yield function is used. Therefore, *further research and measurements of the porosity dependent yield functions of real materials is of paramount importance.*

17. Verification calculations using the QCKP model

This section presents some simple benchmark simulations that demonstrate the overall capabilities of the QCKP model to describe transformation strain, plastic hysteresis, hardening, and shear-dependence of pore collapse.*

EXAMPLE 1: hydrostatic loading

Figures 17.1 and 17.2 show the isotropic stress-strain response of a porous material modeled using the present model in conjunction with the Gurson yield function. Fig 17.1 depicts compressive stress vs. compressive strain showing the phase transformation (first plateau) followed by extended straining and continued linear response until the pores begin to crush out.

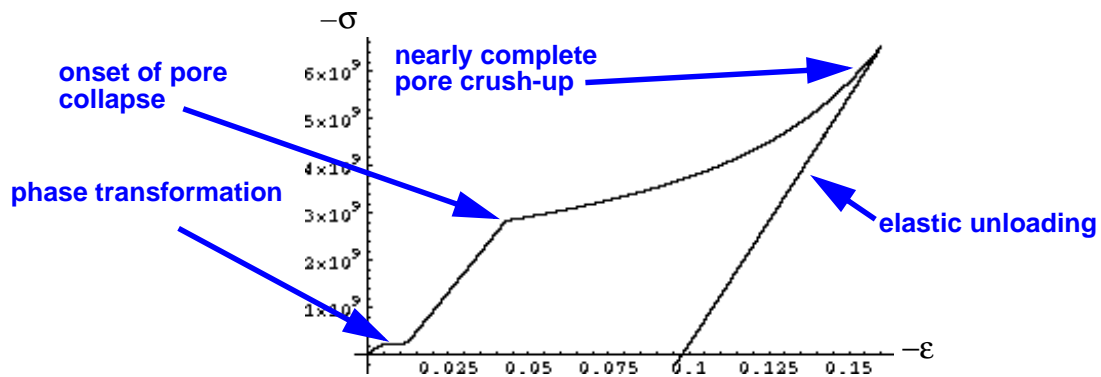


Figure 17.1. Hydrostatic compression with phase transformation. The remainder of sample calculations in this report have transformation “turned off.”

Fig 17.2, shows the results of the CKP model under isotropic loading when phase transformation is turned off and the hardening parameter h is set to zero. The upper-left and upper-right figures show compression followed by expansion (keep in mind that σ_m is negative in compression whereas p is positive in compression). The stress and strain begin at the origin (A) and are loaded elastically in compression with a slope equal to the porous bulk modulus. Crushing of pores allows a rapid increase in compressive strain (B) with very little applied stress. As the pores completely crush out, the slope approaches the *stiffer* elastic bulk modulus of the matrix material (C). Because all pores have been crushed out, the elastic unloading has a slope equal to the *matrix* bulk modulus (D) until the tensile mean stress becomes sufficiently high to permit void nucleation (E). The nucleated voids grow (F)

* For the purpose of these examples, we have used the Gurson yield function. Different yield functions can dramatically affect the quantitative results, but the overall *qualitative* shapes of the stress-strain plots would remain unchanged.

with increasing strain, thereby resulting in decreasing stress. Upon the second strain reversal (G), the elastic modulus is less stiff due to the increased porosity. Pore collapse re-commences (H) at a tensile strain, and continues such that there is residual stress once the strain is returned to zero (J).

The upper-right graph in Fig. 17.2 is a parametric plot of the pore ratio ψ vs. pressure (positive in compression), which is the effective p - ψ curve for this material. Incidentally, ψ remains constant during intervals of elastic loading. This does *not* mean that the porosity remains constant during elastic loading. Recall that we defined ψ to be the *unloaded porosity*, not the actual loaded porosity. The only way that our unloaded ψ can change is by plastic loading.

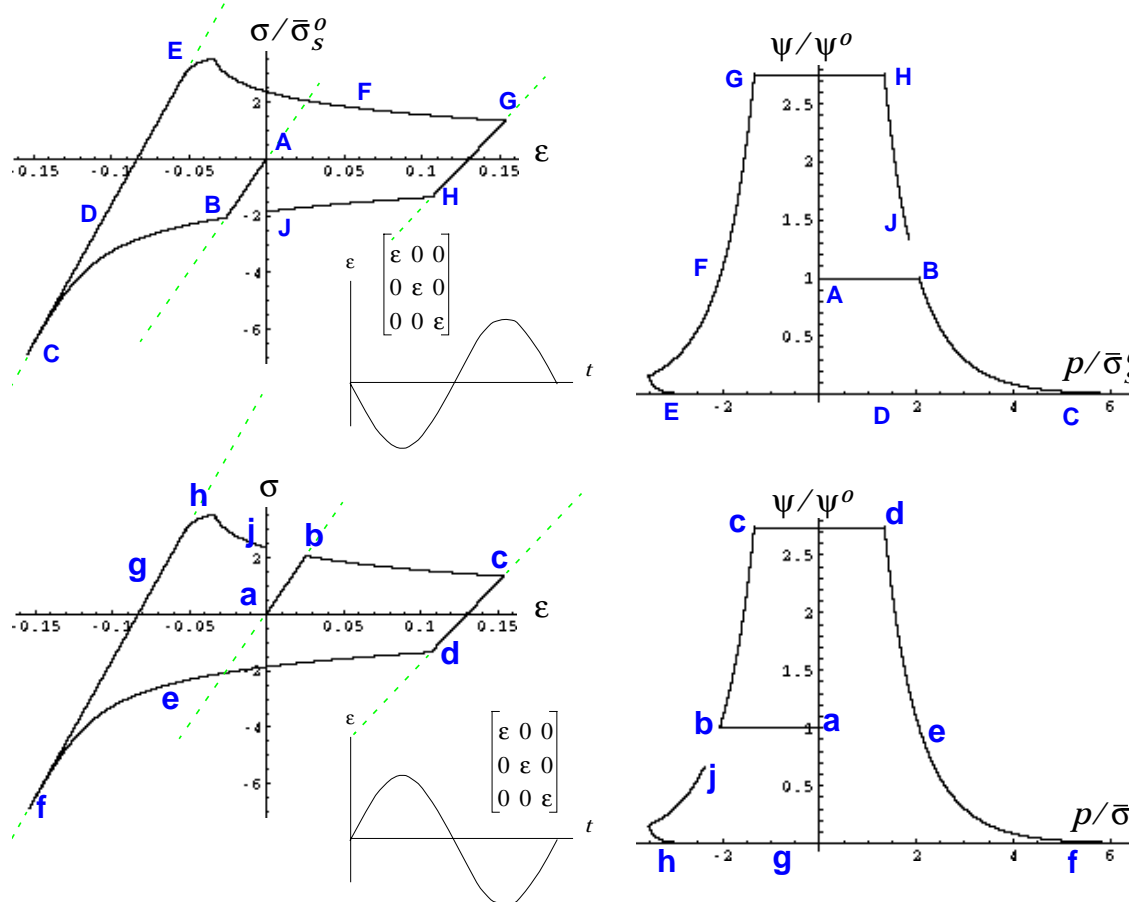


Figure 17.2. Mean stress vs. logarithmic volumetric strain for purely isotropic straining. The top two figures show compression followed by expansion. The bottom two figures show expansion followed by compression. The stress strain curves plot conventional mean stress, $\sigma = (\text{tr}\sigma)/3$ versus logarithmic strain. The dashed lines are drawn for reference to emphasize how the elastic moduli vary with porosity. The p - ψ curves at right parametrically plot the *unloaded* pore ratio ψ vs. the conventional pressure, $p = -\sigma$.

Keep in mind that the CKP model does not initiate pore collapse based on any explicit p - ψ curve. We have merely demonstrated that one can compute an *implicit* p - ψ curve by exercising the model under isotropic loading. Any other loading will generally follow a different path in ψ vs. p space. The

implicit hydrostatic p - ψ curve corresponds to the pressure where the general yield surface intersects the shear free axis in the Rendulic plane. This intersection point depends on the level of porosity. The plot of this intersection pressure vs. porosity is the implied p - ψ curve.

The bottom row of Fig 17.2 shows the same load path except expansion is followed by compression. The two hysteresis loops are similar because the calculations were run *without* matrix hardening (*cf.* Figs 17.5 and 17.6).

EXAMPLE 2: Pure shear with linear hardening

Fig 17.3 shows the result of running a purely deviatoric strain path ($\hat{\underline{d}}:\hat{\underline{I}} = 0$) using Gurson's yield function [9]. This calculation uses a hardening parameter h equal to twice the initial value for $\bar{\sigma}_s$ (thus, the user input **HARDMOD** is given by 2.0).

The stress-strain response indeed reduces to the Von-Mises-like limiting case of Eq. (15.13b).

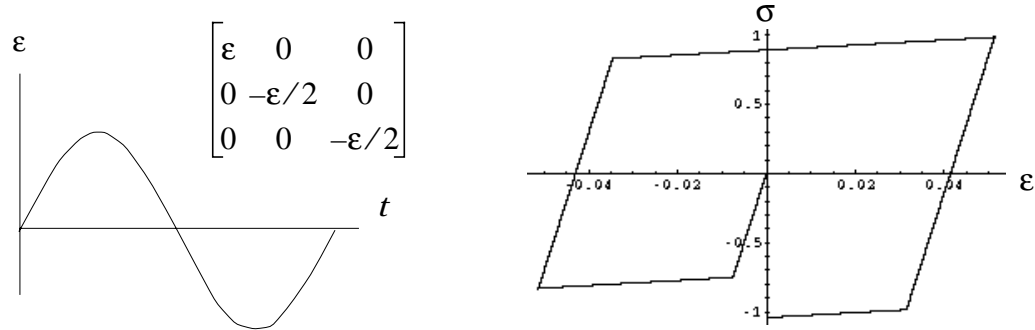


Figure 17.3. Simple linear hardening under uniaxial shear. The loading is strain-prescribed, with the (logarithmic) strain being purely deviatoric, as indicated in the matrix shown in the inset.

The stress-strain response in Fig. 17.3 looks much like the response of classical Von Mises models for metals. This behavior is strictly a by-product of the chosen yield function. For Gurson's model, the yield surface has a zero slope at zero pressure. Hence, since the CKP model presumes plastic normality, Gurson's model is incapable of producing a change in porosity under deviatoric straining. If Gurson's model were abandoned in favor of a yield function that had a nonzero slope at zero pressure, then the new model would be capable of modelling shear-enhanced compaction or dilatation (depending on the sign of the slope).

EXAMPLE 3: Uniaxial strain (mixed) loading

Figure 17.4 shows the stress strain curve for cyclic uniaxial strain-controlled loading using Gurson's yield function. This load path starts at the origin (A) and moves elastically until pore collapse commences (B). At first, the tangent stiffness decreases, but then increases as the pores collapse. The deformation completely collapses the pores (C), and the yield surface becomes a Von Mises type with the tangent stiffness is given by the elastic bulk modulus. The elastic release from point D follows a path with a slope given by the elastic longitudinal wave modulus, $K + 4G/3$. The material yields again (E), but since all the pores have been crushed out, the response is again like conventional Von Mises plasticity, with the plastic tangent modulus equalling the elastic bulk modulus K_m . Re-yielding occurs while the axial stress is compressive due to the assistance of the residual pressure built up in the material during loading that cannot be fully released during the elastic uniaxial extension. Eventually enough tension builds in the specimen to allow pores to re-nucleate (F) at which point they grow, resulting in a decreasing stress with increasing strain (G). Upon the final strain reversal (H), the elastic stiffness has decreased due to the effect of increased porosity on the elastic moduli. Finally, pore collapse commences again (I). When the strain is returned to zero (J), there is a compressive residual stress.

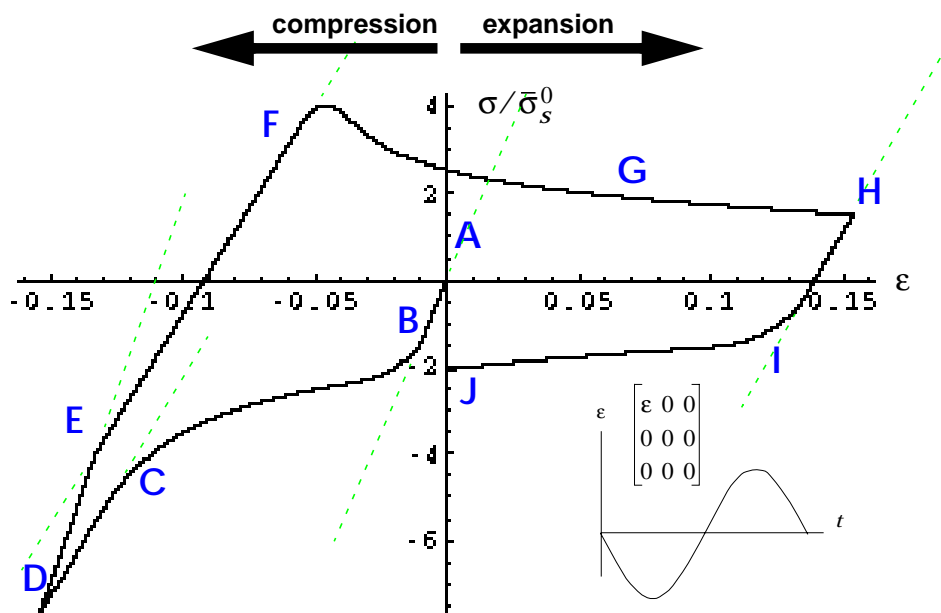


Figure 17.4. Uniaxial stress vs. logarithmic strain for uniaxial strain controlled loading. The load path uniaxially compresses the material, then expands it, and finally returns to a zero-strain configuration (leaving a compressive residual stress).

The upper part of Figure 17.5 shows the same loading path as in Fig. 17.4, but with hardening enabled (upper left) and with superimposed load reversals to show the instantaneous elastic unloading paths.

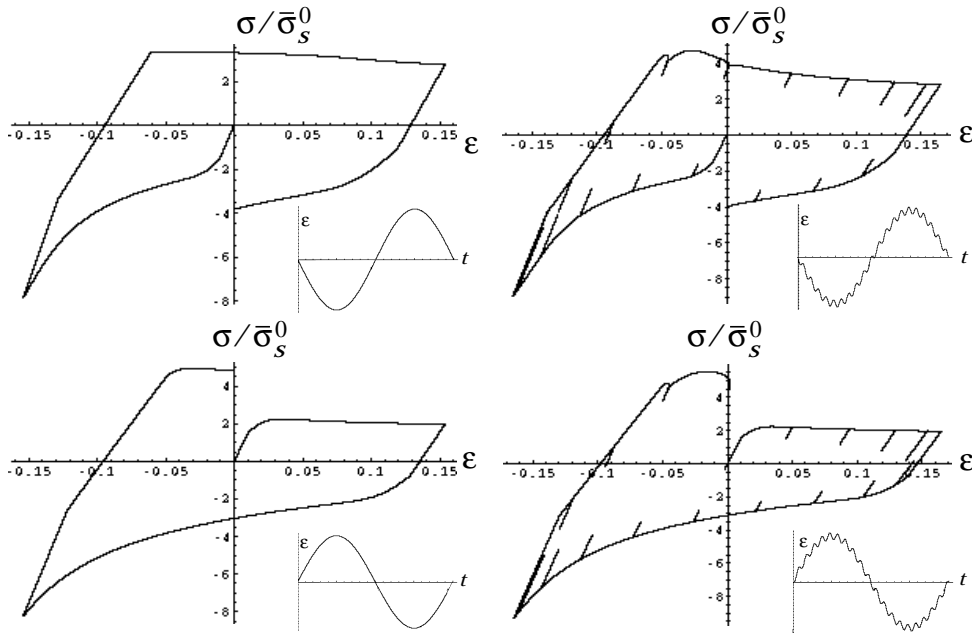


Figure 17.5. Linear hardening and cyclic unloading. The upper-left calculation is identical to Fig. 17.4 except that matrix hardening is enabled with $h = 2\bar{\sigma}$, which corresponds to a user input `HARDMOD=2` in the numerical implementation. The upper right figure is identical except small unloading perturbations are imposed on the strain cycle as indicated in the strain history inset. The lower two figures show these effects for load paths that start in tension and end in compression.

Thus far, all examples have subjected the material to a single strain cycle (e.g. compression to extension back to zero strain). Figure 17.6 shows the response of the material to *thirty* cycles of uniaxial strain. Of course a real material would fatigue and crack upon such severe loading; these calculations merely serve to indicate asymptotic limits of the theory. The hardening material approaches a *linear-elastic* material because the matrix yield stress $\bar{\sigma}_s$ eventually becomes so large that yield can longer occur. By contrast, the non-hardening material immediately achieves a steady-state hysteresis loop.

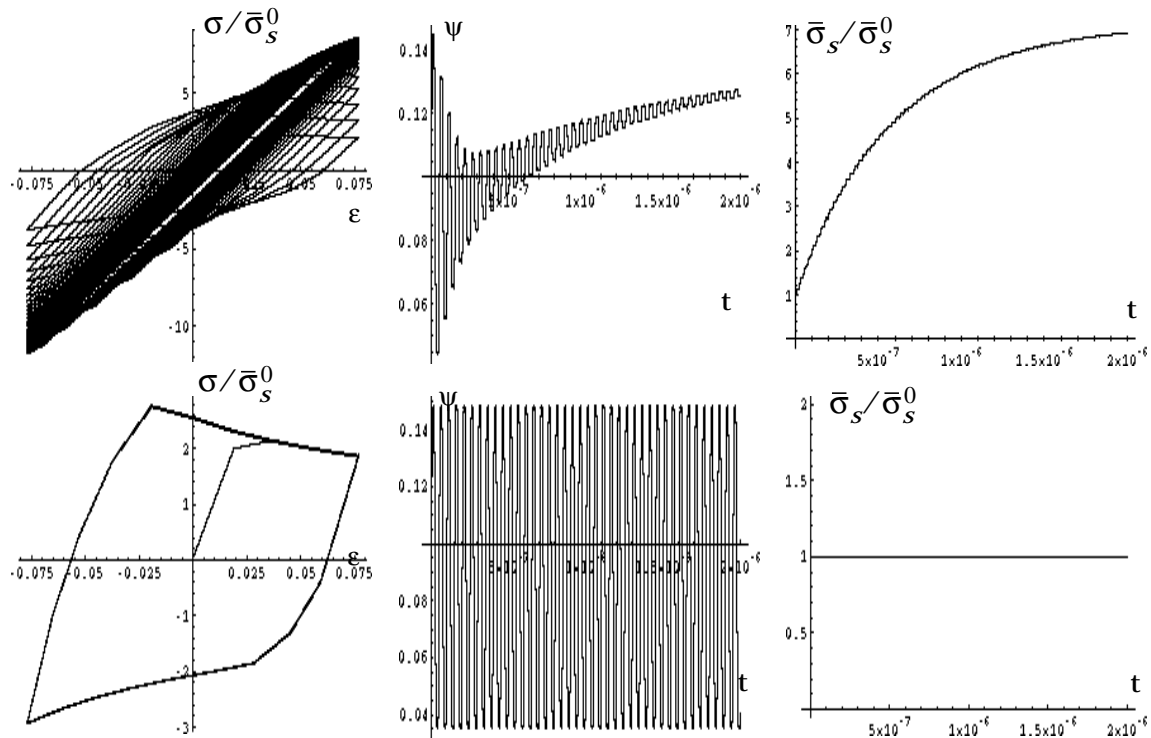


Figure 17.6. Steady state response to multiple uniaxial strain cycles. The top row includes linear strain hardening, while the bottom row is nonhardening.

This calculation is an excellent example of the present inability of the CKP model to predict the effects of pore morphology. In a real material, continued strain cycling would cause the migration and coalescence of the pores, eventually degrading the material enough to induce fracture. Such effects will be incorporated in future versions of this model.

18. Rate dependence

One possible approach to modelling rate dependence in a porous material is to use a rate dependent yield function such as that of Pan *et al.* [37] or Duva and Hutchinson [27]. Our own yield function would become rate dependent if we were to make the matrix yield stress $\bar{\sigma}$ depend on the strain rate. A immediate difficulty with these approaches is a matter of practicality: the governing equations become nonlinear with respect to the rates, and an exact solution (as was found in Section 14 for quasistatic loading) becomes unlikely. To permit rate dependence in a purely phenomenological manner, this version of the CKP model uses an overstress technique. The QCKP solution from Section 14 is regarded as the “equilibrium” solution for which the stress may never exist outside of the yield surface, but the *actual* stress is permitted to lie outside of the yield surface. The actual stress is attracted back toward the equilibrium stress at a rate that is proportional to the distance between them.

The solid arrows in Fig. 18.1 show the stress decomposed into a “consistent kinetics” equilibrium part σ^{eqbm} , which must always lie within or on the yield surface, plus a transient overstress σ^{over} , which allows the dynamic stress state to lie off of the yield surface. Therefore, referring to the sketch,

$$\underline{\underline{\sigma}} = \underline{\underline{\sigma}}^{\text{eqbm}} + \underline{\underline{\sigma}}^{\text{over}} \quad (18.1)$$

The rate of σ^{eqbm} is governed by the quasistatic consistent kinetics equations (QCKP) that were outlined in the earlier sections. Hence, by the time the overstress model is applied, the equilibrium stress rate, $\dot{\underline{\underline{\sigma}}}^{\text{eqbm}}$, may be regarded as known.

The dashed arrows in Fig. 18.1 show that the rate of stress $\dot{\underline{\underline{\sigma}}}$ is taken to equal the (trial) elastic stress rate $\dot{\underline{\underline{\sigma}}}^{\text{trial}}$ plus a restoring stress rate that is directed from the actual dynamic stress toward the equilibrium stress. The magnitude of the restoring stress rate is assumed proportional to the magnitude of the overstress itself. That is,

$$\dot{\underline{\underline{\sigma}}} = \dot{\underline{\underline{\sigma}}}^{\text{trial}} - \frac{\underline{\underline{\sigma}}^{\text{over}}}{\tau} \quad (18.2)$$

where τ is a characteristic dynamic relaxation time parameter, considered to be a material property. From Eq. (18.1), we also have

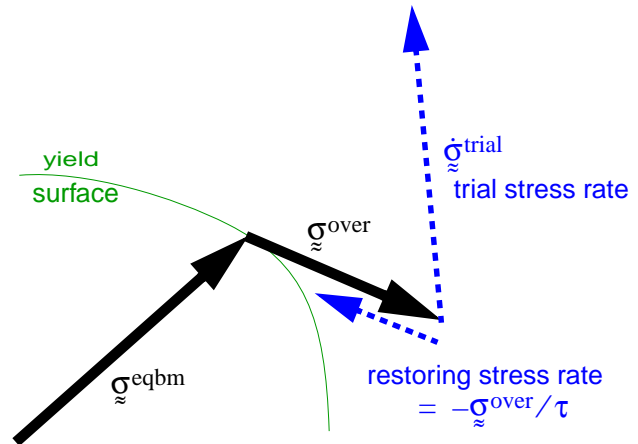


Figure 18.1. Overstress rate dependent stress relaxation. The stress (solid arrows) is the tensor sum of the equilibrium stress plus the overstress. The stress rate (dashed arrows) is the elastic trial stress rate plus a restoring stress rate directed toward the equilibrium state.

Rate dependence

$$\dot{\underline{\underline{\sigma}}} = \dot{\underline{\underline{\sigma}}}^{\text{eqbm}} + \dot{\underline{\underline{\sigma}}}^{\text{over}} \quad (18.3)$$

Combining Eqs. (18.2) and (18.3) gives the differential equation governing the overstress:

$$\dot{\underline{\underline{\sigma}}}^{\text{over}} = \underline{\underline{q}} - \frac{\underline{\underline{\sigma}}^{\text{over}}}{\tau} \quad \text{where} \quad \underline{\underline{q}} = \dot{\underline{\underline{\sigma}}}^{\text{trial}} - \dot{\underline{\underline{\sigma}}}^{\text{eqbm}} \quad (18.4)$$

The tensor $\underline{\underline{q}}$ is the amount by which the elastic trial stress rate exceeds the QCKP equilibrium stress rate. If $\underline{\underline{q}}$ is constant from time t_1 to t_2 , then the solution to Eq. (18.4) is

$$\underline{\underline{\sigma}}^{\text{over}}(t_2) = \tau \underline{\underline{q}} + [\underline{\underline{\sigma}}^{\text{over}}(t_1) - \tau \underline{\underline{q}}] e^{-(t_2 - t_1)/\tau}, \quad (18.5)$$

This solution is used incrementally in numerical simulations, in which overstress is tracked as a separate internal state variable. If the strain rate is held constant, then $\underline{\underline{q}}$ will approach a constant over a long enough period of time, and the overstress then monotonically approaches a limiting value of $\tau \underline{\underline{q}}$. The product $\tau \underline{\underline{q}}$ is small whenever the relaxation time and/or the strain rate are small, which represents the equilibrium limit sketched in Fig. 18.2. For positive relaxation times, the present overstress model has the desirable property that higher strain rates always lead to higher “apparent” yield stresses.

Fig 18.3 shows the effect of rate dependence in our pure-shear numerical verification benchmark problem. Upon reaching yield, the shear stress rate initially remains equal to the *elastic* stress rate. As the stress state deviates further from the equilibrium value, it begins to turn back towards equilibrium. Fig 18.3 compares the transient response for two different load paths. For the constant strain rate (bilinear load path), the actual stress *rate* approaches the equilibrium stress *rate*, while the difference between the actual stress and the equilibrium stress approaches τq_{ij} , as predicted in Eq. (18.5). This apparent increase in the yield stress is approximately $G\tau\dot{\gamma}$, where G is the shear modulus, τ is the relaxation time constant, and $\dot{\gamma}$ is the shear strain rate. The sinusoidal path in Fig 18.3 passes through the same strain states as the linear path, but the strain rate (slope of the strain history) is continually changing. Consequently, the stress response never reaches steady state — the response turns back towards the equilibrium state because the sinusoidal strain rate is *zero* at the peak strain. Fig 18.4 shows the effect of the overstress relaxation time on the results for sinusoidal *isotropic* (shear-free) loading.

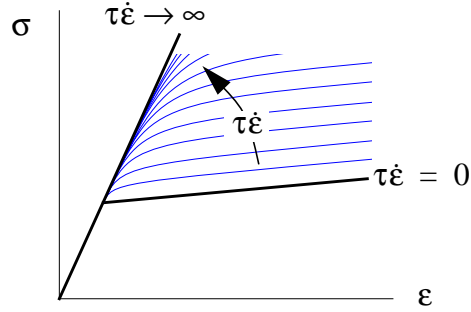


Figure 18.2. Rate-dependent “apparent” yield stress. When the strain rate is held constant, the stress strain curve asymptotes to a value that exceeds the quasistatic yield stress by an amount τq , which is roughly proportional to $\tau \dot{\epsilon}$.

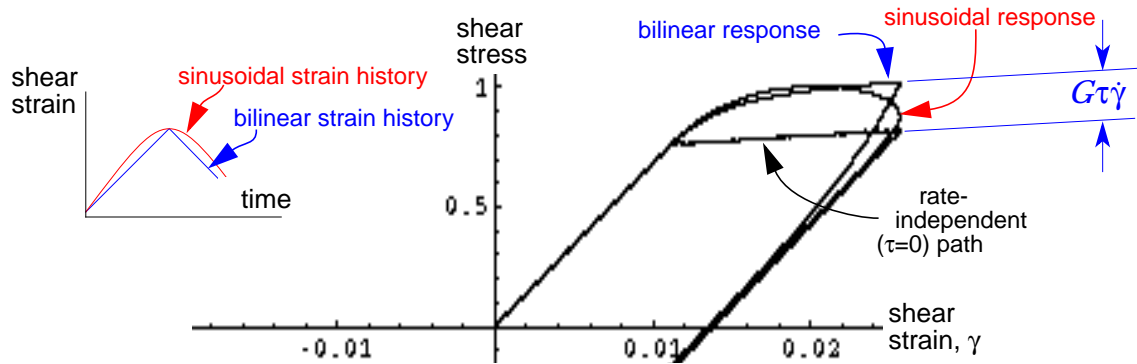


Figure 18.3. Overstress rate dependence in pure shear with Gurson yield function. The figure shows the response under two pure shear strain paths. For the linear path, the loading strain rate is constant and the “apparent” yield stress approaches a steady-state path that runs parallel to the equilibrium yield stress. The sinusoidal strain path illustrates transient effects throughout the loading phase.

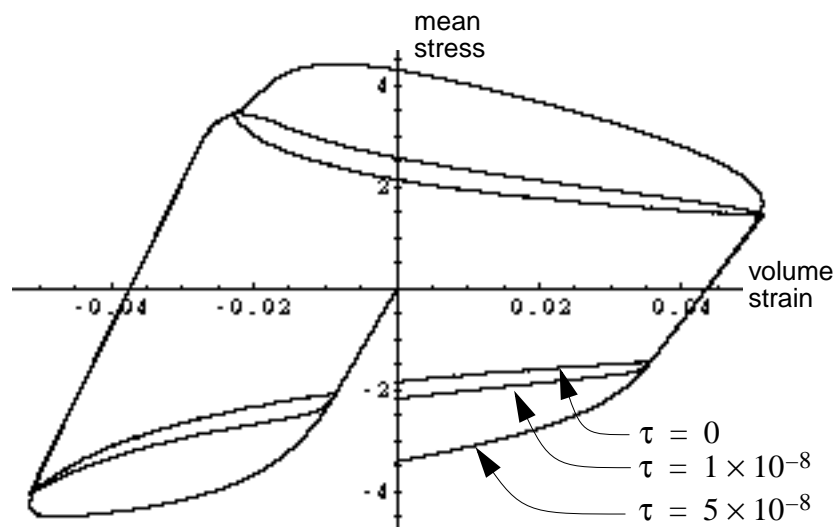


Figure 18.4. Rate dependence in isotropic loading. Note how even pore nucleation is sluggish with this model. The concavity of the response changes at the largest relaxation time because the loading is sinusoidal.

An *ad hoc* way to incorporate the effect of porosity on relaxation time assumes that the *product* of the relaxation time and the macroscopic shock impedance is constant, giving the following formula for the dynamic time constant in terms of (presumably known) initial material properties:

$$\tau = \tau_0 \sqrt{\frac{\rho_0 K_0}{\rho K}} \quad (18.6)$$

This particular relationship is still under review and is not implemented in the present version of the CKP model.

19. Default “dearth of data” (D.O.D.) yield function

Recall that the CKP model does not assume any particular form for the yield function. The numerical implementation of the CKP model has been written such that the yield function and its derivatives can (*should*) be defined by the user. Ideally, the yield function should be measured in the laboratory and implemented as a tabular routine. Unfortunately, however, measurement of a yield function is very labor intensive — it requires numerous careful measurements on numerous (and necessarily identical) samples. Quite often, such experimental measurements are unavailable and the user is faced with the daunting task of having to “guess” a reasonable form for the yield function. One recourse is to use published yield functions such as that of Gurson [9] which was derived based on analytical solutions for a periodic hexagonal array of pores embedded in a rigid-plastic matrix material. Subroutines for the Gurson yield function are provided in Appendix F.

One problem (or virtue, depending on one’s viewpoint) with the Gurson yield function is that it has almost no user-adjustable parameters. This is just fine for materials that are well-modelled under the Gurson theory, but it leaves virtually no flexibility for the user to explore the effect of yield surface shape on the material’s response. Furthermore, the Gurson model tends to be too “rounded” even when applied to the porous metals for which it was designed. Finally, the Gurson model is symmetric with respect to pressure and it therefore violates the admissibility constraint of Eq. (15.10) and cannot model shear-enhanced compaction/dilatation or different yield points in tension and compression which are often observed in real materials.

In this section, we assume that the user does not have a complete yield function for all possible stress paths and porosities, but the user *does* have data for the yield function at various porosities under purely isotropic (hydrostatic) loading. Such a function is frequently called a p - α curve because it can be plotted as pressure versus distention $\alpha = \rho_s/\rho$, where ρ_s is the theoretical solid density and ρ is the actual mass density. This section provides a flexible qualitatively reasonable extension of a known p - α curve into the shear-stress vs. mean-stress plane.

Faced with a dearth of data (D.O.D.), engineers are often stuck with the job of “guessing” a reasonable shape for the yield surface. We seek a multipurpose yield function that can provide the following features:

- Different yield points in isotropic tension and compression
- Dilatation under simple shear.
- Pressure dependent yield.
- Porosity dependent yield.
- Interpolating yield function having elliptical and rectangular limits.
- Optional Drucker-Prager type behavior for the matrix yield stress.
- Optional yield “cap” type behavior.

We start with the most simple yield function, namely a classical p - ψ yield function. Here, the pore ratio ψ is related to distention α by $\psi = \alpha - 1$. In classical p - ψ pore collapse models, yield commences when either σ_m reaches a critical value s_m or when σ_s reaches a critical value s_s . Both s_m and s_s depend only on the porosity. Such a yield criterion corresponds to a *rectangular* yield surface in shear vs. pressure space, as shown in Fig. 19.1. Such a model is clearly very crude. If the stress is at the critical shear surface, it will travel along that shear surface until σ_m reaches s_m ; prior to that moment, there is zero pore collapse.

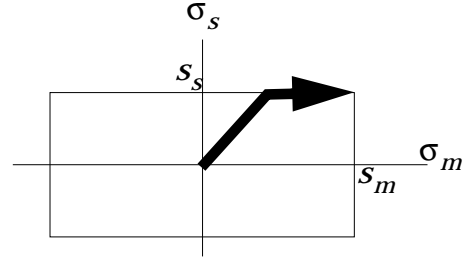


Figure 19.1. A p - ψ yield surface.

The stress path shown by the bold arrow corresponds to uniaxial strain (with a nonhardening matrix material so that the yield surface remains unchanged during the shear phase).

To improve upon the classical rectangular p - ψ yield surface, we introduce some curvature to "round off" the corners. Specifically, we add pressure dependence of yield by changing the yield function to the following form:

$$\left\{ \left(\frac{\sigma_m}{s_m} \right)^{2k} + \left(\frac{\sigma_s}{s_s} \right)^{2k} \right\}^{\frac{1}{2k}} - 1 \quad (19.1)$$

When the parameter k equals 1, the yield surface is ellipsoidal. As $k \rightarrow \infty$, the yield surface approaches the p - ψ rectangular surface. To provide an easier interface for users, the k value is defined *indirectly* through the use of a parameter γ that varies from 0 for an ellipsoidal yield surface to 1 for the rectangular yield surface. The user-specified value for γ is then converted (internally within the subroutines) to a value for k by the formula

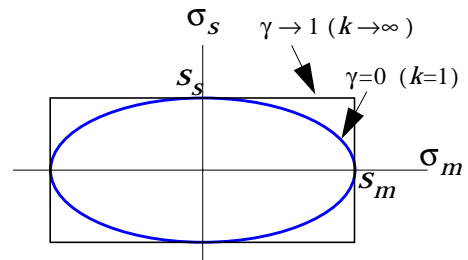


Figure 19.2. A nominal ellipsoidal yield surface.

$$k = \frac{-\ln 2}{2 \ln \left[\gamma + \frac{(1-\gamma)}{\sqrt{2}} \right]} \quad (19.2)$$

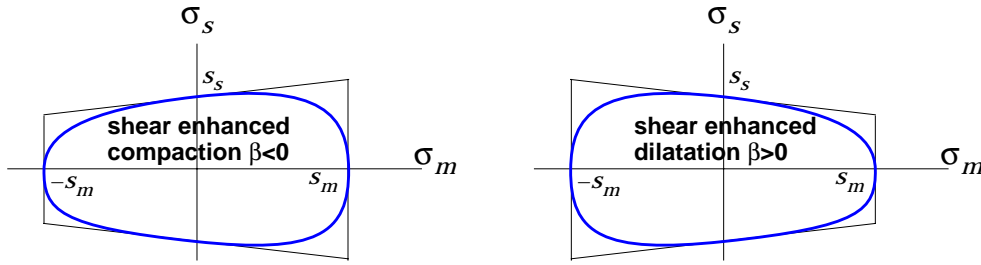


Figure 19.3. Shear-enhanced porosity compaction/dilatation. Consider a state of pure shear ($\sigma_m=0$). The parameter β is the slope of the yield surface outward normal. When $\beta < 0$, the normal to the yield surface has a negative isotropic component, meaning that pores will collapse in pure shear. When $\beta > 0$, the normal to the yield surface has a positive isotropic component, meaning that pores will expand in pure shear.

Now we wish to modify this yield surface so that simple shear can involve dilatation or compaction, as sketched in Fig. 19.3. This is accomplished by replacing s_s by

$$\hat{s}_s = s_s \left(1 - \beta \frac{\sigma_m}{s_m} \right), \quad (19.3)$$

If $\beta > 0$, then \hat{s}_s decreases as σ_m increases. The parameter β may be regarded as the slope of the yield surface’s *normal*. To prevent the yield surface from inverting, admissible values of the parameter β must satisfy

$$-1 < \beta < 1 \quad (19.4)$$

With the replacement defined in Eq. (19.3), the yield function becomes

$$\left\{ \left(\frac{\sigma_m}{s_m} \right)^{2k} + \left(\frac{\sigma_s}{\hat{s}_s} \right)^{2k} \right\}^{\frac{1}{2k}} - 1 \quad (19.5)$$

As sketched in Fig. 19.4, the final modification of the yield function allows s_m to have different values (s_m^T and s_m^C) in tension and compression. To accomplish this modification, the mean stress σ_m is replaced by

$$\hat{\sigma}_m = \sigma_m - \frac{1}{2}(s_m^T + s_m^C) \quad (19.6)$$

and s_m is then replaced by

$$\hat{s}_m = \frac{1}{2}(s_m^T - s_m^C) \quad (19.7)$$

With this, the yield function becomes

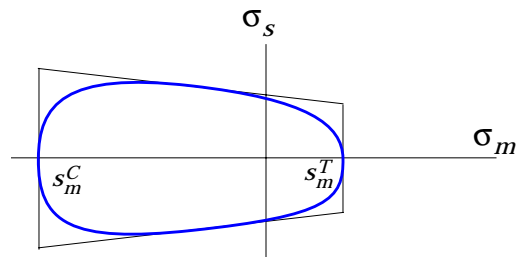


Figure 19.4. Different yield in compression and tension.

$$f(\sigma_m, \sigma_s, \Psi, \zeta) = \left\{ \left(\frac{\hat{\sigma}_m}{\hat{s}_m} \right)^{2k} + \left(\frac{\hat{\sigma}_s}{\hat{s}_s} \right)^{2k} \right\}^{\frac{1}{2k}} - 1 \quad (19.8)$$

where

$$\hat{\sigma}_m = \sigma_m - \frac{1}{2}(s_m^T + s_m^C) \quad \hat{\sigma}_s = \sigma_s \quad (19.9)$$

$$\hat{s}_m = \frac{1}{2}(s_m^T - s_m^C) \quad \hat{s}_s = s_s \left(1 - \beta \frac{\hat{\sigma}_m}{\hat{s}_m} \right) \quad (19.10)$$

In these equations, β , γ , s_s , s_m^C , and s_m^T are material parameters or, in the case of an evolving yield function, they are material functions of the porosity and the internal state variable(s) ζ . To keep things tractable, we will assume that β and γ are independent of Ψ and ζ .

To apply the CKP model, we require formulas for the gradients of the yield function. Referring to Eq. (19.8). To keep the equations manageable, define

$$f = \left\{ \left(\frac{\hat{\sigma}_m}{\hat{s}_m} \right)^{2k} + \left(\frac{\hat{\sigma}_s}{\hat{s}_s} \right)^{2k} \right\}^{\frac{1}{2k}} - 1 \quad (19.11)$$

$$g = \{1 + f\}^{1-2k} = \left\{ \left(\frac{\hat{\sigma}_m}{\hat{s}_m} \right)^{2k} + \left(\frac{\hat{\sigma}_s}{\hat{s}_s} \right)^{2k} \right\}^{\frac{1}{2k}-1} \quad (19.12)$$

$$A_m = \left(\frac{\hat{\sigma}_m}{\hat{s}_m} \right)^{2k-1} g \quad \text{and} \quad A_s = \left(\frac{\hat{\sigma}_s}{\hat{s}_s} \right)^{2k-1} g \quad (19.13)$$

$$\begin{aligned} B_{mm} &= \frac{\partial}{\partial \sigma_m} \left(\frac{\hat{\sigma}_m}{\hat{s}_m} \right) & B_{ms} &= \frac{\partial}{\partial \sigma_m} \left(\frac{\hat{\sigma}_s}{\hat{s}_s} \right) \\ B_{sm} &= \frac{\partial}{\partial \sigma_s} \left(\frac{\hat{\sigma}_m}{\hat{s}_m} \right) & B_{ss} &= \frac{\partial}{\partial \sigma_s} \left(\frac{\hat{\sigma}_s}{\hat{s}_s} \right) \\ B_{\Psi m} &= \frac{\partial}{\partial \Psi} \left(\frac{\hat{\sigma}_m}{\hat{s}_m} \right) & B_{\Psi s} &= \frac{\partial}{\partial \Psi} \left(\frac{\hat{\sigma}_s}{\hat{s}_s} \right) \\ B_{\zeta m} &= \frac{\partial}{\partial \zeta} \left(\frac{\hat{\sigma}_m}{\hat{s}_m} \right) & B_{\zeta s} &= \frac{\partial}{\partial \zeta} \left(\frac{\hat{\sigma}_s}{\hat{s}_s} \right) \end{aligned} \quad (19.14)$$

Here and throughout this section, the independent variables are $\{\sigma_m, \sigma_s, \Psi, \zeta\}$, so there is no need to explicitly indicate what is being held constant in the partial derivatives. By the way, derivatives of the yield function are computed only when the stress is off of the yield surface. Hence, no special treatment is required when $\hat{\sigma}_m = \hat{\sigma}_s = 0$. With the above definitions,

Default “dearth of data” (D.O.D.) yield function

$$\begin{aligned}
 \frac{\partial f}{\partial \sigma_m} &= B_{mm}A_m + B_{ms}A_s \\
 \frac{\partial f}{\partial \sigma_s} &= B_{sm}A_m + B_{ss}A_s \\
 \frac{\partial f}{\partial \psi} &= B_{\psi m}A_m + B_{\psi s}A_s \\
 \frac{\partial f}{\partial \zeta} &= B_{\zeta m}A_m + B_{\zeta s}A_s
 \end{aligned} \tag{19.15}$$

To help with the evaluation of the B_{ij} quantities, we introduce additional convenience quantities:

$$\begin{aligned}
 D_{mm} &= \frac{\partial \hat{\sigma}_m}{\partial \sigma_m} & D_{ms} &= \frac{\partial \hat{\sigma}_s}{\partial \sigma_m} \\
 D_{sm} &= \frac{\partial \hat{\sigma}_m}{\partial \sigma_s} & D_{ss} &= \frac{\partial \hat{\sigma}_s}{\partial \sigma_s} \\
 D_{\psi m} &= \frac{\partial \hat{\sigma}_m}{\partial \psi} & D_{\psi s} &= \frac{\partial \hat{\sigma}_s}{\partial \psi} \\
 D_{\zeta m} &= \frac{\partial \hat{\sigma}_m}{\partial \zeta} & D_{\zeta s} &= \frac{\partial \hat{\sigma}_s}{\partial \zeta}
 \end{aligned} \tag{19.16}$$

$$\begin{aligned}
 E_{mm} &= \frac{\partial \hat{s}_m}{\partial \sigma_m} & E_{ms} &= \frac{\partial \hat{s}_s}{\partial \sigma_m} \\
 E_{sm} &= \frac{\partial \hat{s}_m}{\partial \sigma_s} & E_{ss} &= \frac{\partial \hat{s}_s}{\partial \sigma_s} \\
 E_{\psi m} &= \frac{\partial \hat{s}_m}{\partial \psi} & E_{\psi s} &= \frac{\partial \hat{s}_s}{\partial \psi} \\
 E_{\zeta m} &= \frac{\partial \hat{s}_m}{\partial \zeta} & E_{\zeta s} &= \frac{\partial \hat{s}_s}{\partial \zeta}
 \end{aligned} \tag{19.17}$$

Then

$$\begin{aligned}
 B_{mm} &= \frac{(D_{mm}\hat{s}_m - E_{mm}\hat{\sigma}_m)}{\hat{s}_m^2}, & B_{ms} &= \frac{(D_{ms}\hat{s}_s - E_{ms}\hat{\sigma}_s)}{\hat{s}_s^2} \\
 B_{sm} &= \frac{(D_{sm}\hat{s}_m - E_{sm}\hat{\sigma}_m)}{\hat{s}_m^2}, & B_{ss} &= \frac{(D_{ss}\hat{s}_s - E_{ss}\hat{\sigma}_s)}{\hat{s}_s^2} \\
 B_{\psi m} &= \frac{(D_{\psi m}\hat{s}_m - E_{\psi m}\hat{\sigma}_m)}{\hat{s}_m^2}, & B_{\psi s} &= \frac{(D_{\psi s}\hat{s}_s - E_{\psi s}\hat{\sigma}_s)}{\hat{s}_s^2} \\
 B_{\zeta m} &= \frac{(D_{\zeta m}\hat{s}_m - E_{\zeta m}\hat{\sigma}_m)}{\hat{s}_m^2}, & B_{\zeta s} &= \frac{(D_{\zeta s}\hat{s}_s - E_{\zeta s}\hat{\sigma}_s)}{\hat{s}_s^2}
 \end{aligned} \tag{19.18}$$

Referring to Eqs. (19.9) through (19.10) the D_{ij} and E_{ij} quantities are

$$\begin{aligned}
 D_{mm} &= 1 & D_{ms} &= 0 \\
 D_{sm} &= 0 & D_{ss} &= 1 \\
 D_{\psi m} &= -\frac{1}{2}(s_{m,\psi}^T + s_{m,\psi}^C) & D_{\psi s} &= 0 \\
 D_{\zeta m} &= -\frac{1}{2}(s_{m,\zeta}^T + s_{m,\zeta}^C) & D_{\zeta s} &= 0
 \end{aligned} \tag{19.19}$$

$$\begin{aligned}
 E_{mm} &= 0 & E_{ms} &= -s_s \beta B_{mm} \\
 E_{sm} &= 0 & E_{ss} &= -s_s \beta B_{sm} \\
 E_{\psi m} &= \frac{1}{2}(s_{m,\psi}^T - s_{m,\psi}^C) & E_{\psi s} &= s_{s,\psi} \left(\frac{\hat{s}_s}{s_s} \right) - s_s \beta B_{\psi m} \\
 E_{\zeta m} &= \frac{1}{2}(s_{m,\zeta}^T - s_{m,\zeta}^C) & E_{\zeta s} &= s_{s,\zeta} \left(\frac{\hat{s}_s}{s_s} \right) - s_s \beta B_{\zeta m}
 \end{aligned} \tag{19.20}$$

For computational convenience, we compute the D’s and E’s that end in “m”, followed by the B’s that end in “m”. Then we get the D’s and E’s that end in “s”, followed by the B’s that end in “s”. In our numerical implementation, this work is performed in the routine called `YLLDER`.

The D.O.D. crush curves

Recall that s_s , s_m^T , and s_m^C are presumed to be user-supplied functions of the pore ratio ψ and the internal state variable(s) ζ . If any data are available at all, it is usually the p- ψ curve, which gives the pore ratio as a function of the pressure for isotropic (hydrostatic) compression. Such a function can be inverted to obtain the s_m^C function. Faced with a dearth of data, a good place to start might be to use the (implicit) Gurson crush curves:

$$s_m^C = -\bar{\sigma} \sqrt{2} \ln\left(\frac{1}{f_v}\right) = -\bar{\sigma} \sqrt{2} \ln\left(\frac{1+\psi}{\psi}\right) = \bar{\sigma} \sqrt{2} \ln\left(\frac{\psi}{1+\psi}\right) \tag{19.21}$$

$$s_s = \bar{\sigma}(1 - f_v) = \bar{\sigma} \left(\frac{1}{1+\psi} \right) \tag{19.22}$$

Here, $\bar{\sigma}$ is a user-specified parameter that changes the size of the yield surface without changing its shape. To allow hardening, $\bar{\sigma}$ is interpreted as the internal state variable ζ . For the tensile growth function, s_m^T , a D.O.D. implementation uses the s_m^C curve with $\bar{\sigma}$ effectively reduced by a user-specified factor r (called `YRATIO` in the coding) so that

$$s_m^T = -r s_m^C \tag{19.23}$$

Typically, one would select $0 < r \leq 1$. Choosing $r=0$ would make the material have zero strength in tension. Choosing $r=1$ would make the strength in tension equal to the strength in compression. With the above choices,

Default “dearth of data” (D.O.D.) yield function

$$s_{m, \psi}^C = \frac{\bar{\sigma} \sqrt{2}}{\psi(1 + \psi)} \quad s_{m, \psi}^T = -r s_{m, \psi}^C \quad s_{s, \psi} = \frac{-\bar{\sigma}}{(1 + \psi)^2} \quad (19.24)$$

and

$$s_{m, \zeta}^C = \frac{s_m^C}{\bar{\sigma}} \quad s_{m, \zeta}^T = -r s_{m, \zeta}^C \quad s_{s, \zeta} = \frac{s_s}{\bar{\sigma}} \quad (19.25)$$

Clearly, rather tedious mathematics has been required for us to precisely describe the “dearth of data (D.O.D.)” yield function. Users of this yield function do not need all of the above detail. The key points that users must understand are the effects of the D.O.D. material parameters that are listed in Table 19.1 and graphically defined in Figures 19.1 through 19.4.

Table 19.1: Material parameters defining the evolving yield function

Symbol	ASCII	Description	Restriction
β	YSLOPE	shear-enhanced compaction slope. Choose $\beta=0$ to neglect this effect. Choose β approaching ± 1 to maximize the effect. Choose $\beta > 0$ to cause pores to grow in shear. Choose $\beta < 0$ to make pores collapse in shear.	$ \beta < 1$
γ	YCURVE	yield curvature parameter. =0 for ellipsoidal, =1 for the rectangular p- ψ description.	$0 \leq \gamma < 1$
$\bar{\sigma}$	SBY	Matrix yield stress.	$\bar{\sigma} > 0$
r	YRATIO	ratio of tensile yield to compressive yield in purely isotropic stress.	$0 < r \leq 1$

Verification results

Fig. 19.5 verifies that the pressure follows the user-specified crush curve under isotropic loading.

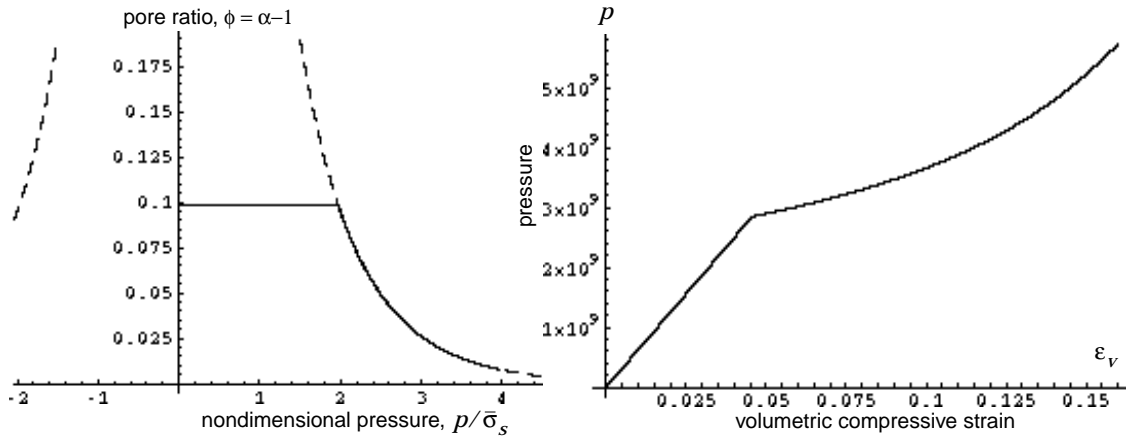


Figure 19.5. p - α curve and stress-strain response. The computed parametric plot (solid line) of pore ratio vs. nondimensional pressure exactly follows the user-specified theoretical p - α function (dashed line). The stress response has a fundamentally different character than the uniaxial response in Fig. 19.7 (which uses identical baseline inputs).

Fig. 19.6 shows the effect of varying β (=YSLOPE) under deviatoric shear strain. For the case where $\beta > 0$, the porosity increases and the σ_{11} stress component decreases. Interestingly, the stress deviator magnitude σ_s increases, which might seem counter-intuitive at first glance since increased porosity usually causes σ_s to decrease. The explanation is that Fig. 19.6 is a *strain controlled* loading.* When pores grow, we know that the *plastic* volumetric strain rate is positive. Therefore, to keep the *total* volumetric strain rate equal to zero (as specified in our strain-controlled path), the *elastic* volumetric strain rate must be negative. Hence, the mean stress must be decreasing. When $\beta > 0$, however, the slope of the yield surface is negative. Thus, if σ_m decreases, σ_s must increase, which is indeed observed in our calculations.

Fig. 19.7 shows the effects of varying YSLOPE, YCURVE, and YRATIO for uniaxial strain. Importantly, *all* of the input sets used in Figs. 19.7 would predict the *same* response (namely, Fig. 19.5) if they were instead loaded under hydrostatic compression. Likewise, all of the inputs used in Figs. 19.7 would also predict the *same* response (namely, Fig. 19.6) if they were loaded under deviatoric strain with YSLOPE=0.0. The distinctions afforded by YSLOPE,

* The situation here is analogous to contrasting behaviors observed for heating a material. If the strain is constrained, then the stress will decrease (become compressive). If the stress is constrained, then the volume will increase. Here we have a strain-controlled loading that produces a stress change that is the opposite of what one would expect under stress-controlled loading.

YCURVE, and YRATIO can be seen only for mixed loadings that are neither pure shear nor pure hydrostatic. This reiterates why materials cannot be fully characterized unless tested under numerous strain paths, including strain reversals.

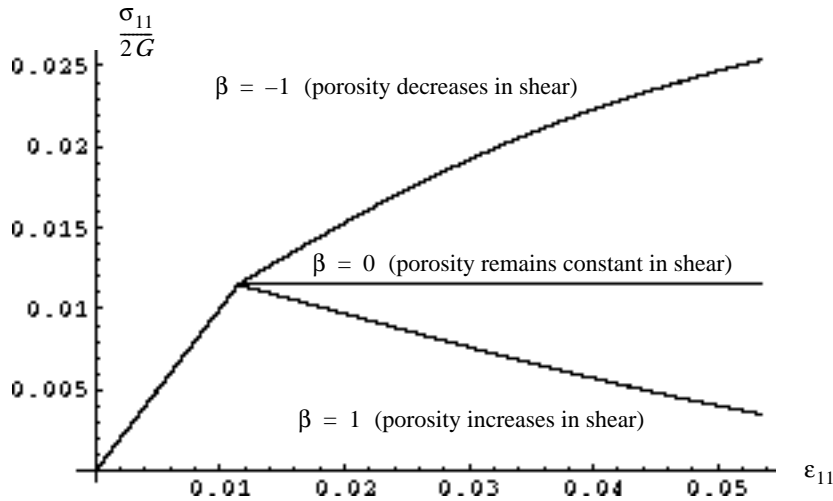


Figure 19.6. Effect of changing YSLOPE. For this strain-controlled calculation, the strain is diagonal and increases linearly in time until $\epsilon_{11} = -0.053 = -2\epsilon_{22} = -2\epsilon_{33}$. Note that this is a volume preserving shearing strain and therefore the mean stress is zero during the elastic loading. However, the means stress changes upon pore growth/expansion. When $\beta=0$, the response (to this strain path) is similar to a traditional Von Mises model under simple shear.

Fig. 19.7(a) shows how changing YCURVE, γ , affects the stress-strain response under uniaxial strain. Initial yield occurs at nearly the same stress level. For $\gamma = 0$, the yield surface is ellipsoidal and (because the outward normal has a volumetric component) yield is immediately accompanied by pore collapse. However, for $\gamma = 1$, yield is initially like a simple Von Mises model (with no pore collapse) until the pressure cap is reached and pore collapse begins in earnest. Consequently, pore collapse initiates at a higher stress for p - α type models. It is important that we illustrated the effect of YCURVE by using a uniaxial strain path because there would be no distinction between the two models for purely isotropic or purely deviatoric strain paths.

Fig. 19.7(b) shows that putting YRATIO=0.5 makes the yield in tension equal to half that of the yield in compression. There is no difference during initial compression, but there would be a difference in *recompression* because the two materials would have evolved porosity differently during the tensile phase.

Fig. 19.7(c) shows the effect of changing the YSLOPE parameter, β , under uniaxial strain. This figure is not as informative as Fig. 19.6 in illustrating the effect of YSLOPE. Interesting structure (such as the double curvature) occurs under uniaxial strain when $\beta < 0$.

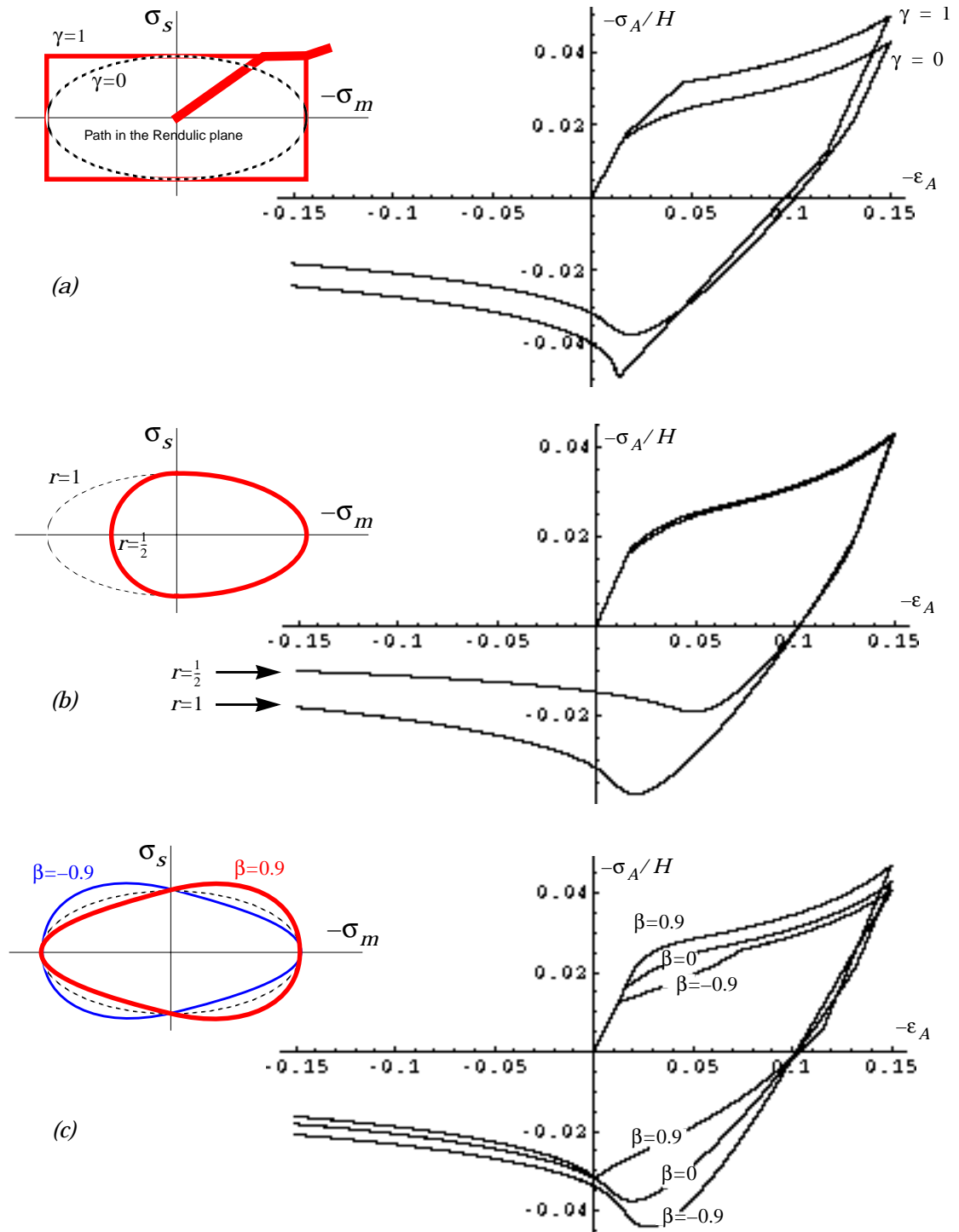


Figure 19.7. Effect of changing (a) YCURVE, (b) YRATIO, and (c) YSLOPE for uniaxial strain compression followed by tension.

Allowing finite crush pressures

The crush curve in Fig 19.5 is the one *implied* by the intercept of the Gurson yield surface on the pressure axis. This implied crush curve (Eq. 19.21) makes the porosity *asymptote* to zero as the pressure increases. Thus, according to the Gurson theory, an infinite amount of pressure is required to reduce the porosity down to zero.*

Physically, users may wish for complete crush to occur a lower pressure than that implied by the nominal crush function. For this reason, we allow the user to specify a critical pressure that corresponds to complete crush. To utilize this parameter, we assume that the crush curve is identical to the nominal (e.g. Gurson) curve up until a critical transition point (ψ^t, s_m^t) , at which point the crush curve goes linearly down to the crush value s_m^{crush} .

Of course, the critical transition point, (ψ^t, s_m^t) , must lie on both the nominal and linear parts of the crush curve. Furthermore, as shown in Fig. 19.8, we demand that the slope be continuous at the (ψ^t, s_m^t) transition point. Thus, given the user-supplied equation for the nominal crush curve (or the default Eq. 19.21) and given the user-specified value for s_m^{crush} , we can compute the coordinates of the (ψ^t, s_m^t) transition point. In our numerical implementation, this computation is performed in the routine called SCNSTRNT. That routine also *imposes* a transition point in the tensile regime so that the slope of the tensile growth curve will never be too shallow (see discussion on page 45).

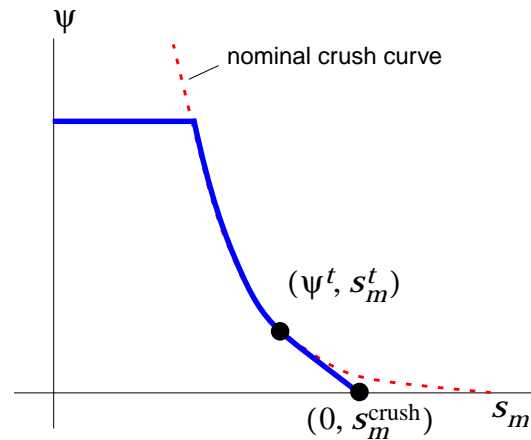


Figure 19.8. Crush transition model.

* Of course, in a finite precision numerical calculation porosity would go to zero at a finite pressure because of numerical underflow.

Measuring a crush curve

In its classical p - α sense, a crush curve is a plot of the distention parameter α (which is the ratio of solid density to porous density) versus pressure p measured under isotropic loading conditions. Suppose this p - α function is denoted by g :

$$\alpha = g(p) \quad (19.26)$$

This function is difficult to measure directly because it is difficult to measure porosity directly. Therefore, we here describe an *indirect* method of converting a measured stress-strain curve into a crush curve. By using this method, a crush curve can be constructed that will almost exactly match any measurement of hydrostatic pressure vs. volumetric strain.

Suppose that the stress strain curve under hydrostatic loading is known to be

$$p = h(\varepsilon) \quad (19.27)$$

where ε is the volumetric strain. Experimentalists differ in how they define strain, so the upcoming analysis will use the Seth-Hill generalized strain measure

$$\varepsilon = -\frac{1}{\beta} \left[\left(\frac{V}{V_o} \right)^\beta - 1 \right] \quad (19.28)$$

where V/V_o is the ratio of the current volume to the initial volume, and β is a parameter that may be set according to how the strain is defined by the experimentalist.*

The plastic strain ε^P is defined by the unloaded volume divided by the initial volume. If V^v and V^s denote the unloaded void and solid volumes respectively, then

$$\varepsilon^P = -\frac{1}{\beta} [\lambda^\beta - 1], \text{ where } \lambda \equiv \frac{V^v + V^s}{V_o^v + V_o^s} = \frac{\psi + 1}{\psi_o + 1} = \frac{\alpha}{\alpha_o} \quad (19.29)$$

In writing the last form for the plastic volumetric stretch λ , we have imposed our assumption that the solid matrix material is plastically incompressible so that $V^s = V_o^s$. Next, we recalled the definition of the pore ratio ψ is void volume divided by solid volume. Finally, we recalled that the distention parameter α is defined by $\alpha = \psi + 1$.

* For example, if the strain is engineering $-(V - V_o)/V_o$, then $\beta=1$. If the strain is logarithmic $\ln(V/V_o)$, then $\beta \rightarrow 0$. If the strain is Lagrangian, then $\beta = 2$, etc.

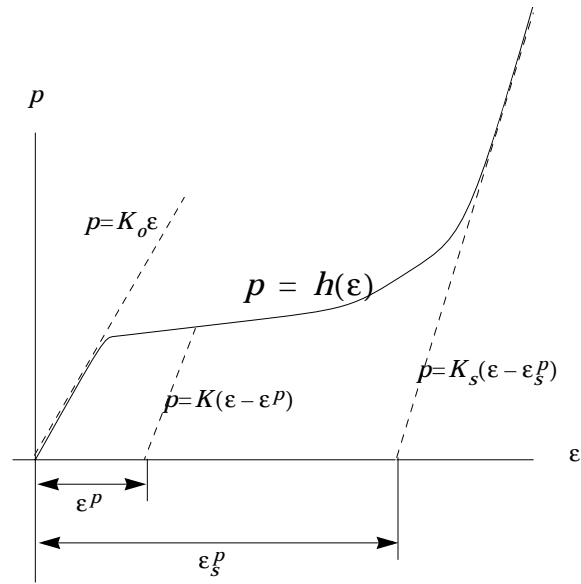


Figure 19.9. Inferring crush data from a hydrostatic stress-strain plot.

The initial slope of the measured stress strain curve is the initial bulk modulus:

$$K_o = h'(0) \quad (19.30)$$

We will assume that the experiment deforms the material to full crush-up so that the final slope of the stress-strain measurement is the solid bulk modulus:

$$K_s = h'(\varepsilon^{\max}) \quad (19.31)$$

These two limiting elastic lines have the equations

$$p = K_o \varepsilon \quad (19.32)$$

and

$$p = K_s(\varepsilon - \varepsilon_s^p) \quad (19.33)$$

we know that this last line passes through the point $(\varepsilon^{\max}, p^{\max})$. Thus, the final “solid” plastic strain must be given by

$$\varepsilon_s^p = \varepsilon^{\max} - \frac{p^{\max}}{K_s} \quad (19.34)$$

This final plastic strain corresponds to completely crushing out the pores. Therefore, the final unloaded volume must equal the solid volume. Recall that the CKP assumes that plastic volume change of the solid matrix material is negligible. Therefore,

$$\varepsilon_s^p = -\frac{1}{\beta} \left[\left(\frac{V_s}{V_o} \right)^\beta - 1 \right] = -\frac{1}{\beta} [(1 - f_v^o)^\beta - 1], \quad (19.35)$$

where f_v^o is the initial volume fraction of pores. Solving for f_v^o gives the initial porosity.

$$f_v^o = 1 - (1 - \beta \varepsilon_s^p)^{1/\beta} \quad (19.36)$$

We are now going to apply similar concepts to express the change of porosity as a function of the loading pressure. The initial and final linear unloading lines intersect at the point (ε^*, p^*) , where

$$\varepsilon^* = \frac{K_s \varepsilon_s^p}{K_s - K_o} \quad \text{and} \quad p^* = K_o \varepsilon^* \quad (19.37)$$

As an approximation, we will assume that all of the unloading lines pass through the same (ε^*, p^*) point. The equation of the intermediate unloading line is

$$p = K(\varepsilon - \varepsilon^p) \quad (19.38)$$

Thus, if this line passes through the point (ε^*, p^*) , then

$$p^* = K(\varepsilon^* - \varepsilon^p) \quad (19.39)$$

We know that the intermediate unloading line also passes through the stress-strain loading curve $h(\varepsilon)$. Thus, we know

$$h(\varepsilon) = K(\varepsilon - \varepsilon^p) \quad (19.40)$$

Combining the last two equations, and solving for ε^p gives

$$\varepsilon^p = \frac{\varepsilon - \varepsilon^* h(\varepsilon)}{1 - h(\varepsilon)} \quad (19.41)$$

Recalling Eq. (19.29) this means that

$$\frac{\alpha}{\alpha_o} = \left[1 - \beta \left(\frac{\varepsilon - \varepsilon^* h(\varepsilon)}{1 - h(\varepsilon)} \right) \right]^{1/\beta} \quad (19.42)$$

By the end of the stress-strain path, we know that all of the pores have crushed out. Therefore, we $\varepsilon = \varepsilon^{\max}$, we know that $\alpha = 1$. Consequently,

$$\alpha_o = \left[1 - \beta \left(\frac{\varepsilon - \varepsilon^* h(\varepsilon^{\max})}{1 - h(\varepsilon^{\max})} \right) \right]^{-\left(\frac{1}{\beta}\right)} \quad (19.43)$$

Once α_o is known, Eq. (19.42), represents the distention parameter α as a function of the load strain ε . Recall that $h(\varepsilon)$ represents pressure as a function of load strain ε . Taken together, $h(\varepsilon)$ and Eq. (19.42) parametrically define the crush curve α as a function of pressure p , which is the function g from Eq. (19.26).

Now that the function g from Eq. (19.26) is known, it may be converted to our isomorphic definition of a crush curve by recognizing

$$\alpha = \psi + 1 \quad (19.44)$$

and $p = s_m / \sqrt{3}$. Furthermore, for our implementation, we need s_m as a function of ψ . Thus, Eq. (19.44) may be written $p = g^{-1}(\alpha)$, or

$$s_m = \sqrt{3} g^{-1}(\psi + 1) \quad (19.45)$$

This is the final expression for the crush curve. In future work, we intend to apply this result to a measured hydrostatic stress-strain function to obtain the crush curve in tabular form. Future implementations of the CKP model will be able to process such tabular crush curves.

20. Concluding remarks

This report has detailed the theory and implementation of a general model for porous solids. The model is called the Consistent Kinetics Porosity (CKP) model because the individual components of the model have been assembled and implemented in a self-consistent manner. To handle material nonlinearity, the model is necessarily presented in rate form, which then permits a closed-form solution for the rate of change of the state. The CKP model includes the following physical features

- Isotropic linear elastic response with porosity dependent moduli.
- A yield criterion that depends on the pressure, equivalent shear stress, porosity, and the yield stress of the matrix material.
- Kinematical connection between porosity and plastic dilatation consistent with plastic incompressibility of the matrix material.
- Normality of the *plastic part* of the strain rate to the yield surface (i.e., the plastic response is “associative”).
- Inelastic strain rates from void nucleation and phase transformation of the matrix material. These rates lead to non-normality of the total inelastic strain rate even though the plastic strain rate is associative.
- Hardening of the matrix yield stress.
- Rigorous plastic consistency that requires the stress to remain on the yield surface throughout any quasistatic interval of plastic straining.
- Overstress rate-dependence that permits the dynamic stress to lie transiently outside the yield surface at large strain rates.
- Satisfaction of the principle of material frame indifference (PMFI) through application of the model in the unrotated polar frame.
- A default yield function that permits users to quickly generalize a simple p - α model to include the effect of shear on pore collapse.

While the above list is certainly extensive, it by no means approaches the full range of complexities that can be encountered for a porous material. The model has been shown capable of reproducing shock-loading response of materials of interest to us, but it is well known that many different material paradigms are *also* capable of matching simple shock loading data. A larger suite of tests is needed to better validate the model. The greatest limitation (or greatest virtue, depending on your point of view) of the CKP model is that *it does not address what the yield function should be*. The CKP model is simply a general framework in which the user can readily explore the effect of different yield functions. We have described a procedure by which *any* isotropic stress-strain curve can be matched *exactly* by defining the isotropic porosity dependence of the yield function appropriately. Much more validation work is needed to test the CKP model (and its user-supplied yield function) under service loadings that include different levels of shear stress and load reversals. We expect that limitations such as the assumption of isotropy will have to be rectified in order to fully realize the potential of the CKP model.

REFERENCES

- ¹ Brannon, R.M. (1999) A consistent kinetics porosity (CKP) model, in: **Shock Compression of Condensed Matter - 1999**, eds. M.D. Furnish, L.C. Chhabildas, and R.S. Hixson, American Institute of Physics publication no. 1-56396-293-8.
- ² Boucheron, E.A., Budge, K.G., Carrol, D.E., Carrol, S.K, Drake, R.R., Hail, T.A., Peery, J.F., Petney, S.V., Robinson, A.C., Summers, R.M., Trucano, T.G., Weatherby, J.R., Wong, M.K.W. (1999) ALEGRA: User Input and Physics Descriptions, *Sandia National Laboratories report No. SAND99-3012*.
- ³ Summers, R.M., et al. (1997), Recent progress in ALEGRA development and application to ballistic impacts, *Int. J. Impact Engng.*, Vol. 20, pp. 779-788.
- ⁴ Brannon, R.M., and Wong, M.K. (1996) MIG Version 0.0 Model Interface Guidelines: Rules to Accelerate Installation of Numerical Models Into Any Compliant Parent Code, *Sandia National Laboratories report No. SAND96-2000*.
- ⁵ Tuttle, B.A., Yang, P., Gieske, J.H., Voigt, J.A., Scofield, T.W., Zeuch, D.H., and Olson, W.R. (2000) Pressure Induced Phase Transformation of Controlled Porosity Pb(Zr_{0.95}Ti_{0.05})O₃ Ceramics., submitted to *Journal of the American Ceramic Society*.
- ⁶ Glass, S.J. (1997) Internal Sandia Memo Jan 15.
- ⁷ Setchell, R.E. (1998) unpublished work for Sandia National Laboratories.
- ⁸ Herrmann, W. (1969) Constitutive equation for the dynamic compaction of ductile porous materials, *J. Appl. Phys.* **40**, 2490-2499.
- ⁹ Gurson, A.L. (1977) Continuum theory of ductile rupture by void nucleation and growth: Part 1 — Yield criteria and flow rules for porous ductile media., *J. Engng Mater. Technol* **99**, pp. 2-15.
- ¹⁰ Haghi, M. and Anand, L. (1992) A constitutive model for isotropic porous elastic-viscoplastic metals, *Mechanics of Materials* **13**, p. 37.
- ¹¹ Lubliner, Jacob (1990) **Plasticity Theory**, MacMillian.
- ¹² Le Roy, G., Embury, J.D., Edwards, G., and Ashby, M.F. (1981) A model of ductile fracture based on the nucleation and growth of voids. *Acta Metall.* **29** 1509-1522.
- ¹³ Tvergaard, V. (1998) Interaction of very small voids with larger voids., *Int. J. Solids and Structures*, **35/30**, pp. 3989-4000.
- ¹⁴ Berg, C.A. (1970) Plastic dilation and void interaction. In: **Inelastic Behavior of Solids**, M.F. Kanninen et al. (eds.), McGraw-Hill, New York, pp. 171-210.
- ¹⁵ Needleman, A. and Tvergaard, V. (1984) An analysis of dimpled rupture in notched bars, *J. Mech. Phys. Solids* **33**, p. 25.
- ¹⁶ Worswick, M.J. and Pick, R.J. (1995) Void growth and coalescence during high velocity impact, *Mechanics of Materials* **19**, 293-309.
- ¹⁷ Kopic, J. and Needleman, A. (1988) Void growth and coalescence in porous plastic solids, *Int J. Solids Structures* **24**, pp. 835-851.
- ¹⁸ Pardoen, T. and Hutchinson, J.W. (2000) An extended model for void growth and coalescence. *J. Mech. Phys. Solids* **48** pp. 2467-2512.
- ¹⁹ Leblond, J.-B. and Perrin, G. (1999) A self-consistent approach to coalescence of cavities in inhomogeneously voided ductile solids. *J. Mech. and Physics of Solids* **47**, pp. 1823-1841.
- ²⁰ Detournay, E., and Cheng, A. H.-D. (1993) Fundamentals of poroelasticity. In: **Comprehensive Rock Engineering**, ed. C. Fairhurst, Pergamon Press, NY.

- ²¹ Zhao, Y.H., Tandon, G.P., and Weng, G.J. (1989) *Acta Mechanica* **76**, p. 105.
- ²² Brannon, R.M., and Drugan, W.J. (1993) Influence of nonclassical elastic-plastic features on shock wave existence and spectral solutions, *J. Mech. Phys. Solids* **41** (2), pp. 297-330.
- ²³ Dienes, John K. (1979) On the analysis of Rotation and Stress Rate in Deforming Bodies, *Acta Mechanica* **32**, 217-232.
- ²⁴ Malvern, L.E. (1969) **Introduction to the Mechanics of a Continuous Medium**, Prentice-Hall, Inc. Englewood Cliffs, NJ.
- ²⁵ Hill, R. (1950) **The mathematical theory of plasticity**, Oxford University Press, New York.
- ²⁶ Chakrabarty, J. (1987) **Theory of Plasticity**, McGraw-Hill.
- ²⁷ Duva, J.M. and Hutchinson, J.W. (1984) Constitutive potentials for dilutely voided nonlinear materials, *Mechanics of Materials* **3** pp. 41-54.
- ²⁸ Brannon, R.M. (1999) Geometric Interpretation of Radial and Oblique Return Algorithms for the numerical solution of Plasticity Equations, Draft available at me.unm.edu/~rmbrann/RadialReturn.pdf, Sandia National Laboratories report in process.
- ²⁹ Wilkens, M.L. (1969) Calculation of Elastic-Plastic Flow, *Lawrence Radiation Laboratory report UCRL-7322* (revised).
- ³⁰ Needleman, A. and Rice, J.R. (1978) in: **Mechanics of Sheet Metal Forming** (edited by D.P. Koistinen and N.-M. Wang), Plenum, NY, p. 237.
- ³¹ Brannon, R.M. (1998) Caveats concerning conjugate stress and strain measures for frame indifferent anisotropic elasticity, *Acta Mechanica* **129** (#1-2) pp. 107-116.
- ³² Brannon, R.M. (2000) Tensile instabilities for porous plasticity models. in: **Proceedings of the International Symposium on Plasticity and its current Applications**, Whistler, CANADA July 17.
- ³³ Ragab, A.R. and Saleh, A.R. (1999) Evaluation of constitutive models for voided solids. *Int. J. Plasticity* **15**, pp. 1041-1065.
- ³⁴ Tvergaard, V. (1982) On localization in ductile materials containing spherical voids. *Int. J. Fract.* **18**, 237-252.
- ³⁵ Tvergaard, V. (1989) Materials failure by void growth to coalescence. *Advances in Appl. Mech.* **27**, 83.
- ³⁶ Carroll, M.M. (1980) Mechanical Response of Fluid-saturated Porous Materials, in **Proc. 15th Int. Cong. on Theoretical and Applied Mechanics**, F.P.J. Rimrott and R. Tabarrok eds., North Holland, NY, pp. 251-262.
- ³⁷ Pan, J., Saje, M., and Needleman, A. (1983) Localization of deformation in rate sensitive porous plastic solids. *Int. J. Fracture* **2**, 261.
- ³⁸ Ramakrishnan, N., and Arunachalam, V.S. (1990) Effective Elastic Moduli of Porous Solids, *J. Mat. Sci.* **25**, pp. 3930-3937.
- ³⁹ Rice, Roy W. (1998) **Porosity of ceramics**, Marcel Decker, Inc. New York, NY.
- ⁴⁰ Biswas, D.R. (1976) Influence of Porosity on the Mechanical Properties of Lead-Zirconate-Titanate Ceramics, *Materials and Molecular Research Division Annual Report*, Lawrence Berkeley Laboratory, University of California, Berkeley, pp. 110-113.
- ⁴¹ Wolfram, S. (1996) **The Mathematica Book**, 3rd Ed., Wolfram Media, Inc. and Cambridge University Press.
- ⁴² Thompson, S.L., and Kmetyk, L.N. (1991) HISPLT: A time-history graphics post processor users' guide, *Sandia National Laboratories report No. SAND91-1767*.

APPENDIX A. Solution of the governing equations

Equations (10.3), (12.3), (11.1b), (11.13a), and (11.13b) form the basic equations for the QCKP model. They are:

$$\dot{\zeta} = h\xi\dot{\lambda} \quad (\text{A.1})$$

$$\dot{\psi} = \sqrt{3}(1 + \psi)F_m\dot{\lambda} + \dot{\psi}^n, \text{ where } \dot{\delta}^n = \frac{\dot{\psi}^n}{\sqrt{3}(1 + \psi)} \quad (\text{A.2})$$

$$F_m\dot{\sigma}_m + F_s\dot{\sigma}_s + F_\psi\dot{\psi} + F_\zeta\dot{\zeta} = 0 \quad (\text{A.3})$$

$$\dot{\sigma}_m = 3K(\mathbf{d}:\hat{\mathbf{I}} - F_m\dot{\lambda} - \dot{\delta}^n) - \kappa_m\sigma_m\dot{\psi} + \dot{\gamma}\sigma_m \quad (\text{A.4})$$

$$\dot{\sigma}_s = 2G(\mathbf{d}:\hat{\mathbf{S}} - F_s\dot{\lambda}) - \gamma_m\sigma_s\dot{\psi} + \dot{\gamma}\sigma_s \quad (\text{A.5})$$

This set of five equations is to be solved for the following five unknowns:

- $\dot{\sigma}_m$, the rate of the isomorphic projected mean stress.
- $\dot{\sigma}_s$, the rate of the isomorphic projected effective shear stress.
- $\dot{\psi}$, the rate of the pore ratio.
- $\dot{\lambda}$, the “plastic segment” (= magnitude of the plastic strain rate divided by ξ).
- $\dot{\zeta}$, the rate of the internal state variable(s).

This appendix presents the solution of the above equations in a form that is best suited for numerical implementation. From Eqs. (A.1) and (A.2), we see that $\dot{\zeta}$ and $\dot{\psi}$ become known as soon as $\dot{\lambda}$ is known. Hence, we focus on solving for $\dot{\lambda}$. First incorporate Eqs. (A.1) and (A.2) into the remaining equations so that the governing system can be reduced to following three equations and three unknowns:

$$F_m\dot{\sigma}_m + F_s\dot{\sigma}_s + (\sqrt{3}(1 + \psi)F_mF_\psi + F_\zeta h\xi)\dot{\lambda} + \dot{\psi}^n F_\psi = 0 \quad (\text{A.6})$$

$$\dot{\sigma}_m = 3K(\mathbf{d}:\hat{\mathbf{I}} - \dot{\delta}^n) - \dot{\psi}^n \kappa_m \sigma_m + \dot{\gamma}\sigma_m - (3KF_m + \sqrt{3}(1 + \psi)F_m\kappa_m\sigma_m)\dot{\lambda} \quad (\text{A.7})$$

$$\dot{\sigma}_s = 2G\mathbf{d}:\hat{\mathbf{S}} - \dot{\psi}^n \gamma_m \sigma_s + \dot{\gamma}\sigma_s - (2GF_s + \sqrt{3}(1 + \psi)F_m\gamma_m\sigma_s)\dot{\lambda}. \quad (\text{A.8})$$

Putting (A.7) and (A.8) into (A.6) gives

$$\begin{aligned} & F_m(3K(\mathbf{d}:\hat{\mathbf{I}} - \dot{\delta}^n) - \dot{\psi}^n \kappa_m \sigma_m + \dot{\gamma}\sigma_m) - F_m(3KF_m + \sqrt{3}(1 + \psi)F_m\kappa_m\sigma_m)\dot{\lambda} \\ & + F_s(2G\mathbf{d}:\hat{\mathbf{S}} - \dot{\psi}^n \gamma_m \sigma_s + \dot{\gamma}\sigma_s) - F_s(2GF_s + \sqrt{3}(1 + \psi)F_m\gamma_m\sigma_s)\dot{\lambda} \\ & + (\sqrt{3}(1 + \psi)F_mF_\psi + F_\zeta h\xi)\dot{\lambda} \\ & + \dot{\psi}^n F_\psi = 0. \end{aligned} \quad (\text{A.9})$$

APPENDIX A. Solution of the governing equations

Solving this equation for $\dot{\lambda}$ gives

$$\dot{\lambda} = \frac{F_m((3K(\underline{\underline{\mathbf{d}}}:\underline{\underline{\hat{\mathbf{I}}}} - \dot{\delta}^n) - \dot{\psi}^n \kappa_m \sigma_m + \dot{\Upsilon} \sigma_m) + F_s(2G\underline{\underline{\mathbf{d}}}:\underline{\underline{\hat{\mathbf{S}}}} - \dot{\psi}^n \gamma_m \sigma_s + \dot{\Upsilon} \sigma_s) + \dot{\psi}^n F_\psi)}{F_m(3KF_m + \sqrt{3}(1+\psi)F_m \kappa_m \sigma_m) + F_s(2GF_s + \sqrt{3}(1+\psi)F_m \gamma_m \sigma_s) - (\sqrt{3}(1+\psi)F_m F_\psi + F_\zeta h \xi)} \quad (\text{A.10})$$

With a little rearrangement, this becomes

$$\dot{\lambda} = \frac{3KF_m(\underline{\underline{\mathbf{d}}}:\underline{\underline{\hat{\mathbf{I}}}} - \dot{\delta}^n) + 2GF_s\underline{\underline{\mathbf{d}}}:\underline{\underline{\hat{\mathbf{S}}}} + \dot{\psi}^n(F_\psi - \kappa_m \sigma_m F_m - \gamma_m \sigma_s F_s) + \dot{\Upsilon}(F_m \sigma_m + F_s \sigma_s)}{3KF_m^2 + 2GF_s^2 + \sqrt{3}(1+\psi)F_m(\kappa_m \sigma_m F_m + \gamma_m \sigma_s F_s - F_\psi) - h \xi F_\zeta}. \quad (\text{A.11})$$

Note that

$$\underline{\underline{\mathbf{d}}}: \underline{\underline{\hat{\mathbf{I}}}} = \frac{\underline{\underline{\mathbf{d}}}: \underline{\underline{\mathbf{I}}}}{\sqrt{3}} = \frac{\text{tr } \underline{\underline{\mathbf{d}}}}{\sqrt{3}}. \quad (\text{A.12})$$

Recall from Eq. (7.1) that

$$\underline{\underline{\mathbf{d}}}^n = \dot{\delta}^n \underline{\underline{\hat{\mathbf{I}}}}. \quad (\text{A.13})$$

The nucleation strain rate is determined during the computation of the elastic trial stress and may be subtracted from the total strain rate at that point. We therefore find it convenient to compute an effective elastic plastic strain rate as

$$\underline{\underline{\mathbf{d}}}^{\text{ep}} \equiv \underline{\underline{\mathbf{d}}} - \underline{\underline{\mathbf{d}}}^n. \quad (\text{A.14})$$

Thus, the expression in the first term in the numerator of Eq. (A.11) can be written

$$\underline{\underline{\mathbf{d}}}: \underline{\underline{\hat{\mathbf{I}}}} - \dot{\delta}^n = \underline{\underline{\mathbf{d}}}^{\text{ep}} : \underline{\underline{\hat{\mathbf{I}}}} = \frac{\underline{\underline{\mathbf{d}}}^{\text{ep}} : \underline{\underline{\mathbf{I}}}}{\sqrt{3}} = \frac{\text{tr } \underline{\underline{\mathbf{d}}}^{\text{ep}}}{\sqrt{3}}, \quad (\text{A.15})$$

from which we obtain our final expression for the plastic segment:

$$\dot{\lambda} = \frac{\sqrt{3}KF_m \text{tr } \underline{\underline{\mathbf{d}}}^{\text{ep}} + 2GF_s\underline{\underline{\mathbf{d}}}: \underline{\underline{\hat{\mathbf{S}}}} + \dot{\psi}^n(F_\psi - \kappa_m \sigma_m F_m - \gamma_m \sigma_s F_s) + \dot{\Upsilon}(F_m \sigma_m + F_s \sigma_s)}{3KF_m^2 + 2GF_s^2 + \sqrt{3}(1+\psi)F_m(\kappa_m \sigma_m F_m + \gamma_m \sigma_s F_s - F_\psi) - h \xi F_\zeta}, \quad (\text{A.16})$$

which is the expression cited in Eq. (14.1) of the main text.

APPENDIX B.

Porosity dependence of the elastic moduli

This appendix presents graphs of how the elastic moduli and sound speeds vary with porosity according to the equations employed in the CKP model. Page B-6 concludes the discussion with a detailed description of how a Newton-Raphson solver is used in the code to back out the moduli of the matrix material given the initial macroscopic porous moduli.

The ZTW model.

The Zhao, Tandon, Weng (ZTW) model [21] for the dependence of the elastic shear modulus G and bulk modulus K on porosity is*

$$\frac{G}{G_m} = (1 + \gamma_m \psi)^{-1} \quad \text{where} \quad \gamma_m = \frac{5(4G_m + 3K_m)}{8G_m + 9K_m}. \quad (\text{B.1a})$$

$$\frac{K}{K_m} = (1 + \kappa_m \psi)^{-1} \quad \text{where} \quad \kappa_m = \frac{4G_m + 3K_m}{4G_m}, \quad (\text{B.1b})$$

where G_m and K_m are the shear and bulk moduli of the matrix material, and the ‘‘pore ratio’’ ψ is equals the volume fraction of void divided by the volume fraction of solid (thus it varies from zero to infinity).

The ZTW dependence of the elastic moduli on porosity is illustrated in Fig. B.2. In these plots, the horizontal axis is the pore ratio ψ . The traditional measure of porosity (i.e., the volume fraction of pores) is related to the pore ratio by $f = \psi / (1 + \psi)$. Hence, the plots in Fig. B.2 correspond to porosities ranging from 0.0 to about 66%. Such a large porosity range is shown strictly to verify qualitatively sensible trends; the ZTW model is intended for applications at or below ~10% porosity (it is not intended for highly porous media such as foams). Poisson’s ratio is related to the shear and bulk moduli by

$$\nu = \frac{3K - 2G}{2(3K + G)}. \quad (\text{B.2})$$

Poisson’s ratio of the matrix material is given by

$$\nu_m = \frac{3K_m - 2G_m}{2(3K_m + G_m)}. \quad (\text{B.3})$$

* The specific form of Equations (B.1) was first presented in Ref. [22]. The actual equations that appear in the ZTW paper are specified in terms of traditional porosity (volume fraction of voids) and are far less transparent in structure.

APPENDIX B. Porosity dependence of the elastic moduli

Both K and G become smaller with increasing porosity, so the behavior of ν depends on whether the numerator in Eq. (B.2) decreases faster or slower than the denominator. In Fig. B.2, Poisson's ratio is seen to increase with porosity when $\nu_m < 0.2$ but decreases when $\nu_m > 0.2$. Such behavior is also reported in Ref. [38] but is opposed in Ref. [39] where the authors appeal to intuition to ask why Poisson's equation should ever increase with porosity. The porous ceramic of interest to us has a Poisson's ratio very near 0.2, and recent measurements [5] have indeed shown that its Poisson's ratio is indeed nearly independent of porosity.

For the ZTW model, the initial slope of the relative *Young's modulus* E/E_m is approximately 2.0 for all values of ν_m . This behavior is observed or predicted for some materials Ref. [39], but other data in the same reference show that the initial slope of the relative Young's modulus can be steeper by a factor of ~ 2 . Data from Biswas [40] indicate that the initial slope of the relative Young's modulus curve should be about 2.6 for PZT ceramics.

When the relative shear modulus, G/G_m , is plotted as a function of ψ , the initial slope (at $\psi=0$) is given by $-\gamma_m$. The scalar κ_m is interpreted similarly for the plot of K/K_m . Thus γ_m and κ_m are to be compared with the parameter "b" used in Ref. [39]. As shown in Fig. B.1, the ZTW model predicts that both γ_m and κ_m depend only on the matrix material's Poisson's ratio ν_m .

In general, since $\psi \approx f$ as $f \rightarrow 0$, we note that

$$\kappa_m = -\frac{1}{K_m} \left(\frac{dK}{df} \Big|_{f \rightarrow 0} \right) \quad (\text{B.4})$$

and

$$\gamma_m = -\frac{1}{G_m} \left(\frac{dG}{df} \Big|_{f \rightarrow 0} \right). \quad (\text{B.5})$$

In our numerical implementation of the CKP model, the user may specify *measured* values for γ_m and κ_m . Otherwise, the code uses the ZTW expressions to set default values for γ_m and κ_m .

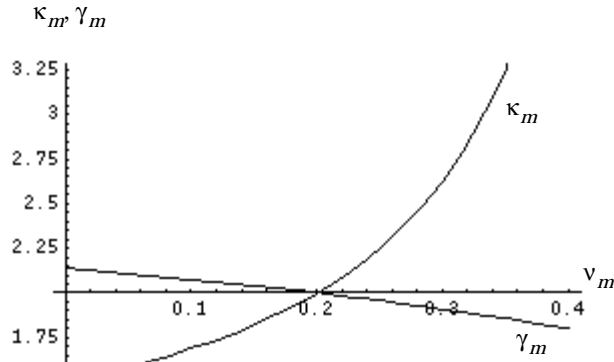


Fig. B.1. Dependence of the relative moduli on the matrix Poisson's ratio. The scalar κ_m is the derivative of the relative bulk modulus (K/K_m) with respect to porosity in the limit as porosity goes to zero; γ_m is the similar measure for relative shear modulus (G/G_m).

APPENDIX B. Porosity dependence of the elastic moduli

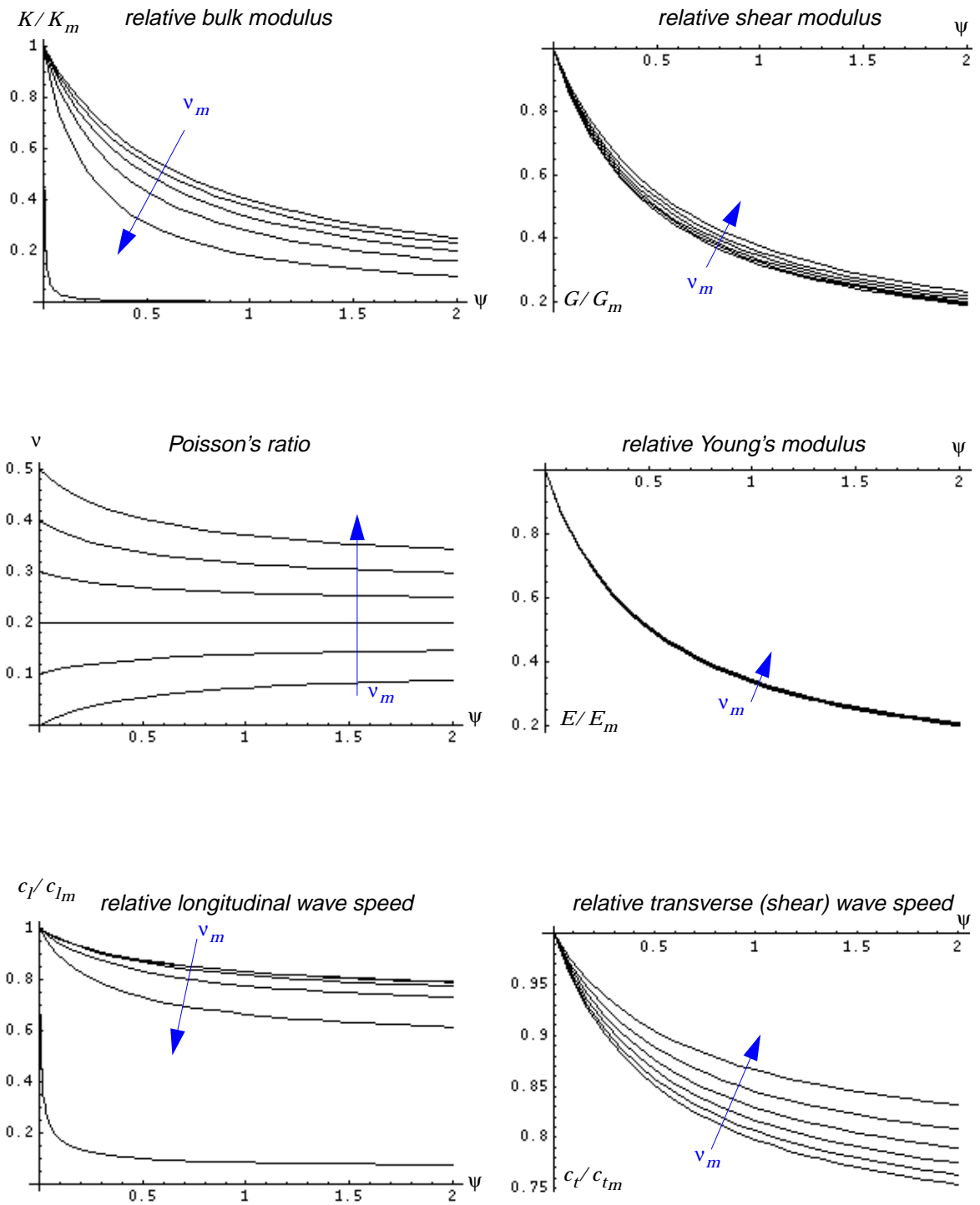


Fig. B.2. Effect of porosity on the elastic moduli. The plots show relative elastic moduli (i.e., modulus divided by the matrix modulus) and relative wave speeds as a function of pore ratio ψ for six values of the matrix Poisson's ratio ν_m ranging from 0.0 to 0.5 in the direction indicated by the arrows.

The exponential model

The ZTW model shows that the porous *compliances* are simple one-term expansions with respect to the pore ratio ψ . Thus, for small porosities, the ZTW model is approximately equivalent to an *exponential* model for which

$$\frac{G}{G_m} = e^{-\gamma_m \psi} \quad (\text{B.6a})$$

$$\frac{K}{K_m} = e^{-\kappa_m \psi}. \quad (\text{B.6b})$$

This is a convenient approximation since it gives analytically simple expressions for the time rates of the moduli:

$$\frac{\dot{G}}{G} = -\gamma_m \dot{\psi} \quad (\text{B.7a})$$

$$\frac{\dot{K}}{K} = -\kappa_m \dot{\psi}, \quad (\text{B.7b})$$

where we have assumed that the matrix moduli do not vary with time (this assumption will later be released when the material is undergoing a phase transition).

The simpler analytical form for the moduli rates is the principal motivation for using the above exponential model. The analysis and numerical experiments presented in this report employ the exponential model because, for our own applications, we are interested in materials having porosities less than about 10%. As shown in Fig. B.3, the exponential model is roughly equivalent to the ZTW model at these moderately low porosities.

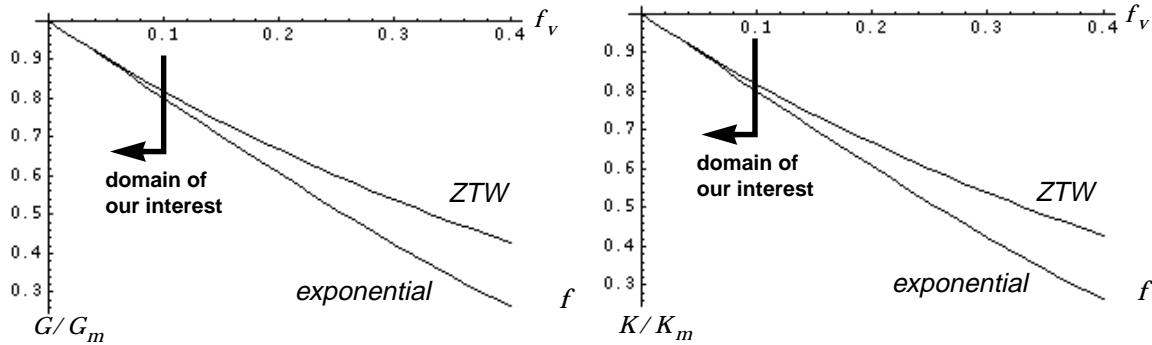


Fig. B.3. The ZTW and exponential models of porosity dependence of elastic moduli. These plots show the relative shear modulus G/G_m and the relative bulk modulus K/K_m vs. porosity for a matrix Poisson's ratio of $\nu_m=0.2$. The distinction between the models is more pronounced for larger values of ν_m .

Figure B.4 compares predictions Young's modulus for the full range of porosities. The ZTW model appears superior in the domain of extremely large porosities because it qualitatively agrees better with experiments reported in Reference [39]. Both models are roughly equivalent for low porosities except

that the exponential model shows strong dependence on the matrix Poisson's ratio ν_m as it approaches 1/2. For the exponential model, both the shear and bulk moduli would be linear on a semi-log plot, but Young's modulus is *not* linear because it is given by a nonlinear function of shear and bulk moduli.

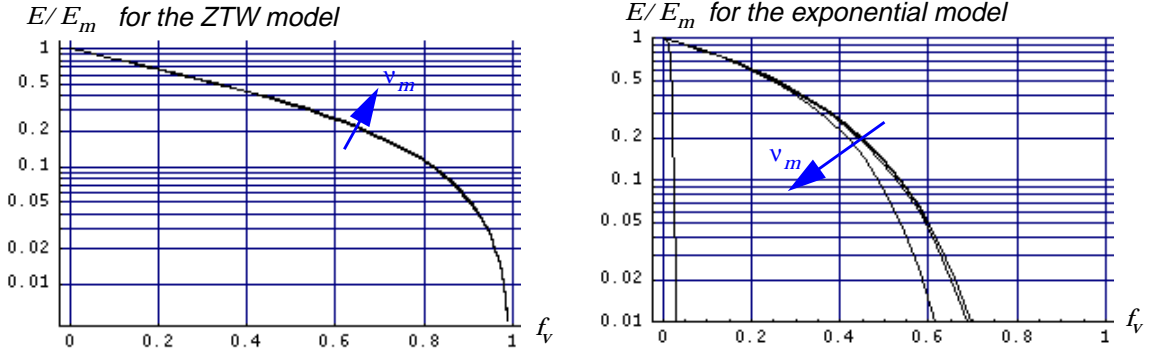


Fig. B.4. Dependence of Young's modulus on porosity. These plots show the relative Young's modulus E/E_m for values of the matrix Poisson's ratio increasing from 0.0 to 0.5 in a direction indicated by the arrows.

The ZTW model predicts negligible dependence of the relative Young's modulus on ν_m , and the slope of the linear region is

$$\frac{d(E/E_m)}{df_v} \approx 2.0 \text{ for the ZTW model.} \quad (\text{B.8})$$

This report uses the exponential model for convenience. If one is interested in large porosities, the derivation presented in this report could be readily generalized using the ZTW model of Eq. (2.1). Better yet, the analysis could be generalized such that the moduli are given by any desired *user-supplied* functions, f and g such that

$$\begin{aligned} K &= f(K_m, G_m, \psi) \\ G &= g(K_m, G_m, \psi). \end{aligned} \quad (\text{B.9})$$

One should question, however, the usefulness of such generality. Defining such functions to be accurate at large porosities would be helpful only for problems involving small macroscopic distortions.* Otherwise, deformation-induced anisotropy (even in the elastic regime) would render K and G meaningless. Deformation-induced anisotropy is an important issue for *any* isotropic porosity model. Realistically, the model can be expected to provide good results only in the small distortion realm. A future extension of this report's model will allow deformation-induced material anisotropy.

* A deformation involves large distortions if the body significantly changes its *shape*, not just its size or orientation. For large distortions, initially spherical pores collapse to ellipsoidal pores or (in the limit) to cracks.

User inputs for the elastic constants.

Both the ZTW model and the exponential model are special cases of Eq. (B.9). Regardless of which model is used, the independent variables in these functions are the matrix elastic moduli and the porosity. The user of this model may be reasonably expected to supply a value for porosity f_v , which can in turn be converted to the pore ratio ψ by applying Eq. (2.2). However, the elastic properties K_m and G_m of the *matrix* material are generally not known or easily measured. Instead, the user typically knows only the *macroscopic* moduli K and G at the initial state.

The model to be derived in this report allows the porosity to change from its initial user-supplied value ψ_o as a result of plastic flow of the matrix material. The elastic properties K_m and G_m of the *matrix* material are presumed unchanged by plastic flow. Hence, it makes sense to perform a time-zero set-up calculation in which Eq. (B.9) is inverted using the user-supplied initial values for K , G , and ψ to obtain the true material constants K_m and G_m . An analytical inversion of Eq. (B.9) is typically unavailable, so a Newton solver must be used, as detailed in the next section.

Newton solver for matrix moduli

Recall the general form of Eq. (B.9) for the macroscopic moduli as a function of the matrix moduli and porosity:

$$\begin{aligned} K &= f(K_m, G_m, \psi) \\ G &= g(K_m, G_m, \psi). \end{aligned} \tag{B.10}$$

The user provides values for the initial *macroscopic* moduli. Given that

$$\begin{aligned} K &= K^{\text{user}} \\ G &= G^{\text{user}} \\ \psi &= \psi^{\text{user}}, \end{aligned} \tag{B.11}$$

we wish to invert Eq. (B.9) to solve for the matrix moduli K_m and G_m . Employing a Newton-Raphson solver, one must establish a first “guess” $\{K_m^0, G_m^0\}$. In our numerical implementation, we take the user-specified matrix moduli to equal the macroscopic porous moduli as our first guess:

$$K_m^o = K^{\text{user}} \text{ and } G_m^o = G^{\text{user}}. \tag{B.12}$$

Given a guess $\{K_m^i, G_m^i\}$ for the matrix moduli, the Newton-Raphson improved guess is given by

$$\begin{bmatrix} G_m^{i+1} \\ K_m^{i+1} \end{bmatrix} = \begin{bmatrix} G_m^i \\ K_m^i \end{bmatrix} - [S]^{-1} \begin{bmatrix} G^i - G^{\text{user}} \\ K^i - K^{\text{user}} \end{bmatrix}, \tag{B.13}$$

where

$$\begin{aligned} G^i &\equiv g(K_m^i, G_m^i, \Psi) \\ K^i &\equiv f(K_m^i, G_m^i, \Psi), \end{aligned} \quad (\text{B.14})$$

and $[S]$ is a matrix defined

$$[S] = \begin{bmatrix} \frac{\partial g}{\partial G_m} & \frac{\partial g}{\partial K_m} \\ \frac{\partial f}{\partial G_m} & \frac{\partial f}{\partial K_m} \end{bmatrix} \text{ evaluated at } \{G_m^i, K_m^i\}. \quad (\text{B.15})$$

Consider, for example, the exponential model of Eq. (2.4):

$$\frac{G}{G_m} = e^{-\gamma_m \Psi} \quad \text{where} \quad \gamma_m = \frac{5(4G_m + 3K_m)}{8G_m + 9K_m} \quad (\text{B.16})$$

$$\frac{K}{K_m} = e^{-\kappa_m \Psi} \quad \text{where} \quad \kappa_m = \frac{4G_m + 3K_m}{4G_m}. \quad (\text{B.17})$$

First we can apply the chain rule to write

$$\frac{\partial G}{\partial G_m} = e^{-\gamma_m \Psi} + G_m e^{-\gamma_m \Psi} \left(-\Psi \frac{\partial \gamma_m}{\partial G_m} \right). \quad (\text{B.18})$$

Simplifying,

$$\frac{\partial G}{\partial G_m} = \frac{G}{G_m} (1 - \Psi G_m \gamma_{,G}), \quad (\text{B.19})$$

where

$$\gamma_{,G} \equiv \frac{\partial \gamma_m}{\partial G_m} = \frac{600 K_m}{(8G_m + 9K_m)^2}. \quad (\text{B.20})$$

Again applying the chain rule, we find that

$$\frac{\partial G}{\partial K_m} = -\Psi G \gamma_{,K}, \quad (\text{B.21})$$

$$\text{where } \gamma_{,K} \equiv \frac{\partial \gamma_m}{\partial K_m} = -\gamma_{,G} \frac{G_m}{K_m}. \quad (\text{B.22})$$

Similarly,

$$\frac{\partial K}{\partial K_m} = \frac{K}{K_m} (1 - \Psi K_m \kappa_{,K}), \quad (\text{B.23})$$

$$\text{where } \kappa_{,K} \equiv \frac{\partial \kappa_m}{\partial K_m} = \frac{3}{4G_m}, \quad (\text{B.24})$$

APPENDIX B. Porosity dependence of the elastic moduli

and

$$\frac{\partial K}{\partial G_m} = -\psi K \kappa_{,G} , \quad (\text{B.25})$$

$$\text{where } \kappa_{,G} \equiv \frac{\partial \kappa_m}{\partial G_m} = \frac{-3 K_m}{4 G_m^2}. \quad (\text{B.26})$$

Analogous formulas exist for the derivatives of the bulk modulus. Hence, the $[S]$ matrix used in the Newton-Raphson solver is given by

$$[S] = \begin{bmatrix} \frac{\partial G}{\partial G_m} & \frac{\partial G}{\partial K_m} \\ \frac{\partial K}{\partial G_m} & \frac{\partial K}{\partial K_m} \end{bmatrix} \text{ evaluated using } \{ G_m^i, K_m^i \}. \quad (\text{B.27})$$

Show below is the actual FORTRAN code fragment for the Newton-Raphson solver for the exponential moduli model. In this coding, SHMOD and BKMOD are the user-supplied macroscopic shear and bulk moduli.

```

c      As first guess, take the matrix properties to equal
c      the user-specified porous properties.
      RGM=SHMOD                                     <----- apply Eq. (B.12)
      RKM=BKMOD
      DO 7 I=1,200
Apply Eq. (B.16)
      RGAMM=PFIVE*( PFOUR*RGM+PTHREE*RKM) / ( PEIGHT*RGM+PNINE*RKM)
      RKAPM=( PFOUR*RGM+PTHREE*RKM) / ( PFOUR*RGM)
      RG=RGM*EXP( -RGAMM*PSI )                       <----- Apply Eq. (B.14)
      RK=RKM*EXP( -RKAPM*PSI )

Check for convergence
      IF(          ABS(RG/SHMOD-PONE).LT.PRND4
      &          .AND.ABS(RK/BKMOD -PONE).LT.PRND4 )GO TO 8
C      ...first compute derivative of rgamm and rkapm
Apply Eqs. (B.20), (B.22), (B.26), and (B.24) respectively
      DGDGM=0.6D2*RKM/(( PEIGHT*RGM+PNINE*RKM)**PTWO)
      DGDKM=-DGDGM*RGM/RKM
      DKDGM=-PTHREE*RKM/PFOUR/RGM/RGM
      DKDKM=PTHREE/PFOUR/RGM
C      ...Now get derivatives of rG and rK
Apply Eqs. (B.19), (B.23), (B.21), and (B.25) respectively
      DGDGM=( PONE-PSI*RGM*DGDGM)*RG/RGM
      DKDKM=( PONE-PSI*RKM*DKDKM)*RK/RKM
      DGDKM=-PSI*RG*DGDKM
      DKDGM=-PSI*RK*DKDGM

Compute the determinant of the [S] matrix:
      DET=DGDGM*DKDKM-DKDGM*DGDKM
Apply Eq. (B.13) to improve the guess of the matrix properties
      RGM=MAX( PZERO, RGM+( DKDKM*( SHMOD-RG)-DGDKM*( BKMOD-RK) )/DET)
      RKM=MAX( PZERO, RKM+( DGDGM*( BKMOD-RK)-DKDGM*( SHMOD-RG) )/DET)
7      CONTINUE
      CALL FATERR(IAM,'Matrix properties did not converge')
8      CONTINUE

```

APPENDIX C.

Proper application of return algorithms

This appendix outlines a proof that, for general plasticity equations (for which CKP is a special instance), the updated stress may be computed by projecting the elastic trial stress back to the yield surface. The trial stress must be projected back to the yield surface along a line parallel to $\underline{\underline{A}} = \underline{\underline{E}}:\underline{\underline{M}}$, where $\underline{\underline{E}}$ is the elastic stiffness and $\underline{\underline{M}}$ is the direction of the plastic strain rate. Thus, if the model assumes plastic normality, then the correct direction to return to the yield surface is *not* generally normal to the yield surface.

We finish this appendix by showing that the popular shear/mean stress measures $\tau \equiv \|\underline{\underline{S}}\|$ and $p \equiv \frac{1}{3}\text{tr}\underline{\underline{\sigma}}$ are not isomorphic to stress space. Consequently, the normal to the yield surface in the τ vs. p plane does *not* correspond to the normal to the yield surface in six-dimensional stress space! To return to the nearest point on the yield surface in stress space, the correct (τ, p) point is *not* the nearest point on the yield curve in the τ vs. p plane! By rejecting τ vs. p in favor of our isomorphic stress measures σ_s vs. σ_m , we avoid such non-intuitive behavior.

Return algorithms in generality

Consider the basic equations of non-hardening plasticity:

$$\underline{\underline{B}}:\underline{\underline{\dot{\sigma}}} = 0 \quad (\text{this form holds only for non-hardening yield surfaces}^*) \quad (\text{C.1})$$

$$\underline{\underline{\dot{\epsilon}}} = \underline{\underline{\dot{\epsilon}}^e} + \underline{\underline{\dot{\epsilon}}^p} \quad (\text{C.2})$$

$$\underline{\underline{\dot{\epsilon}}^p} = \dot{\lambda}\underline{\underline{M}} \quad (\text{C.3})$$

$$\underline{\underline{\dot{\sigma}}} = \underline{\underline{E}}:\underline{\underline{\dot{\epsilon}}^e}. \quad (\text{C.4})$$

In these equations, the following quantities are presumed known:

$\underline{\underline{B}}$, gradient of the yield function at the current state ($B_{ij} = \partial f / \partial \sigma_{ij}$)

$\underline{\underline{\dot{\epsilon}}}$, the total strain rate.

$\underline{\underline{E}}$, the fourth-order elastic tangent stiffness tensor.

$\underline{\underline{M}}$, the unit tensor in the direction of the plastic strain rate.

* A yield function is nonhardening if it depends only on stress, not on other internal state variables such as porosity or equivalent plastic strain. We consider non-hardening only for simplicity. For hardening (or softening), the yield function is of the form $f(\underline{\underline{\sigma}}, \zeta)$ where ζ is an internal state variable (e.g., for porous media, it could be the pore ratio ψ or the matrix yield stress). Consistency requires that $\dot{f}=0$, or $\frac{\partial f}{\partial \underline{\underline{\sigma}}}:\underline{\underline{\dot{\sigma}}} + \frac{\partial f}{\partial \eta}\dot{\zeta} = 0$. Again define $\underline{\underline{B}}=\partial f/\partial \underline{\underline{\sigma}}$ and assume that the evolution equation for ζ is of the form discussed in Eq. (10.2) on page -28; namely, $\dot{\zeta} = \underline{\underline{G}}:\underline{\underline{\dot{\epsilon}}^p$. Then the hardening generalization of Eq. (C.1) becomes $\underline{\underline{B}}:\underline{\underline{\dot{\sigma}}} + \underline{\underline{g}}:\underline{\underline{\dot{\epsilon}}^p} = 0$, where $\underline{\underline{g}}=\frac{\partial f}{\partial \eta}\underline{\underline{G}}$.

See <http://www.me.unm.edu/~rnbrann/gobag.html> for a generalization of this appendix that permits hardening.

APPENDIX C. Proper application of return algorithms

The following quantities are unknown:

$\dot{\underline{\underline{\sigma}}}$, the rate of stress

$\dot{\underline{\underline{\epsilon}}}^e$, the elastic part of the strain rate

$\dot{\underline{\underline{\epsilon}}}^p$, the plastic part of the strain rate.

$\dot{\lambda}$, the magnitude of the plastic part of the strain rate.

The above equations are valid under the following conditions:

- Arbitrary elastic anisotropy.
- Arbitrary plastic anisotropy.
- Nonhardening yield surface.*
- Genuine nonlinear elasticity. In other words, the stress is *truly* a proper function of the elastic strain. The function may permissibly be nonlinear. Because the function is assumed proper, the stress *rate* will be linear in the strain *rate*, where the linear transformation is given by the elastic tangent stiffness tensor, which depends only on the elastic strain.
- Yield functions that obey the sign convention that elastic stresses correspond to negative values and forbidden stresses correspond to positive values (this is needed so that the outward normal can indeed be given by the yield function gradient and so that trial stresses may be categorized to be above or below yield by checking the sign of the yield function[†]).
- Strain definitions that permit the decomposition of strain rates.
- Stress and strain definitions that permit the use of true rates rather than objective rates. A popular choice is to use the “unrotated” reference configuration.
- Strain rate direction being dependent only on the material state, not on the rate of change of state.

Notice that we do *not* require the yield surface to be convex or that the plastic strain rate be directed away from the yield surface. We don’t even require that the elastic stiffness be positive definite. Rational models will indeed have such properties, but those concerns merely dictate appropriate choices for the quantities listed as “known” on page C-1. To prove the radial and oblique return theorems, we will only need to presume that

$$\underline{\underline{B}} : \underline{\underline{E}} : \underline{\underline{M}} \neq 0. \quad (\text{C.5})$$

Equations (C.1) through (C.4) constitute a linear set of four equations that may be solved for the four unknowns. The solution for the stress rate is

* As shown in <http://www.me.unm.edu/~rbrann/RadialReturn.pdf>, this restriction can be released without changing the fundamental ideas derived here.

† Tresca yield function is often erroneously cited in an intoxicatingly appealing invariant form as $f(\underline{\underline{\sigma}}) = 4J_2^3 - 27J_3^2 - 36k^2J_2^2 + 96k^4J_2 - 64k^6$, but this yield function is invalid because there exist stress states outside the Tresca yield surface for which $f(\underline{\underline{\sigma}}) < 0$. The sign convention is crucial!

$$\underline{\underline{\dot{\sigma}}} = \underline{\underline{\dot{\sigma}}}^{\text{trial}} - \frac{\underline{\underline{\mathbf{A}}}(\underline{\underline{\mathbf{B}}}: \underline{\underline{\dot{\sigma}}}^{\text{trial}})}{\underline{\underline{\mathbf{A}}}: \underline{\underline{\mathbf{B}}}} \quad (\text{C.6})$$

where $\underline{\underline{\dot{\sigma}}}^{\text{trial}}$ and $\underline{\underline{\mathbf{A}}}$ are just shorthand notations for

$$\underline{\underline{\dot{\sigma}}}^{\text{trial}} = \underline{\underline{\mathbf{E}}}: \underline{\underline{\dot{\epsilon}}}, \quad (\text{C.7})$$

$$\underline{\underline{\mathbf{A}}} \equiv \underline{\underline{\mathbf{E}}}: \underline{\underline{\mathbf{M}}}. \quad (\text{C.8})$$

The above solution for the stress rate is geometrically equivalent to the oblique projection of a vector $\underline{\mathbf{x}}$ onto a plane illustrated in Fig. C.1. The normal to the plane is specified by the vector $\underline{\mathbf{b}}$ and the projection direction is given by the vector $\underline{\mathbf{a}}$, neither of which must be unit vectors. The formula for the projection of $\underline{\mathbf{x}}$ is

$$\underline{\mathbf{p}} = \underline{\mathbf{x}} - \frac{\underline{\mathbf{a}}(\underline{\mathbf{b}} \cdot \underline{\mathbf{x}})}{\underline{\mathbf{a}} \cdot \underline{\mathbf{b}}} \quad (\text{C.9})$$

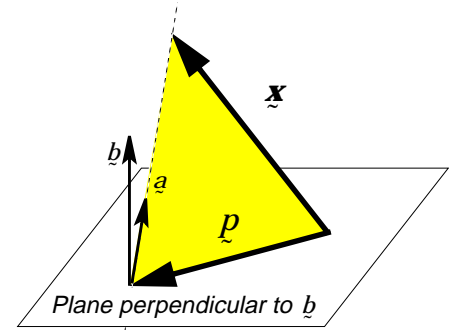


Fig. C.1. Oblique projection. The path obliquely intersects the plane.

Equations (C.6) and (C.7) are identical in structure, with the double dot ($:$) tensor inner product playing a role in 6D stress space that is similar to the role played by the single dot vector inner product in 3D physical space. In Eq. (C.6), the tensor $\underline{\underline{\mathbf{B}}}$ is normal to the target surface. Since $\underline{\underline{\mathbf{B}}}$ is normal to the yield surface, Eq. (C.6) says that *the actual stress rate $\underline{\underline{\dot{\sigma}}}$ is a projection of the trial stress rate $\underline{\underline{\dot{\sigma}}}^{\text{trial}}$ onto the yield surface.* The projection direction must be parallel to the tensor $\underline{\underline{\mathbf{A}}} \equiv \underline{\underline{\mathbf{E}}}: \underline{\underline{\mathbf{M}}}$. Similar conclusions also go through for hardening or softening yield surfaces of the type used in our CKP porous model (see <http://www.me.unm.edu/~rmbrann/gobag.html>). The only difference for evolving yield surfaces is that only the *tangential* part of $\underline{\underline{\dot{\sigma}}}$ equals the projection of $\underline{\underline{\dot{\sigma}}}^{\text{trial}}$; the normal part of $\underline{\underline{\dot{\sigma}}}$ is constrained to exactly match the normal velocity of the yield surface's expansion or contraction. Return algorithms are very appealing because they allow the trial elastic stress to be projected back to the yield surface to obtain the updated stress. Wilkens [29] demonstrated that this approach is second-order accurate even if the computational interval is partially elastic.

Importantly, the projection direction $\underline{\underline{\mathbf{A}}}$ is not generally parallel to the plastic strain rate direction $\underline{\underline{\mathbf{M}}}$. Thus, even if the plastic strain rate is normal to the yield surface, *the correct direction to return to the yield surface is not generally normal to the yield surface.* For elastic isotropy,

$$\underline{\underline{\mathbf{A}}} \equiv \underline{\underline{\mathbf{E}}}: \underline{\underline{\mathbf{M}}} = 2G\underline{\underline{\mathbf{M}}}^d + 3K\underline{\underline{\mathbf{M}}}^i, \quad (\text{C.10})$$

where G is the shear modulus, K is the bulk modulus, $\underline{\underline{\mathbf{M}}}^d$ is the deviatoric part of $\underline{\underline{\mathbf{M}}}$ and $\underline{\underline{\mathbf{M}}}^i$ is the isotropic part of $\underline{\underline{\mathbf{M}}}$. Thus, the projection direction $\underline{\underline{\mathbf{A}}}$ is parallel to the plastic strain rate direction $\underline{\underline{\mathbf{M}}}$ only if $\underline{\underline{\mathbf{M}}}$ is purely isotropic or purely deviatoric. The latter case expresses the common assumption for solid metals that the material is plastically incompressible, but such an assumption is grossly inadequate for porous media. Thus, for porous media, return algorithms *must* involve an oblique return to the yield surface. If you encounter a model that nevertheless returns to the nearest point on the yield surface, then that model is implicitly assuming $\underline{\underline{\mathbf{A}}}$ to be proportional to the yield surface normal $\underline{\underline{\mathbf{B}}}$. Since $\underline{\underline{\mathbf{A}}} \equiv \underline{\underline{\mathbf{E}}}: \underline{\underline{\mathbf{M}}}$, you may conclude that any model that returns to the nearest point on the yield surface is implicitly taking the direction of plastic strain rate as $\underline{\underline{\mathbf{M}}} \propto \underline{\underline{\mathbf{E}}}^{-1}: \underline{\underline{\mathbf{B}}}$. Thus, in general, such a model is implicitly nonassociative!

Geometric perils of return operations

The return operation must be done in full six-dimensional stress space. Often, however, the yield surface is defined in terms of scalar measures of stress. An extremely common choice is to write $F(\underline{\underline{\sigma}}) = f(\tau, p)$, where

$$\tau \equiv \|\underline{\underline{\mathbf{S}}}\| \quad \text{and} \quad p \equiv \frac{1}{3}\text{tr}\underline{\underline{\sigma}}, \quad (\text{C.11})$$

where $\underline{\underline{\mathbf{S}}}$ is the stress deviator. The yield surface is the set of stress states for which $f(\tau, p)=0$. Geometrically, this represents an axisymmetric surface of revolution about an axis in stress space parallel to the identity tensor $\underline{\underline{\mathbf{I}}}$. With the above stress measures, we note that

$$\underline{\underline{\sigma}} = \tau \hat{\underline{\underline{\mathbf{S}}}} + p \underline{\underline{\mathbf{I}}}, \quad (\text{C.12})$$

where $\hat{\underline{\underline{\mathbf{S}}}}$ is the unit tensor in the direction of the stress deviator and $\underline{\underline{\mathbf{I}}}$ is the identity tensor. The tensor $\hat{\underline{\underline{\mathbf{S}}}}$ plays a role similar to the radial base vector $\underline{\underline{\mathbf{e}}}_r$ used in cylindrical coordinates. The identity tensor $\underline{\underline{\mathbf{I}}}$ defines the symmetry axis of the cylinder, *but $\underline{\underline{\mathbf{I}}}$ is not analogous to the cylindrical axis base vector $\underline{\underline{\mathbf{e}}}_z$ because $\underline{\underline{\mathbf{I}}}$ is not a unit tensor!*

There's nothing wrong with the (τ, p) choice *per se*, but one must then be extremely careful when casting stress space into the reduced space of τ vs. p and vice versa. The normal to the yield surface *in stress space* is proportional to the gradient of the yield function $\underline{\underline{\mathbf{B}}}$. Applying the chain rule,

$$\underline{\underline{\mathbf{B}}} = \frac{dF}{d\underline{\underline{\sigma}}} = \frac{\partial f}{\partial \tau} \left(\frac{d\underline{\underline{\sigma}}}{d\tau} \right) + \frac{\partial f}{\partial p} \left(\frac{d\underline{\underline{\sigma}}}{dp} \right) = \frac{\partial f}{\partial \tau} (\hat{\underline{\underline{\mathbf{S}}}}) + \frac{\partial f}{\partial p} \left(\frac{1}{3} \underline{\underline{\mathbf{I}}} \right). \quad (\text{C.13})$$

The factor of 3 (equal to the square magnitude of $\hat{\mathbf{I}}$) in the last term of Eq. (C.13) arises because $\hat{\mathbf{I}}$ is not a unit tensor. Again, so long as the chain rule is applied properly, then the yield function gradient $\hat{\mathbf{B}}$ may be computed regardless of what stress measures you adopt. The problem comes when attempting to visualize the 6D yield surface normal in the reduced 2D space of τ vs. p .

To illustrate the issue most concretely, suppose that you have a trial stress $\hat{\boldsymbol{\sigma}}^t$ that lies outside the yield surface and (despite all the lessons learned in the preceding section) you wish to return this stress to the *nearest* point on the yield surface to obtain a *new* updated stress $\hat{\boldsymbol{\sigma}}^n$. Then the difference $\hat{\boldsymbol{\sigma}}^t - \hat{\boldsymbol{\sigma}}^n$ must be parallel to the yield surface normal $\hat{\mathbf{B}}$. That is,

$$\hat{\boldsymbol{\sigma}}^t - \hat{\boldsymbol{\sigma}}^n \propto \hat{\mathbf{B}}, \quad (\text{C.14})$$

or

$$(\tau^t - \tau^n)\hat{\mathbf{S}} + (p^t - p^n)\hat{\mathbf{I}} \propto \frac{\partial f}{\partial \tau}(\hat{\mathbf{S}}) + \frac{\partial f}{\partial p}\left(\frac{1}{3}\hat{\mathbf{I}}\right). \quad (\text{C.15})$$

From which we conclude that

$$\frac{\tau^t - \tau^n}{p^t - p^n} = 3\left(\frac{\partial f/\partial \tau}{\partial f/\partial p}\right). \quad (\text{C.16})$$

The ratio in the parenthesis is the slope of the normal to the yield curve in τ vs. p space. Hence, the factor of 3 in the above equation tells us that projecting *normal* to the yield surface in 6D *stress space* must be accomplished by projected with a slope *three times as steep* as the normal in 2D τ vs. p space! While p is certainly the *de facto* standard measure of mean stress, we conclude that it is *not* the natural or intuitive choice when attempting to represent 6D axisymmetric stress space in two dimensions. Our σ_s vs. σ_m stress measures are exact analogs of cylindrical coordinates.

With our isomorphic stress measures, the stress tensor may be written as $\hat{\boldsymbol{\sigma}} = \sigma_s\hat{\mathbf{S}} + \sigma_m\hat{\mathbf{I}}$. The *unit* tensor $\hat{\mathbf{I}}$ is now a direct analog of the \mathbf{e}_z cylindrical base vector, and a return to the nearest point in stress space also corresponds to a return to the nearest point in σ_s vs. σ_m space.

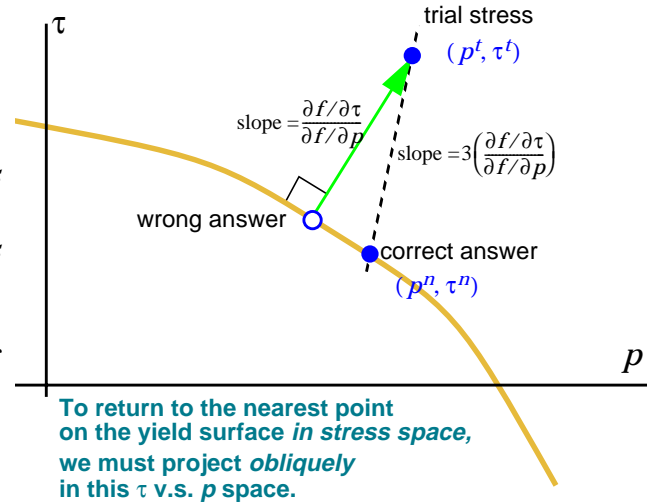


Fig. C.2. Counterintuitive behavior with non-isomorphic stress measures.

APPENDIX C. Proper application of return algorithms

This page intentionally left blank.

APPENDIX D. The predictor-corrector QCKP algorithm

Consider a computational step that starts at time t^{old} and ends at time t^{new} . The “rate” of deformation $\underline{\underline{d}}$ is assumed constant during the step. It is not known *a priori* whether the step will be elastic. We will write the algorithm assuming that the time step $\Delta t \equiv t^{\text{new}} - t^{\text{old}}$ consists of two parts: Δt_e during which the deformation is “elastic,” followed by Δt_p during which plastic flow occurs and pores collapse. For the algorithm, Δt_e will be written as a fraction of the total time step: $\Delta t_e = \mu \Delta t$ where $0 \leq \mu \leq 1$.

step 1. Compute variables at the beginning of the step. For example,

$$\text{Elastic moduli: } G = G_m e^{-\gamma_m \Psi} \text{ and } K = K_m e^{-\kappa_m \Psi}.$$

$$\text{Initial scalar stress measures: } \sigma_m^{\text{old}} = \frac{1}{\sqrt{3}} \text{tr}(\underline{\underline{\sigma}}^{\text{old}}) \text{ and } \sigma_s^{\text{old}} = \left\| (\underline{\underline{\sigma}}')^{\text{old}} \right\|.$$

Compute the nucleation rate at the beginning of the step and use

$$\text{Eqs. (12.2) and (12.3) to compute } \text{tr} \underline{\underline{d}}^n = \frac{\dot{\Psi}^n}{(1 + \Psi)}.$$

step 2. Supposing that the step *might* be entirely elastic, compute a trial elastic stress using Eqs. (6.5) and (6.6) as follows:

$$\Delta \sigma_m = \sqrt{3} K (\text{tr} \underline{\underline{d}} - \dot{\nu}) \Delta t \quad (\text{D.1})$$

$$\Delta \underline{\underline{S}} = 2 G \underline{\underline{d}}' \Delta t \quad (\text{D.2})$$

$$\sigma_m^{\text{trial}} = \sigma_m^{\text{old}} + \Delta \sigma_m \quad (\text{D.3})$$

$$\underline{\underline{S}}^{\text{trial}} = \underline{\underline{S}}^{\text{old}} + \Delta \underline{\underline{S}} \quad (\text{D.4})$$

$$\sigma_s^{\text{trial}} = \left\| (\underline{\underline{S}})^{\text{trial}} \right\|. \quad (\text{D.5})$$

step 3. Check whether the trial stress is at or below yield. If

$F(\sigma_m^{\text{trial}}, \sigma_s^{\text{trial}}, \Psi, \zeta) < 0$, then set $\mu = 1$ and go to STEP 5. Otherwise, continue.

step 4. Determine what fraction of the step is elastic. Do this by solving the following equation for the factor μ .

$$F(\sigma_m^{\text{old}} + \mu \Delta \sigma_m, \left\| \underline{\underline{S}}^{\text{old}} + \mu \Delta \underline{\underline{S}} \right\|, \Psi + \mu \Delta \Psi, \zeta) = 0, \quad (\text{D.6})$$

or

$$F(\sigma_m^{\text{old}} + \mu \Delta \sigma_m, \sqrt{(\sigma_s^{\text{old}})^2 + A\mu + B\mu^2}, \Psi + \mu \Delta \Psi, \zeta) = 0, \quad (\text{D.7})$$

where

APPENDIX D. The predictor-corrector QCKP algorithm

$$A \equiv 2 \underline{\underline{\mathbf{S}}}^{\text{old}} : \Delta \underline{\underline{\mathbf{S}}} \quad \text{and} \quad B \equiv \Delta \underline{\underline{\mathbf{S}}} : \Delta \underline{\underline{\mathbf{S}}}. \quad (\text{D.8})$$

Note: the quantities $\Delta \sigma_m$ and $\Delta \underline{\underline{\mathbf{S}}}$ have already been computed in an earlier step (STEP 2) and are considered constants during the Newton-Raphson search procedure outlined below:

- (i) Compute $A \equiv 2(\underline{\underline{\sigma}}')^{\text{old}} : (\Delta \underline{\underline{\sigma}}')$ and $B \equiv \Delta \underline{\underline{\sigma}}' : \Delta \underline{\underline{\sigma}}'$.
(ii) Initialize guess $\mu = 1/2$, Then compute

$$\sigma_m^{\text{elas}} = \sigma_m^{\text{old}} + \mu \Delta \sigma_m, \quad (\text{D.9})$$

$$\sigma_s^{\text{elas}} = \sqrt{(\sigma_s^{\text{old}})^2 + A\mu + B\mu^2}, \quad (\text{D.10})$$

$$\psi^{\text{elas}} = \psi^{\text{old}} + \mu \Delta \psi. \quad (\text{D.11})$$

- (iii) If $\sigma_s^{\text{elas}} = 0$, replace it by $\sigma_s^{\text{elas}} + \&$ where (recall) the “&” denotes a small stress. (This is for later division protection and artificial computation of a limit.)
(iv) Compute

$$F^{\text{elas}} = F(\sigma_m^{\text{elas}}, \sigma_s^{\text{elas}}, \psi^{\text{elas}}, \zeta) \quad (\text{D.12})$$

$$F_m^{\text{elas}} \equiv \left. \frac{\partial F(\sigma_m, \sigma_s, \psi, \zeta)}{\partial \sigma_m} \right|_{\sigma_m^{\text{elas}}, \sigma_s^{\text{elas}}, \psi^{\text{elas}}, \zeta} \quad (\text{D.13})$$

$$F_s^{\text{elas}} \equiv \left. \frac{\partial F(\sigma_m, \sigma_s, \psi, \zeta)}{\partial \sigma_s} \right|_{\sigma_m^{\text{elas}}, \sigma_s^{\text{elas}}, \psi^{\text{elas}}, \zeta} \quad (\text{D.14})$$

$$F_\psi^{\text{elas}} \equiv \left. \frac{\partial F(\sigma_m, \sigma_s, \psi, \zeta)}{\partial \psi} \right|_{\sigma_m^{\text{elas}}, \sigma_s^{\text{elas}}, \psi^{\text{elas}}, \zeta}. \quad (\text{D.15})$$

- (v) Save μ into a temporary variable $\mu^{\text{save}} = \mu$. Then replace μ with improved estimate:

$$\mu := \mu^{\text{save}} - \frac{F^{\text{elas}}}{F_\psi^{\text{elas}} \Delta \psi + F_m^{\text{elas}} \Delta \sigma_m + \frac{F_s^{\text{elas}} (A + 2B\mu^{\text{save}})}{2\sigma_s^{\text{elas}}}}. \quad (\text{D.16})$$

The earlier division protection for σ_s^{elas} guards against division by zero and helps ensure correct computation of

$$\lim_{\sigma_s^{\text{elas}} \rightarrow 0} \frac{F_s^{\text{elas}}(\sigma_m^{\text{elas}}, \sigma_s^{\text{elas}}, \psi, \zeta)}{\sigma_s^{\text{elas}}}.$$

- (vi) Replace with limiter: $\mu := \text{Min}[\text{Max}(\mu, 0), 1]$.
(vii) If $1 - \mu < \&$, set $\mu = 1$.
(viii) With the new μ , update the elastic stresses:

$$\sigma_m^{\text{elas}} = \sigma_m^{\text{old}} + \mu \Delta \sigma_m \quad (\text{D.17})$$

$$\sigma_s^{\text{elas}} = \sqrt{(\sigma_s^{\text{old}})^2 + A\mu + B\mu^2}. \quad (\text{D.18})$$

(ix) If $|\mu - \mu^{\text{save}}| < \text{small number}$, then continue on to iteration step (x). Otherwise, go back to iteration step (iii).

(x) Update the stress deviator to the end of the elastic time step:

$$\underline{\underline{\mathbf{S}}}^{\text{elas}} = \underline{\underline{\mathbf{S}}}^{\text{old}} + \mu \Delta \underline{\underline{\mathbf{S}}}. \quad (\text{D.19})$$

This concludes the elastic substep.

(xi) Return to the next step in the main algorithm.

step 5. Update or partially update the stress:

$$\sigma_m = \sigma_m^{\text{elas}} \quad \text{and} \quad \sigma_s = \sigma_s^{\text{elas}} \quad (\text{D.20})$$

$$\underline{\underline{\sigma}}^{\text{elas}} = \frac{\sigma_m^{\text{elas}} \underline{\underline{\mathbf{I}}}}{\sqrt{3}} + (\underline{\underline{\sigma}}')^{\text{elas}}; \quad \underline{\underline{\sigma}} = \underline{\underline{\sigma}}^{\text{elas}} \quad (\text{D.21})$$

$$\hat{\underline{\underline{\mathbf{S}}}}^{\text{elas}} = \begin{cases} (\underline{\underline{\sigma}}')^{\text{elas}} / \sigma_s^{\text{elas}} & \text{if } \sigma_s^{\text{elas}} \neq 0 \\ \Delta \underline{\underline{\epsilon}}' / \|\Delta \underline{\underline{\epsilon}}'\| & \text{if } \|\Delta \underline{\underline{\epsilon}}'\| \neq 0 \\ \underline{\underline{\mathbf{0}}} & \text{otherwise} \end{cases}; \quad \hat{\underline{\underline{\mathbf{S}}}} = \hat{\underline{\underline{\mathbf{S}}}}^{\text{elas}}. \quad (\text{D.22})$$

Also update the pore ratio to the end of the elastic step. (Keep in mind that porosity change during the elastic step can occur *only* by void nucleation, not by void growth or collapse due to plastic flow of the matrix material.)

step 6. Check if $1 - \mu < \text{small number}$. If so, go to STEP 19 because the step is entirely elastic. Otherwise continue.

step 7. For numerical reasons, this algorithm integrates the plastic step in *two* distinct half steps. Therefore set the plastic time step to *half* of the actual plastic time step.

$$\text{Set } \Delta t^P = \frac{1}{2}(1 - \mu)\Delta t.$$

Set KOUNT=0.

Set $\psi^{\text{save}} = \psi^{\text{old}}$, where ψ^{old} is now the value of ψ at the end of the elastic step.

step 8. Compute the pore rate from nucleation and subtract this contribution from the strain rate.

step 9. Compute the yield function derivatives.

$$F_m \equiv \frac{\partial F(\sigma_m, \sigma_s, \psi)}{\partial \sigma_m} \quad (\text{D.23})$$

APPENDIX D. The predictor-corrector QCKP algorithm

$$F_s \equiv \frac{\partial F(\sigma_m, \sigma_s, \psi)}{\partial \sigma_s} \quad (\text{D.24})$$

$$F_\psi \equiv \frac{\partial F(\sigma_m, \sigma_s, \psi)}{\partial \psi}. \quad (\text{D.25})$$

step 10. Compute the unit tensor in the direction of the stress deviator. Or in the direction of $\underline{\underline{d}}$ if the stress deviator is zero.

step 11. Compute the plasticity parameter $\hat{\lambda}$ using Eq. (14.1):

$$\hat{\lambda} = \frac{\sqrt{3} K F_m \text{tr} \underline{\underline{d}}^{\text{ep}} + 2 G F_s \underline{\underline{d}} : \underline{\underline{S}} + \psi^n (F_\psi - \kappa_m \sigma_m F_m - \gamma_m \sigma_s F_s) + \dot{\gamma} (F_m \sigma_m + F_s \sigma_s)}{3 K F_m^2 + 2 G F_s^2 + \sqrt{3} (1 + \psi) F_m (\kappa_m \sigma_m F_m + \gamma_m \sigma_s F_s - F_\psi) - h \xi F_s}. \quad (\text{D.26})$$

During iterations, we allow $\hat{\lambda}$ to be negative, but the final result for $\Delta \lambda$ over the entire time step is rigorously enforced to be positive.

step 12. Compute the rates of state variables. For example,

$$\text{Rate of pore ratio} = \dot{\psi} = \sqrt{3} (1 + \psi) F_m \hat{\lambda} \quad (\text{D.27})$$

$$\text{Rate of } \sigma_m = \dot{\sigma}_m = 3 K (\underline{\underline{d}} : \underline{\underline{I}} - F_m \hat{\lambda}) - \kappa_m \sigma_m \dot{\psi} \quad (\text{D.28})$$

$$\text{Rate of } \sigma_s = \dot{\sigma}_s = 2 G (\underline{\underline{d}} : \underline{\underline{S}} - F_s \hat{\lambda}) - \gamma_m \sigma_s \dot{\psi} \quad (\text{D.29})$$

$$\text{total stress rate: } \underline{\underline{\dot{\sigma}}} = \dot{\sigma}_m \underline{\underline{I}} + \dot{\sigma}_s \underline{\underline{S}} + 2 G [\underline{\underline{d}} - \underline{\underline{S}} (\underline{\underline{S}} : \underline{\underline{d}})]. \quad (\text{D.30})$$

Use one of the techniques on page 33 of the main report to integrate the last term all the way through to the end of the step.

step 13. If KOUNT=0, partially update values to their estimate at the half step:

$$\psi^{\text{half}} = \psi^{\text{old}} + \dot{\psi} \Delta t^p$$

$$\underline{\underline{\sigma}}^{\text{half}} = \underline{\underline{\sigma}}^{\text{elas}} + \underline{\underline{\dot{\sigma}}} \Delta t^p.$$

Keep in mind that Δt^p is actually *half* of the length of the time step, so this update brings us up to the middle of the step via forward differencing. For the second half of the step, we use a crude predictor-corrector technique to approximately use backward differencing for the second half of the step. This method improves the overall order of accuracy of the solution.

step 14. Regardless of value of the KOUNT iterator, update the variables to end of step. The effect of separating these steps is to approximate a second-order differencing scheme (a very crude predictor-corrector method).

When KOUNT is 0, this update is a simple forward difference to approximate the updated variables at the *end* of the step. Then KOUNT is incremented and the end-values estimates are used to approximate the rates $\dot{\lambda}$ and $\dot{\zeta}$ at the end of the step. Thus, when KOUNT > 0, this step effectively averages the rates at the beginning and end of the step, thereby resulting in an approximate second-order difference.

$$\psi = \psi^{\text{half}} + \frac{\dot{\psi} \Delta t^P}{2}$$

$$\underline{\underline{\sigma}} = \underline{\underline{\sigma}}^{\text{half}} + \underline{\underline{\dot{\sigma}}} \Delta t.$$

- step 15. Note: because we explicitly segregated the time step into elastic and plastic parts, there will be no need to return the stress state to the yield surface. In other words, the stress state will be “close” to the yield surface within differencing errors. The error here is third-order and is caused by yield surface curvature. Nevertheless, this step in the calculation may be used to force the predicted stress to lie exactly on the yield surface.
- step 16. Save the tentative updated stress tensor.
- step 17. Increase the iteration counter KOUNT:=KOUNT+1
- step 18. If KOUNT<KNTMAX and $|\psi - \psi^{\text{save}}| > 0$, then set $\psi^{\text{save}} = \psi$. Also update the moduli $K(\psi)$ and $G(\psi)$ and the scalar stress measures (σ_m and σ_s). Then return to STEP 9. Otherwise, if KOUNT=KNTMAX, give up on achieving convergence (print a warning and go to STEP 19.) If KOUNT<KNTMAX and $\psi = \psi^{\text{save}}$ to within tolerable error, then the predictor-corrector scheme successfully converged. See Fig. D.1 on page D-6.
- step 19. Stop. The stress and all other state variables have now been updated to the end of the step.
- step 20. If applicable, perform supplemental models such as rate dependence and/or PMFI rotation of the predicted state back to the current frame.

APPENDIX D. The predictor-corrector QCKP algorithm

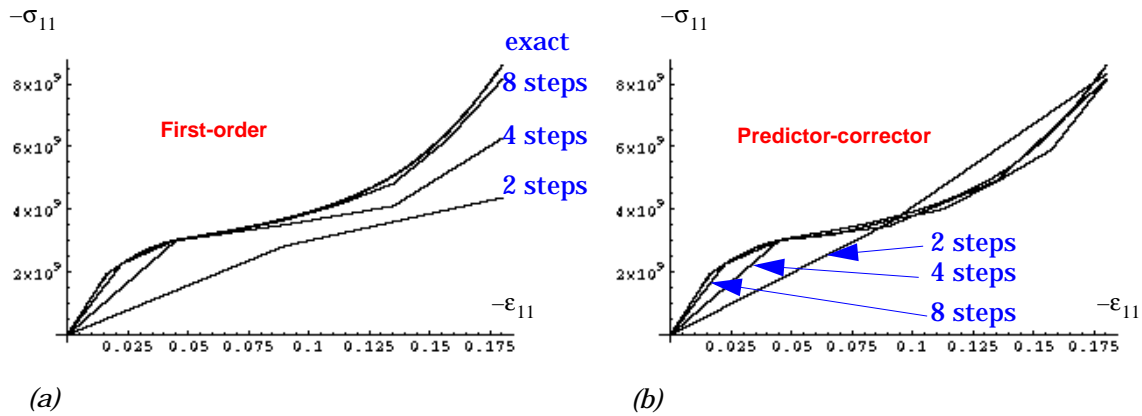


Fig. D.1. The effect of predictor-corrector scheme. The above plots show convergence behavior for simulation of pore collapse under uniaxial compression for (a) forward difference and (b) predictor corrector. Note that the predictor-corrector scheme has almost no error at the time step points — most of the visible error comes from linear interpolation of the solution between the steps.

APPENDIX E. The CKP coding

Below is the principal code fragment that applies this physics of the model. The steps listed in the comments correspond to those in Appendix D. By the time this code fragment is executed, user inputs have been read and reformulated. The complete set of routines for the CKP model will be made available at our discretion. Complete installation instructions are given in Appendix G.

```

C      -----
C      step 1: Compute variables at beginning of step
C      -----
C
C      Volumetric strain rate = trace of rate of deformation
C      DKK=D(1,I)+D(2,I)+D(3,I)
C      DKKX=PTHIRD*DKK
C
C      ... elastic moduli (Eq. 2.1 in SAND report)
C      RK=RKM*EXP(-RKAPM*PSI)
C      RG=RGM*EXP(-RGAMM*PSI)
C
C      Increase the relaxation time as the material is compressed.
C      (Apply Eq. 18.6 from SAND report.
C      TRELAX=TREL0*SQRT(RHO(I)*RK/(RHO0*RKM))
C
C      ... Old value of Sig_m
C      SIGMO=(SIG(1,I)+SIG(2,I)+SIG(3,I))/ROOT3
C
C      ... Old value of psidN, which is the rate of PSI from nucleation.
C      Compute this value using Eq.12.3 from SAND report:
C      PSIDNO=MIN(MAX(
$         ROOT3*(PONE+PSIO)*ALFN*(SIGMO*(PONE+PSIO)/(EPSN*RKM)-PONE)
$         ,PZERO),PSIDNM)
C
C      In this coding, we let DEP denote the effective elastic
C      plastic strain "rate" obtained by removing transformation
C      strain rate (which was done by the calling routine) and
C      by removing the part of the strain rate from nucleation.
C      We have a pretty bone-headed nucleation model that
C      assumes that the strain rate from nucleation is purely
C      isotropic. (See Eq. 7.1 in SAND report.)
C      From Eq.12.2 in SAND report, we know that the trace
C      of the strain rate from nucleation is equal to the rate
C      of psi from nucleation divided by (1+psi). In the following
C      line, we subtract this from the trace of D to obtain an
C      effective volumetric strain rate from everything BUT
C      nucleation and transformation:
C
C      TRDEP=DKK-PSIDNO/(PONE+PSI)
C
C      ... Old pressure
C      PRES=- (SIG(1,I)+SIG(2,I)+SIG(3,I))/PTHREE
C      PRESO=PRES
C
C      ... Old stress deviator
C      T10=SIG(1,I)+PRESO
C      T20=SIG(2,I)+PRESO
C      T30=SIG(3,I)+PRESO
C      T40=SIG(4,I)
C      T50=SIG(5,I)

```

APPENDIX E. The CKP coding

```

      T6O=SIG(6,I)
C
C   ... Old value of the isomorphic shear measure, Sig_s
      SIGSO=
&   SQRT(T1O*T1O+T2O*T2O+T3O*T3O+PTWO*(T4O*T4O+T5O*T5O+T6O*T6O))
C
C   -----
C   step 2: Compute a trial elastic stress
C   -----
C
C   ...trial increment in pressure and isomorphic mean stress:
      DPRES=-RK*TRDEP*DT
      DSIGM=ROOT3*RK*TRDEP*DT
C
C   ...trial increment in stress deviator:
      TWOGDT=PTWO*RG*DT
      DT1=TWOGDT*D(1,I)
      DT2=TWOGDT*D(2,I)
      DT3=TWOGDT*D(3,I)
      DT4=TWOGDT*D(4,I)
      DT5=TWOGDT*D(5,I)
      DT6=TWOGDT*D(6,I)
      DUM=PTHIRD*(DT1+DT2+DT3)
      DT1=DT1-DUM
      DT2=DT2-DUM
      DT3=DT3-DUM
C
C   ...Trial updated sigm (isomorphic mean stress)
      SIGM=SIGMO+DSIGM
C   ...Trial updated stress deviator
      T1=T1O+DT1
      T2=T2O+DT2
      T3=T3O+DT3
      T4=T4O+DT4
      T5=T5O+DT5
      T6=T6O+DT6
C
C   ...Updated value for trial sigs (isomorphic shear stress)
      SIGS=SQRT(T1*T1+T2*T2+T3*T3+PTWO*(T4*T4+T5*T5+T6*T6))
C
C   -----
C   step 3: Check if this is an elastic step
C   -----
C
C   ...Call the yield function. See Eq. 4.1 in SAND report
C   Throughout this model, the yield function is treated
C   as a black-box. There are no assumptions about the yield
C   function other than its independent arguments must be
C   as shown in the call below.
C
      FVAL=YIELDF(SIGM,SIGS,PSI,RSV)
C
C   ...The yield function is user-adjustable, so it is possible
C   for the user to employ a perverse yield function that
C   allows the pores to grow at zero stress. In a very loose
C   sense, we attempt to handle this possibility through the
C   use of PSIFRC, which is the value of PSI above which the
C   material is regarded to have fractured. This treatment is
C   quite ad-hoc, so we highly recommend avoiding it.
C   Henceforth, all references to PSIFRC have to do with this
C   fracture model, so we will not annotate those sections of
C   the code.
C
      IF(PSI.GT.PSIFRC)THEN
```

```

        IF(SIGM*DKK.GT.PZERO)THEN
            FVAL=PONE
        ELSE
            FVAL=-PONE
        END IF
    END IF

C
    IF(FVAL.LT.PZERO)THEN
C
C    ...To get inside this if-block, the yield function FVAL
C    must have given a negative number, which means that the
C    trial stress is INSIDE the yield surface and is therefore
C    elastic. That means that the fraction of the step that
C    is elastic must be 100%. Hence, we put RMUEL=1.0
C
        RMUEL=PONE

C
C    ...Pore nucleation is possible even under elastic loading.
C    Use Eq. 12.3 from SAND report to find the rate of PSI
C    from nucleation:
        PSIDN=PHALF*(PSIDNO+
$       MIN(MAX(
$         ROOT3*(PONE+PSI)*ALFN*(SIGM*(PONE+PSI)/(EPSN*RKM)-PONE)
$         ,PZERO),PSIDNM)
$     )
C
C    ...Apply Eq. 12.2 from SAND report to subtract off the
C    nucleation strain rate from the total strain rate.
        TRDEP=DKK-PSIDN/(PONE+PSI)

C
C    ...Update the pore ratio
        PSI=PSIO+PSIDN*DT*RMUEL
        CALL PSIVAR(PSI,FV)

C
C    Recall that we are inside this if-block because the
C    interval was determined to be 100% elastic. Therefore
C    we can skip the next section and go straight to
C    updating the stress.
        GO TO 5
    END IF

C
C
C
C    -----
C    step 4: Determine what fraction of step is elastic
C    -----
C
C    To reach this section of the coding, the trial elastic
C    stress state was found to lie outside the yield surface
C    and the interval is therefore at least partly elastic.
C
C    We let RMUEL denote the fraction of the step that is
C    elastic. We know that the stress at the END of the
C    elastic interval is
C
C
C        sig_end = sig_old + sigdot_trial*RMUEL*dt
C
C    We know that sig_end must lie exactly ON the yield
C    surface. If the yield function is f(sig,...) then
C    we wish to satisfy the condition that f(sig_end,...)=0.
C    Hence, we seek the value of RMUEL such that
C
C
C        f(sig_old + sigdot_trial*RMUEL*dt,...) = 0
C
C    The CKPore model presumes that the internal state
C    variables (denoted by "... " above) do not change during
C    elastic loading. Thus, the above equation contains only

```

APPENDIX E. The CKP coding

```

C      one unknown, RMUEL.
C
C      The following coding finds RMUEL via standard
C      Newton-Raphson methods.
C      For more details, see "step 4" of Appendix D
C      in SAND report
C
C      ... (i) Compute parameters used in Newton-Raphson
C      A=PTWO*(
$          T10*DT1+T20*DT2+T30*DT3
$          +PTWO*(T40*DT4+T50*DT5+T60*DT6)      )
C
C
C      B=
$          DT1*DT1+DT2*DT2+DT3*DT3
$          +PTWO*(DT4*DT4+DT5*DT5+DT6*DT6)
C      ... (ii) Initial guess
C      RMUEL=PHALF
C      SIGM=SIGMO+RMUEL*DSIGM
C      PSIDN=PHALF*(PSIDNO+
$          MIN(MAX(
$          ROOT3*(PONE+PSI)*ALFN*(SIGM*(PONE+PSI)/(EPSN*RKM)-PONE)
$          ,PZERO),PSIDNM)
$          )
C      TRDEP=DKK-PSIDN/(PONE+PSI)
C      PSI=PSIO+PSIDN*DT*RMUEL
C      CALL PSIVAR(PSI,FV)
C      SIGS=SQRT(MAX(PZERO,SIGSO*SIGSO+A*RMUEL+B*RMUEL*RMUEL))
C
C      kntNR is a parameter equal to max allowable iterations.
C      DO 77 KNT=1,KNTNR
C      ... (iii) Impose a division protection on sigs
C      SIGS=MAX(SIGS,SMLSTS)
C
C      IF(PSI.GT.PSIFRC)THEN
C          RMUSAV=RMUEL
C          RMUEL=PZERO
C      ELSE
C      ... (iv) Compute the yield function and its derivatives
C          FVAL=YIELDF (SIGM,SIGS,PSI,RSV)
C          CALL YLDDER(PSI,RSV)
C          FM =DFDSIGM(SIGM,SIGS,PSI,RSV)
C          FS  =DFDSIGS(SIGM,SIGS,PSI,RSV)
C          FPSI=DFDPSI (SIGM,SIGS,PSI,RSV)
C      ... (v) Save rmuel and then improve estimate
C          RMUSAV=RMUEL
C          DUM=FPSI*PSIDN*DT+FM*DSIGM+FS*(A+2*B*RMUSAV)/PTWO/SIGS
C          IF(DUM.NE.PZERO)THEN
C              RMUEL=RMUSAV-FVAL/DUM
C          ELSE
C              RMUEL=PONE
C          END IF
C      ... (vi) Limit rmuel to lie between 0 and 1
C          RMUEL=MIN(MAX(RMUEL,PZERO),PONE)
C      ... (vii) To avoid a lot of work for a puny plastic step,
C      replace rmuel by one if it is already close to one.
C          IF(PONE-RMUEL.LT.SMALL)RMUEL=PONE
C      END IF
C
C      ... (viii) Update the elastic stresses
C          SIGM=SIGMO+RMUEL*DSIGM
C          PSIDN=PHALF*(PSIDNO+
$          MIN(MAX(
$          ROOT3*(PONE+PSI)*ALFN*(SIGM*(PONE+PSI)/(EPSN*RKM)-PONE)
$          ,PZERO),PSIDNM)

```

```

$      )
      TRDEP=DKK-PSIDN/(PONE+PSI)
      PSI=PSIO+MIN(PSIMI,PSIDN*DT*RMUEL)
      CALL PSIVAR(PSI,FV)
      SIGS=SQRT(MAX(PZERO,SIGSO*SIGSO+A*RMUEL+B*RMUEL*RMUEL))
C      ... (ix) Check for convergence
      IF (ABS(RMUSAV-RMUEL).LT.SMALL) GO TO 7710
77      CONTINUE
C      call logmsp('WARNING: elastic step didnt cnvg')
      RMUEL=PONE
C
C
7710      CONTINUE
C
C
C      -----
C      step 5: Update the stress to the end of the elastic step
C      -----
5      CONTINUE
C      ... Update the elastic stress deviator
      T1=T10+RMUEL*DT1
      T2=T20+RMUEL*DT2
      T3=T30+RMUEL*DT3
      T4=T40+RMUEL*DT4
      T5=T50+RMUEL*DT5
      T6=T60+RMUEL*DT6
C
C      ... Convert sigm to conventional mean stress
      DUM=SIGM/ROOT3
C
      SIG(1,I)=T1+DUM
      SIG(2,I)=T2+DUM
      SIG(3,I)=T3+DUM
      SIG(4,I)=T4
      SIG(5,I)=T5
      SIG(6,I)=T6
      PRES      = - ( SIG(1,I) + SIG(2,I) + SIG(3,I) ) / PTHREE
C
C      Update the porosity (from nucleation) to end of elastic step
      PSIA(I)=PSI
C
C
C      -----
C      step 6: Check if the entire step is elastic
C      -----
      IF(PONE-RMUEL.LT.SMALL)GO TO 19
C
C
C      -----
C      step 7: Set the plastic time step and initialize iterations
C      -----
C
C      This implementation of the CKPore model uses a fairly
C      simplistic (but so-far robust) predictor-corrector method of
C      integrating the plastic equations. For standard finite
C      differences, we know that the updated value of some quantity y
C      is given by
C
C          ynew = yold + ydot*dt
C
C      The scheme is second order if
C
C          ydot = (1/2) (ydot_old + ydot_new)
C      In this case,

```

APPENDIX E. The CKP coding

```

C
C      ynew = yold + ydot_old*dt/2 + ydot_new*dt/2
C
C      That's the same as using the initial slope ydot_old to integrate
C      halfway through the step and then using ydot_new to integrate
C      through the remaining half step.
C
C      Of course, the difficulty is that ydot_new is not known until
C      ynew itself is known. In our iterative scheme, we use the
C      forward difference solution for ynew as a predictor. Then we
C      recompute ydot_new using this predictor. We re-evaluate the
C      second-half-step integration to correct our prediction.
C      The iteration continues until the predicted end state no longer
C      changes.
C
C      ...Set dtp to HALF the plastic time step.
      DTP=PHALF*(PONE-RMUEL)*DT
      KOUNT=0                ! iteration counter
      PSISAV=PSI             ! value of psi at last iteration
      RSVSAV=RSV            ! value of rsv at last iteration
C
C
C  9  CONTINUE
C
C      -----
C      step 8: Compute the pore rate due to nucleation
C      -----
C      Use Eq.12.3 from SAND report to find the rate of PSI
C      from nucleation:
      PSIDN=
$      MIN(MAX(
$      ROOT3*(PONE+PSI)*ALFN*(SIGM*(PONE+PSI)/(EPSN*RKM)-PONE)
$      ,PZERO),PSIDNM)
      TRDEP=DKK-PSIDN/(PONE+PSI)
C
C      -----
C      step 9: Compute the yield function derivatives
C      -----
C
C      ...Find the value of the yield function
C      (See Eq. 4.1 in SAND report)
      FVAL =YELDF (SIGM,SIGS,PSI,RSV)
      IF(PSI.GT.PSIFRC)FVAL=PONE
      IF(KOUNT.EQ.0)FVAL=MAX(FVAL,PZERO)
C
C      ...Find the values of Fm,Fs,Fpsi, and Fisv from Eq. 4.4 in
C      SAND report
      CALL YLDDER(PSI,RSV)
      FM =DFDSIGM(SIGM,SIGS,PSI,RSV)
      FS =DFDSIGS(SIGM,SIGS,PSI,RSV)
      FISV=DFDISV (SIGM,SIGS,PSI,RSV)
C
C      ...Apply Eq. 4.13 from SAND report
      YXI=SQRT(FM*FM+FS*FS)
      IF(PSI.LT.PSIFRC)THEN
          FPSI=DFDPSI (SIGM,SIGS,PSI,RSV)
      ELSE
C
C      This is a special case for "fracture"
C      This definition forces the elastic rate of deformation
C      to be zero. Again, this stuff is highly ad-hoc. If you
C      wish to model a material that fractures, then you should
C      consider installing a real fracture model.
          FPSI=RKAPM*SIGM*FM+RGAMM*SIGS*FS
$      -HHHH*YXI*FISV/ROOT3/(PONE+PSI)/FM

```

```

END IF

C
C
C -----
C step 10: Compute the S-hat unit tensor
C -----
C The tensor S-hat is just a unit tensor in the direction of the
C stress deviator. Thus, it equals the stress deviator divided by
C sigs. If the stress deviator is zero, then sigs=0.
C In this case, it turns out that S-hat is not really needed.
C It may be set for convenience. When sigs=0, I choose to
C set shat to be a unit tensor in the direction of the
C deviatoric strain rate.
C
C As explained in SAND report, the rate of change of the
C S-hat tensor is governed solely by the part of the trial
C elastic stress rate that is perpendicular to the Rendulic
C plane. With conventional radial return algorithms, the
C updated value of the stress has a new S-hat that is exactly
C equal to the unit tensor in the direction of the trial stress
C deviator. In this code, however, we do not use return methods.
C Instead, we integrate the equations directly. This approach
C requires explicit treatment of the S-hat tensor.
C
IF(SIGS.GT.PZERO)THEN
  SHAT1=T1
  SHAT2=T2
  SHAT3=T3
  SHAT4=T4
  SHAT5=T5
  SHAT6=T6
ELSE IF(SIGS.LT.PZERO)THEN
  CALL BOMBED('negative sigs')
ELSE
  SHAT1=D(1,I)
  SHAT2=D(2,I)
  SHAT3=D(3,I)
  SHAT4=D(4,I)
  SHAT5=D(5,I)
  SHAT6=D(6,I)
ENDIF
C ...Force Shat to be a deviatoric tensor
DUM=PTHIRD*(SHAT1+SHAT2+SHAT3)
SHAT1=SHAT1-DUM
SHAT2=SHAT2-DUM
SHAT3=SHAT3-DUM
C ...Force Shat to be a unit tensor
DUM=SQRT( SHAT1**2+SHAT2**2+SHAT3**2
$ +PTWO*(SHAT4**2+SHAT5**2+SHAT6**2))
IF(DUM.GT.SMALL)THEN
  SHAT1=SHAT1/DUM
  SHAT2=SHAT2/DUM
  SHAT3=SHAT3/DUM
  SHAT4=SHAT4/DUM
  SHAT5=SHAT5/DUM
  SHAT6=SHAT6/DUM
ELSE
  SHAT1=PZERO
  SHAT2=PZERO
  SHAT3=PZERO
  SHAT4=PZERO
  SHAT5=PZERO
  SHAT6=PZERO
END IF

```

APPENDIX E. The CKP coding

```

C -----
C step 11: Compute the plasticity parameter rlmidot.
C -----
C The following section of coding evaluates Eq. 14.1
C from SAND report. This is the most important equation
C of all. It gives the value for the "plastic segment"
C parameter lambda_dot, which we call RLMDOT here in
C the coding. Once RLMDOT is known, all of the other
C rates (of stress, porosity, etc.) are easily computed.
C
C
C ..evaluate d doubledot S-hat that appears in the second
C term (numerator of Eq. 14.1 , SAND report).
C DXXSH= (D(1,I)-DKKX)*SHAT1
$      +(D(2,I)-DKKX)*SHAT2
$      +(D(3,I)-DKKX)*SHAT3
$ + PTWO*( D(4,I)      *SHAT4
$          +D(5,I)      *SHAT5
$          +D(6,I)      *SHAT6 )
C
C ..denominator -- see modification 980630 --
C DUM=PTHREE*RK*FM*FM+PTWO*RG*FS*FS
$ +ROOT3*(PONE+PSI)*FM*(RKAPM*SIGM*FM+RGAMM*SIGS*FS-FPSI)
$ -HHHH*YXI*FISV
C
C IF(DUM.NE.PZERO)THEN
C   RLMDOT=(
$     ROOT3*RK*FM*TRDEP+PTWO*RG*FS*DXXSH
$     +PSIDN*(FPSI-RKAPM*SIGM*FM-RGAMM*SIGS*FS)
$     +UPSDOT(I)*(FM*SIGM+FS*SIGS)
$     )/DUM
C   IF(KOUNT.LE.0.AND.RLMDOT.LT.PZERO)THEN
C     CALL BOMBED('negative plastic segment')
C   ENDIF
C   IF(KOUNT.LE.0)RLMDOT=MAX(RLMDOT,PZERO)
C ELSE
C   RLMDOT=PZERO
C END IF
C
C
C -----
C step 12: Compute rates of the state variables
C -----
C ..Apply Eq. 14.3 from SAND report
C RSVDOT=HHHH*YXI*RLMDOT
C
C ..Apply Eq. 14.4 from SAND report
C PSIDOT=ROOT3*(PONE+PSI)*FM*RLMDOT+PSIDN
C
C ..Apply Eq. 14.5 and 14.5 from SAND report
C SIGMDOT=PTHREE*RK*(TRDEP/ROOT3-FM*RLMDOT)-RKAPM*SIGM*PSIDOT
C SIGSDOT=PTWO*RG*(DXXSH-FS*RLMDOT)-RGAMM*SIGS*PSIDOT
C
C IF(PSI.GT.PSIFRC)THEN
C   PSIDOT=(PONE+PSI)*DKK
C   RSVDOT=HHHH*DXXSH
C   SIGMDOT=-RKAPM*SIGM*PSIDOT
C   SIGSDOT=-RGAMM*SIGS*PSIDOT
C END IF
C
C IF(KOUNT.EQ.0.AND.SIGS.GT.PZERO)THEN
C ..Apply Eq. 14.7
C   SSSD1=PTWO*RG*(D(1,I)-DKKX-SHAT1*DXXSH)

```

```

SSSD2=PTWO*RG*(D(2,I)-DKKX-SHAT2*DXXSH)
SSSD3=PTWO*RG*(D(3,I)-DKKX-SHAT3*DXXSH)
SSSD4=PTWO*RG*(D(4,I)      -SHAT4*DXXSH)
SSSD5=PTWO*RG*(D(5,I)      -SHAT5*DXXSH)
SSSD6=PTWO*RG*(D(6,I)      -SHAT6*DXXSH)
DUM=PTHIRD*(SSSD1+SSSD2+SSSD3)
SSSD1=SSSD1-DUM
SSSD2=SSSD2-DUM
SSSD3=SSSD3-DUM
C
C
C   ...Notice that this chunk of coding is inside an if-block
C   that applies only when KOUNT=0, which is the forward
C   difference part of the calculation. Recall that the
C   rate of S-hat is determined completely by the ELASTIC
C   trial stress rate, which does not change during iterations
C   because the total deformation rate is constant throughout
C   the time step. Hence, in the interest of better efficiency,
C   Finding the updated value of S-hat does not require any
C   iterations. This is especially true since we perform
C   the integration using "infinite" order accuracy using
C   the technique described on page 33 in SAND report.
C
C   Since we are going to perform the integration over the
C   ENTIRE step (not just the half step), we must keep in
C   mind that dtp is actually equal to the half step. That's
C   why we multiply it by two below.
C
C   ...Compute the magnitude of sssd1 times ptwo*dtp/sigs
C   This is the quantity delta-s in Eq. 11.15 from SAND report
C
C   DUM=SQRT(          SSSD1*SSSD1+SSSD2*SSSD2+SSSD3*SSSD3
$           +PTWO*(SSSD4*SSSD4+SSSD5*SSSD5+SSSD6*SSSD6))
$           *PTWO*DTP/SIGS
C   IF(DUM.GT.PZERO)THEN
C   ...Compute the quantity "b" from Eq.(11.21) . Multiply
C   it by the time step (2*dtp) and divide it by
C   SIGS. Store the result into DUM2
C   DUM2=PTWO*DTP*TANH(DUM)/DUM/SIGS
C   ...Compute the quantity "a" from Eq.(11.21)
C   DUM=pone/COSH(DUM)
C
C   ...Apply Eq. 11.16 to update S-hat all the way to the
C   end of the step (not just the half step)
C   SHAT1=DUM2*SSSD1+DUM*SHAT1
C   SHAT2=DUM2*SSSD2+DUM*SHAT2
C   SHAT3=DUM2*SSSD3+DUM*SHAT3
C   SHAT4=DUM2*SSSD4+DUM*SHAT4
C   SHAT5=DUM2*SSSD5+DUM*SHAT5
C   SHAT6=DUM2*SSSD6+DUM*SHAT6
C   END IF
C   END IF
C
C
C   -----
C   step 13: Apply forward difference to half-update the state
C   -----
C   --> Keep in mind: dtp is actually HALF the plastic step.
C
C   IF(KOUNT.EQ.0)THEN
C   ..Save values at the half step to use as starting values
C   for integrating the second half of the step.
C   PSIH=MAX(PSI+PSIDOT*DTP,PZERO)
C   RSVH=MAX(RSV+RSVDOT*DTP,PZERO)

```

APPENDIX E. The CKP coding

```

      SIGMH=SIGM+SIGMDOT*DTP
      SIGSH=SIGS+SIGSDOT*DTP
END IF
C
C
C
C -----
C step 14: Update state to the very END of the step
C -----
C We have already computed and saved the half-updated state
C at the middle of the step. Here we use the rates at the
C end of the step to complete the integration. In the
C predictor-corrector scheme, we initially use the forward
C difference rates as our guess for the backward difference
C rates.
C
C --> Keep in mind: DTP is actually HALF the plastic step,
C     so the following gets us to the end of the step.
RSV=MAX(RSVH+RSVDOT*DTP,PZERO)
PSI=MAX(PSIH+PSIDOT*DTP,PZERO)
CALL PSIVAR(PSI,FV)
PSIA(I)=PSI
RSVA(I)=RSV
C
      SIGM=SIGMH+SIGMDOT*DTP
      SIGS=SIGSH+SIGSDOT*DTP
      IF(SIGS.LT.PZERO)THEN
C         Keep in mind that sigs is the magnitude of the stress
C         deviator, so it must be always positive. However, under
C         finite difference integration, the predicted value of
C         sigs might turn out to be negative. Physically, this
C         means that the stress deviator has simply changed
C         direction. The following coding reflects this fact.
          SIGS=-SIGS
          SHAT1=-SHAT1
          SHAT2=-SHAT2
          SHAT3=-SHAT3
          SHAT4=-SHAT4
          SHAT5=-SHAT5
          SHAT6=-SHAT6
          DXXSH=-DXXSH
      ENDIF
      DUM1=SIGM
      DUM2=SIGS
C
C
C
C -----
C step 15: Ensure that updated stress is at or below yield
C -----
      IF(PSI.LT.PSIFRC.AND.RLMDOT.NE.PZERO)THEN
C
C     ...Third-order integration errors
C     (caused by yield surface curvature) might cause
C     the predicted stress to lie slightly off of the yield
C     surface. The following coding uses a Newton
C     scheme to project the stress to the nearest point
C     on the yield surface.
C
C     ...Put the stress on the yield surface
      SIGMO=SIGM
      SIGSO=SIGS
      DO 22 M=1,20
      FVAL =YIELDF (SIGM,SIGS,PSI,RSV)
      IF(FVAL.LT.PZERO.AND.M.LT.2)GOTO 68
      CALL YLDDER(PSI,RSV)

```

```

IF(PSI.GT.0.1D-10.AND.SIGM/SBY.GT.-0.1D2)THEN
  FM =DFDSIGM(SIGM,SIGS,PSI,RSV)
ELSE
  FM=PZERO
END IF
FS =DFDSIGS(SIGM,SIGS,PSI,RSV)
DUM=FM*FM+FS*FS
IF(DUM.LE.PUNY)GO TO 68
SIGM=SIGM-FVAL*FM/DUM
SIGS=SIGS-FVAL*FS/DUM
IF(((SIGM-SIGMO)/SBY)**2
$   +((SIGS-SIGSO)/SBY)**2.LT.PUNY)THEN
  GO TO 68
ELSE
  SIGMO=SIGM
  SIGSO=SIGS
END IF
22  CONTINUE
    CALL LOGMSP('WARNING: stress off yield')
    SIGM=DUM1
    SIGS=DUM2
68  CONTINUE
END IF
C   sigsdot=(sigs-sigsh)/dtp
C   sigmdot=(sigm-sigmh)/dtp
C
C
C   -----
C   step 16: Update the stress tensor
C   -----
C   ...Apply Eq. 14.8, noting that sigm times I-hat equals
C   -PRES times the ordinary identity I.
    PRES=-SIGM/ROOT3
    SIG(1,I)=SIGS*SHAT1-PRES
    SIG(2,I)=SIGS*SHAT2-PRES
    SIG(3,I)=SIGS*SHAT3-PRES
    SIG(4,I)=SIGS*SHAT4
    SIG(5,I)=SIGS*SHAT5
    SIG(6,I)=SIGS*SHAT6
C
C   -----
C   step 17: Increment the iteration
C   -----
    KOUNT=KOUNT+1
C
C   -----
C   step 18: Check for convergence or iteration limit.
C   -----
    We will consider the solution to have converged when
    the updated porosity and updated yield stress no longer
    change.
C
    IF(KOUNT.LT.KNTMAX.AND.
$   ( ABS(PSIA(I)-PSISAV).GT.SMALL
$     .OR.ABS(RSVA(I)-RSVSAV).GT.SMALL*RSV0 )
$   )THEN
    IF(10*KOUNT.LT.KNTMAX.OR.PSIA(I).GT.PZERO)THEN
C   The if-statement for this block prevents
C   nonconvergence at the cycle when the porosity
C   goes to zero. At that point, you can get into
C   nonconvergence because the yield in hydrostatic
C   compression is suddenly prohibited.
    PSISAV=PSIA(I)
    RSVSAV=RSVA(I)

```

APPENDIX E. The CKP coding

```

    RG=RGM*EXP(-RGAMM*PSI)
    RK=RKM*EXP(-RKAPM*PSI)
    GO TO 9
  ENDF
ELSE IF(KOUNT.GE.KNTMAX)THEN
  IERFLG = 1
  KNTERR=KNTERR+1
  IF(KNTERR.LT.MAXMES)THEN
    CALL LOGMSP('plastic iteration did not converge')
  ENDF
END IF
C
C -----
C step 19: STOP (Computation of new psi and SIG complete)
C -----
19  CONTINUE
C  ...check to be sure the stress is on or in yld surface
    TEST=YIELDF(SIGM,SIGS,PSI,RSV)
    IF(TEST.GT.0.05)THEN
      CALL BOMBED('stress off yield')
    ENDF
C
C -----
C step 20: Apply supplemental model features
C -----
C  At this point, the stress is simply the EQUILIBRIUM stress.
C  If rate dependence is turned on (i.e., if TRELAX.ne.0.0),
C  then we need to compute the overstress and add it to the
C  equilibrium stress.
C
C  Add the rate-dependent contribution
    IF(TRELAX.GT.PZERO)THEN
      C  Compute the tensor q*trelax, where q is the
      C  trial stress rate minus the equilibrium stress rate.
      C  This is Eq. 18.4 in SAND report
      DUM=TRELAX/DT
      DUMA(1)=DUM*(DT1-DPRES-SIG(1,I)+T10-PRESO)
      DUMA(2)=DUM*(DT2-DPRES-SIG(2,I)+T20-PRESO)
      DUMA(3)=DUM*(DT3-DPRES-SIG(3,I)+T30-PRESO)
      DUMA(4)=DUM*(DT4      -SIG(4,I)+T40)
      DUMA(5)=DUM*(DT5      -SIG(5,I)+T50)
      DUMA(6)=DUM*(DT6      -SIG(6,I)+T60)
C
      C  ...update overstress, which is the difference b/w sig
      C  and sig_equilibrium.
      C  Thus, apply Eq.18.5 from SAND report
      DUM=EXP(-DT/TRELAX)
      OVER(1,I)=DUMA(1)+(OVER(1,I)-DUMA(1))*DUM
      OVER(2,I)=DUMA(2)+(OVER(2,I)-DUMA(2))*DUM
      OVER(3,I)=DUMA(3)+(OVER(3,I)-DUMA(3))*DUM
      OVER(4,I)=DUMA(4)+(OVER(4,I)-DUMA(4))*DUM
      OVER(5,I)=DUMA(5)+(OVER(5,I)-DUMA(5))*DUM
      OVER(6,I)=DUMA(6)+(OVER(6,I)-DUMA(6))*DUM
C
      C  ...Now convert the stress from eqbm to actual.
      C  Apply Eq.18.1 from SAND report
      SIG(1,I)=SIG(1,I)+OVER(1,I)
      SIG(2,I)=SIG(2,I)+OVER(2,I)
      SIG(3,I)=SIG(3,I)+OVER(3,I)
      SIG(4,I)=SIG(4,I)+OVER(4,I)
      SIG(5,I)=SIG(5,I)+OVER(5,I)
      SIG(6,I)=SIG(6,I)+OVER(6,I)
    END IF

```

APPENDIX F. Coding for the Gurson yield criterion

The routines below show the computation of the Gurson yield function and its derivatives

$$F(\sigma_m, \sigma_s, \psi) \quad (\text{F.1})$$

$$F_m \equiv \frac{\partial F(\sigma_m, \sigma_s, \psi)}{\partial \sigma_m} \quad (\text{F.2})$$

$$F_s \equiv \frac{\partial F(\sigma_m, \sigma_s, \psi)}{\partial \sigma_s} \quad (\text{F.3})$$

$$F_\psi \equiv \frac{\partial F(\sigma_m, \sigma_s, \psi)}{\partial \psi} \quad (\text{F.4})$$

The functions include an ad hoc means of allowing pore nucleation after pores have completely crushed up. Namely, if pore collapse causes the porosity to fall below some critical value, then the tensile side of the yield surface stops co-evolving (this is clearly nonphysical, but sufficient for present purposes).

```

c-----1-----2-----3-----4-----5-----6-----7--
      FUNCTION YieldF(sigm,sigs,psi,sby)
*****
C      PURPOSE: This routine computes the yield function in the
C      consistent porosity model.
C
C input
C -----
C   sigm: The projected mean stress = trace(stress)/SQRT(3)
C   sigs: The stress deviator magnitude
C   psi: porosity ratio (pore volume divided by solid volume)
C   isv: internal state variable for matrix material (yield in shr)
C
C output
C -----
C   YieldF: value of the yield function at the specified state.
C
C MODIFICATION HISTORY
C 12/17/97:rmbrann:created routine
C
      INCLUDE 'implicit.h'
C.....parameters
c      numbers
      parameter (pzero=0.0d0,pone=0.1d1,ptwo=0.2d1)
      parameter (smallf=0.1d-5)

```


APPENDIX F. Coding for the Gurson yield criterion

```

endif
RETURN
END
c---.---1---.---2---.---3---.---4---.---5---.---6---.---7---
      FUNCTION dFdsigs(sigm,sigs,psi,sby)
*****
C      PURPOSE: This routine computes the derivative of the yield
C      function with respect to sigs.
C
C input
C -----
C      sigm: The projected mean stress = trace(stress)/SQRT(3)
C      sigs: The stress deviator magnitude
C      psi: porosity ratio (pore volume divided by solid volume)
C      isv: internal state variable for matrix material (yield in shr)
C
C output
C -----
C      dFdsigs: value of the derivative
C
C
C      MODIFICATION HISTORY
C      12/17/97:rnbrann:created routine
C
      INCLUDE 'implicit.h'
C.....parameters
c      numbers
      parameter (pzero=0.0d0,pone=0.1d1,ptwo=0.2d1)
c---->hardwired
      parameter (smallf=0.1d-5)
      CHARACTER*6 IAM
      PARAMETER (IAM='HCRUSH')

C.....common
CCCCCCCCCCCCCCCCCCCCCCCCCCCCCCCCCCCCCCCCCCCCCCCCCCCCCCCCCCCCCCCC
      dFdsigs=ptwo*sigs/sby/sby
      RETURN
      END
c---.---1---.---2---.---3---.---4---.---5---.---6---.---7---
      FUNCTION dFdpsi(sigm,sigs,psi,sby)
*****
C      PURPOSE: This routine computes the derivative of the yield
C      function with respect to psi.
C
C input
C -----
C      sigm: The projected mean stress = trace(stress)/SQRT(3)
C      sigs: The stress deviator magnitude
C      psi: porosity ratio (pore volume divided by solid volume)
C      isv: internal state variable for matrix material (yield in shr)

```

APPENDIX F. Coding for the Gurson yield criterion

```
C
C output
C -----
C   dFdpsi: value of the derivative
C
C
C MODIFICATION HISTORY
C 12/17/97:rmbrann:created routine
C
C   INCLUDE 'implicit.h'
C.....parameters
c   numbers
C   parameter (pzero=0.0d0,pone=0.1d1,ptwo=0.2d1)
c---->hardwired
C   parameter (smallf=0.1d-5)
C   CHARACTER*6 IAM
C   PARAMETER (IAM='HCRUSH')

C.....common
CCCCCCCCCCCCCCCCCCCCCCCCCCCCCCCCCCCCCCCCCCCCCCCCCCCCCCCCCCCCCCCCCCCCCCCC
C   root2=SQRT(ptwo)
C   f=psi/(pone+psi)
C   if(f.gt.smallf)then
C   dFdpsi=ptwo*(pone-f)**2*(COSH(sigm/root2/sby)-f)
C   else
C   dFdpsi=pzero
C   endif
C   RETURN
C   END

c---.----1----.----2----.----3----.----4----.----5----.----6----.----7--
C   FUNCTION dFdisv(sigm,sigs,psi,sby)
*****
C   PURPOSE: This routine computes the derivative of the yield
C   function with respect to isv.
C
C input
C -----
C   sigm: The projected mean stress = trace(stress)/SQRT(3)
C   sigs: The stress deviator magnitude
C   psi: porosity ratio (pore volume divided by solid volume)
C   isv: internal state variable for matrix material (yield in shr)
C
C output
C -----
C   dFdpsi: value of the derivative
C
C
C MODIFICATION HISTORY
C 12/17/97:rmbrann:created routine
C
```

APPENDIX F. Coding for the Gurson yield criterion

```

        INCLUDE 'implicit.h'
C.....parameters
c      numbers
        parameter (pzero=0.0d0,pone=0.1d1,ptwo=0.2d1,pthree=0.3d1)
c---->hardwired
        CHARACTER*6 IAM
        PARAMETER (IAM='HCRUSH')

C.....common
CCCCCCCCCCCCCCCCCCCCCCCCCCCCCCCCCCCCCCCCCCCCCCCCCCCCCCCCCCCCCCCCCCCC
        root2=SQRT(ptwo)
        f=psi/(pone+psi)
        dFdisv=- (
$      ptwo*sigs*sigs/sby+root2*f*sigm*sinh(sigm/root2/sby)
$
        RETURN
        END
c---.----1----.----2----.----3----.----4----.----5----.----6----.----7--
        FUNCTION smfnt(fv)
*****
C      PURPOSE: This routine computes the value of the sm function
C      in the interpolated Gurson model.
C
C input
C -----
C   fv: The void volume fraction
C
C output
C -----
C   smfnt: value of the modified/normalized p-alpha function
C
C
C MODIFICATION HISTORY
C 01/05/98:rnbrann:created routine
C
        INCLUDE 'implicit.h'

C.....parameters
c      numbers
        parameter (pzero=0.0d0,pone=0.1d1,ptwo=0.2d1,pthree=0.3d1)
        parameter (seG=0.357192d1,scG=0.1d2)
        parameter (sGdif=scG-seG)
        external grfnt

C.....common
        SAVE /SMDAT/
        COMMON /SMDAT/ psi0,aaa,bbb,psi
CCCCCCCCCCCCCCCCCCCCCCCCCCCCCCCCCCCCCCCCCCCCCCCCCCCCCCCCCCCCCCCCCCCC
C----- Basic Gurson
c      smfnt=grfnt(fv)

```

APPENDIX F. Coding for the Gurson yield criterion

```

C----- Stretched Gurson
      grval=grfnt(fv)
      if(aaa*bbb.gt.pzero)then
        smfnt=aaa*LOG(bbb*grval+pone)
      else
        smfnt=aaa*grval
      endif
C----- linear
      root3=SQRT(pthree)
      se= root3*1.5d0
      sc= root3*5.0d0
      fv0=0.08
      psi0=fv0/(pone-fv0)
      psi=fv/(pone-fv)
      smfnt=se+(pone-psi/psi0)*(sc-se)
C-----
      RETURN
      END

c---.---1---.---2---.---3---.---4---.---5---.---6---.---7---
      FUNCTION smprim(fv)
*****
C      PURPOSE: This routine computes the derivative of smfnt
C      function with respect to its independent variable.
C
C input
C -----
C   fv: The void volume fraction
C
C output
C -----
C   smprim: value of the derivative of sm wrt fv
C
C
C MODIFICATION HISTORY
C 01/05/98:rmbrann:created routine
C
      INCLUDE 'implicit.h'
C.....parameters
c      numbers
      parameter (pzero=0.0d0,pone=0.1d1,ptwo=0.2d1,pthree=0.3d1)
      parameter (seG=0.357192d1,scG=0.1d2)
      parameter (sGdif=scG-seG)
      external grprim
c.....common
      SAVE /SMDAT/
      COMMON /SMDAT/ psi0,aaa,bbb,psi
CCCCCCCCCCCCCCCCCCCCCCCCCCCCCCCCCCCCCCCCCCCCCCCCCCCCCCCCCCCC
C----- Basic Gurson
c      smprim=grprim(fv)

```

APPENDIX F. Coding for the Gurson yield criterion

```

C----- Stretched Gurson
c   grder=grprim(fv)
      if(aaa*bbb.gt.pzero)then
          smprim=grprim(fv)*aaa*bbb/ABS(bbb*grfnt(fv)+pone)
      else
          smprim=aaa*grprim(fv)
      endif
C----- linear
c   root3=SQRT(pthree)
c   se= root3*1.5d0
c   sc= root3*5.0d0
c   fv0=0.08
c   psi0=fv0/(pone-fv0)
c   psi=fv/(pone-fv)
c   smprim=- (sc-se)/psi0/((pone-fv)**2)
C-----
      RETURN
      END

c-----1-----2-----3-----4-----5-----6-----7--
      FUNCTION grfnt(fv)
*****
C   PURPOSE: This routine computes the value of the Gurson sm function
C   in the interpolated Gurson model.
C
C input
C -----
C   fv: The void volume fraction
C
C output
C -----
C   grfnt: value of Gurson modified/normalized p-alpha function
C
C
C   MODIFICATION HISTORY
C   01/13/98:rmbrann:created routine
C
      INCLUDE 'implicit.h'
C.....parameters
c   numbers
      parameter (pzero=0.0d0,pone=0.1d1,ptwo=0.2d1,pthree=0.3d1)
      parameter (puny=1.d-20)

C.....common
CCCCCCCCCCCCCCCCCCCCCCCCCCCCCCCCCCCCCCCCCCCCCCCCCCCCCCCCCCCCCCCC
      grfnt=-SQRT(ptwo)*LOG(MAX(fv,puny))
      RETURN
      END

```

APPENDIX F. Coding for the Gurson yield criterion

```
c---.----1----.----2----.----3----.----4----.----5----.----6----.----7--
      FUNCTION grprim(fv)
*****
C     PURPOSE: This routine computes the derivative of the gurson smfnt
C     function with respect to its independent variable.
C
C input
C -----
C   fv: The void volume fraction
C
C output
C -----
C   grprim: value of the derivative of the gurson smfnt wrt fv
C
C
C MODIFICATION HISTORY
C 01/05/98:rnbrann:created routine
C
      INCLUDE 'implicit.h'
C.....parameters
c     numbers
      parameter (pzero=0.0d0,pone=0.1d1,ptwo=0.2d1,pthree=0.3d1)
      parameter (puny=1.d-20)

C.....common
CCCCCCCCCCCCCCCCCCCCCCCCCCCCCCCCCCCCCCCCCCCCCCCCCCCCCCCCCCCCCCCCCCCC
      grprim=-SQRT(ptwo)/MAX(fv,puny)
      RETURN
      END
```

```
c---.----1----.----2----.----3----.----4----.----5----.----6----.----7--
      SUBROUTINE psivar(
C input
      $ psi,psifrc,
C output
      $ fv,smval,smdr,sigmGr,grval,grder)
*****
C     PURPOSE: This routine computes variables that depend on psi
C     and must be updated whenever psi changes.
C
```

APPENDIX F. Coding for the Gurson yield criterion

```

C input
C -----
C   PSI: The pore ratio (void volume)/(solid volume)
C
C output
C -----
C   FV: void volume fraction
C   SMVAL: Yield stretching function
C   SMDER: Derivative of Yield stretching function
C   SIGMGR: Ratio of sigm to smval
C
C
C   MODIFICATION HISTORY
C   980113:rmb:created routine
C
C       INCLUDE 'implicit.h'
C.....parameters
C       CHARACTER*6 IAM
C       PARAMETER (IAM='PSIVAR')
C       parameter(pzero=0.0d0, pone=0.1d1)
C       parameter(psicut=0.1d-4)
c       parameter(psifrc=0.11d0)

C.....common
c.....passed
C.....function (functions instead of subroutines)
C.....external
c.....local (not saved)
C.....local (saved)
C.....data
C.....statement functions
CCCCCCCCCCCCCCCCCCCCCCCCCCCCCCCCCCCCCCCCCCCCCCCCCCCCCCCCCCCCCCCCCCCCCCCC
    fv=psi/(pone+psi)
    grval=grfnt(fv)
    grder=grprim(fv)
    smval=smfnt(fv)
    if(psi.lt.psicut)then
        smval=grfnt(fv)
        smder=grprim(fv)
        sigmGr=pone
    elseif(psi.gt.psifrc)then
        smval=pzero
        smder=pzero
        sigmGr=pone
    else
        smder=smprim(fv)
        sigmGr=ABS(grval/smval)
    end if
RETURN
END

```

APPENDIX F. Coding for the Gurson yield criterion

This page intentionally left blank.

APPENDIX G.

Manuals for VERSION 001009* of the CKP model

Instructions for model installers

This section contains information about how to install the CKP model into a host code. This model conforms to the (MIG) Model Interface Guidelines [4] which specify how to assemble a material model in such a manner that maximizes its portability from code to code and across computational platforms. In conformance to MIG, there are three key subroutines (all contained in the file called `ckpore.F`):

- **CKPCHK**: Ensures that the user input is sensible. Importantly, this routine also initializes commons and changes some user input to different meanings that are more useful in the CKP model.† This data check routine also uses the user input to compute supplemental material constants.
- **CKPRXV**: Requests extra variables from the host code. This routine outputs a list of desired internal state variables along with their plotting keywords. It is the responsibility of the host code to actually allocate sufficient storage for the requested field variables.
- **CKPORE**: Applies the physics of the CKP model. Inputs and outputs from this routine are listed both in the subroutine prolog and in Appendix H of this report.

The above three routines are the *only* routines called directly by the host code. Other routines are called internally by the model, not by the host code. These private routines reside in the file called `hcrush.F`. This private file contains the functions that define the yield function $F(\sigma_m, \sigma_s, \psi, \zeta)$ and its derivatives F_m , F_s , F_ψ , and F_ζ , [See Eqs. (4.1) and (4.4) in this report]. The version of `hcrush.F` that comes with the standard CKP source code is an implementation of the D.O.D. yield function described in Section 19 on page 62 of this report. As such, `hcrush.F` contains a helper function called `smfnt` that is roughly equivalent to a p - α function except that the stress measures are isomorphic [see Eq. (3.14) in this report] and the porosity measure is ψ instead of α . The default version of `smfnt` that comes in `hcrush.F` is the crush function *implied* by the pressure intercept of the standard Gurson yield surface (see the discussion on page 42 of the main report). If desired, `smfnt` may be replaced by the p - α function for the particular material of interest to the user. Likewise, the derivative of this function `smprim` would also be modified appropriately. A future version of the CKP model will likely support tabular crush curves so that the user will not have to recompile the code in order to use a new yield function.

* The version number is based on the date (yyymmdd) of the most recent physics modification.

† For example, the user specifies the classically-defined porosity f , which is the volume fraction of pores. The CKPCHK routine replaces f by the pore ratio $\psi = f/(1 - f)$ used everywhere else in the coding.

The host code is responsible for reading the user inputs and storing them into a single array in the order specified in the prologue of the CKPCHK routine. Before any calculations begin, the host code must call CKPCHK to check the user inputs and to perform several essential time-zero start-up tasks. If the host code supports restarts, the CKPCHK routine must also be called upon restarting.

Also at time-zero start-up, the host code must call the routine CKPRXV that requests extra variables for the CKP model. As explained in the MIG documentation [4], this extra variable routine does nothing but *ask* for the extra variables. The host code is responsible for actually granting the request and allocating appropriate storage. As explained in the MIG documentation [4], the host code must set default values for all arguments to CKPRXV before calling it. After calling CKPRXV, the host code must establish storage for all internal state variables requested from the routine. The CKPRXV routine does *not* request variables such as stress or rate-of-deformation. These variables are “migrationary” variables that are expected to already exist within the host code. Instead, the CKPRXV routine requests only those internal state variables that are essentially unique to CKP materials.

Once all start-up tasks are complete, the host code begins to sweep over every element/cell for each time step. For the elements that contain CKP material, the host code calls the CKPORE driver routine to obtain updated values for the stress and internal state variables.

Verification benchmarks. Most of the stress-strain plots generated in this report were created by running a stand-alone single cell “demo” program that permits the user to exercise the model under an arbitrary homogeneous deformation history. The demo program then writes the resulting stress history (as well as the histories of all other state variables) in a format that is readable and plot-able by *mathematica* or HISPLT. The installer might want to request from us (at our discretion) a copy of this demo driver as a means of learning how the CKP model is installed in a very simple host code. By using the demo driver, a new installation may be verified by comparing its prediction under the controlled strain conditions against predictions of the demo program.

MIG host utilities. The CKP model conforms to MIG specifications [4]. As such, it assumes that the host code contains certain helper routines such as BOMBED (which stops the calculation) and LOGMES (which prints messages to the host code’s output file). Any “missing” subroutines discovered by attempting to compile the CKP model are probably these MIG utilities. The host code architect should refer to MIG specifications [4] for details about how these simple helper utilities should be written.

User instructions

To determine the manner in which this CKP model is invoked, you must consult the manual for the host code where it is installed. Of course any implementation will require you to specify material property data, as defined in Tables G.1 and G.2. Your CKP material inputs are saved within a single array. Most host codes will write a copy of your input to the log file for the calculation. However, you should be aware that the CKP model performs several modifications of the user inputs. It may happen that the particular host code on which the CKP model resides echos the user-input values *after* they have been modified (for example, porosity f_v is converted into pore ratio ψ). You should be able to easily tell whether the host code echos the original or the modified user inputs by simply seeing if the value of porosity has changed.

Once the material data have been supplied to the host code, the calculation proceeds just as it would for any other material model. The final results will therefore permit you to plot stress versus strain (or density if the code does not have a strain variable). Additional CKP internal state variables available for plotting are:

- **PORRAT**: The porosity ratio $\psi = f_v / (1 - f_v)$, where f_v is the volume fraction of voids. Under isotropic loading, you may parametrically plot PORRAT vs. pressure to obtain the *effective* p - α crush curve for the material. Under a different load path (such as uniaxial strain), this parametric plot will appear quite different, thereby demonstrating that shear dependence means that the p - α crush curve is *not* a fundamental material function in the CKP paradigm.
- **MTRXYLD**: The matrix isomorphic yield stress $\bar{\sigma}_s$, which changes over time only if hardening is invoked ($\text{HARDMOD} > 0$). Referring to Eq. (3.14) of the main report, note that this is initially equal to YIELDM times $\sqrt{2}$, where YIELDM is a user input equal to the matrix yield in shear (see Table G.1).
- **OVERxx**: the xx-component of the overstress tensor $\underline{\underline{\sigma}}^{\text{over}}$ (see Eq. 18.1)
OVERyy: the yy-component of the overstress tensor, etc.
 Overstress is non-zero only if rate dependence is invoked ($\text{TRELAX} > 0$)

For getting started, this model comes with a default yield function. To use the default yield function in its simplest form, you must provide a value of the matrix yield stress in shear (YIELDM, defined in Table G.1). The other yield function parameters (YRATIO, YCURVE, and YSLOPE, defined in Table G.2) may be used to further modify the behavior of the default yield function.

The default yield function has very limited capabilities. If measurements of the material yield function are available, then you should modify the default yield subroutines in the source code file called `hcrush.F`. If you do not have complete information about the material yield function, but you do have a measured hydrostatic p - α crush curve, then you should at least modify the function SMFNT (which is essentially the p - α curve expressed using a nor-

malized isomorphic mean stress $\sigma_m/\bar{\sigma}_s$ instead of p and using the pore ratio ψ instead of α) and its derivative SMPRIM. Future versions of this model will permit the user to specify a crush curve through the use of a table to avoid re-compiling the code.

Essential input keywords for the CKP model are listed in Table G.1. The column labeled “typical values” merely shows the orders of magnitude expected for a typical material. The user-specified value may permissibly fall outside the ranges given in the last column. The allowable range for each user input is specified in the “description” column.

Table G.1: Essential USER INPUT

keyword	description	typical value(s)
POROSITY	The volume fraction of voids, f_v . Allowable range: $0 \leq f_v < 1$ ^(a) . Default = 0.0. Within the numerical coding, this user-supplied value will be replaced by the pore ratio, $\psi = f_v/(1 - f_v)$ defined in Eq. (2.2) of the main documentation.	0.0 to 0.15
SHMOD	The porous shear modulus G . Allowable range: $G > 0$. No default. See page 13 of the main documentation for more details.	40×10^9 Pa
BKMOD	The porous bulk modulus K . Allowable range: $K > 0$. No default. See page 13 of the main documentation for more details.	60×10^9 Pa
YIELDM	The yield in shear τ^{yield} for the matrix material. Allowable range: $\tau^{\text{yield}} > 0$. No default. Within the coding, this user value is converted into an isomorphic shear using Eq. (3.14) in the main documentation.	1×10^9 Pa
RHO0	The initial mass density ρ_o of the porous material, equal to the solid density times the solid volume fraction. (That is, $\rho_o = \rho_{\text{solid}}(1 - f_v)$). Allowable range: $\rho_o > 0$. No default.	1000 to $8000 \frac{\text{kg}}{\text{m}^3}$

a. The model is not expected to be accurate for materials such as foams that have porosities approaching 1.0, but it should be nevertheless robust.

Supplemental user keywords that exercise advanced features of the CKP model are listed in Table G.2. If left unspecified, the numerical implementation of the CKP model will set appropriate defaults as indicated.

Table G.2: Supplemental (advanced) USER INPUT

keyword	description	typical value(s)
HARDMOD	The <i>dimensionless</i> value of the hardening modulus, defined to equal the hardening modulus h divided by $\bar{\sigma}_s$. This input should be regarded as the conventional hardening modulus divided by YELDM. The value must be positive. Default=0.0. After checking data, this value will be replaced by the actual value of h as defined in Eq. (10.3) of the main text.	0. to 5.
TRELAX	Relaxation time τ for the rate dependent model discussed on page 59 of the main documentation. The value must be positive. Default=0.0. If TRELAX is zero (instantaneous relaxation), then the response will correspond to the rate independent QCKP model.	0 to 1×10^{-8} sec.
YSLOPE	The slope β of the D.O.D. yield curve at zero pressure. Value must lie between -1 and 1. Default=0.0. If YSLOPE>0, then the material will exhibit shear-enhanced dilatation (porosity will increase under simple shear). If YSLOPE<0, it will have shear-enhanced compaction. If YSLOPE is close to ± 1 , then the yield model will behave like a linear Mohr-Coulomb envelope with a pressure cap. See page 62 of the main documentation for more details.	-0.1 to 0.1
YCURVE	The parameter γ that controls the “squareness” of the D.O.D. yield surface. Use 0.0 for an ellipsoid or 1.0 for a box (which is the value one would use to compare CKP with a typical p - α model). See page 62 of the main documentation for more details.	0.0 to 0.4
YRATIO	The ratio r of yield in isotropic tension to yield in isotropic compression used in the D.O.D. yield function. Value must be positive. Default=1.0. See page 62 of the main documentation for more details.	0.1 to 1.0
RGM	The shear modulus G_m of the matrix material. If left unspecified, the value of G_m will be inferred from the porous moduli by using the Newton solver described on page B-6 of Appendix B. However, if G_m is specified, then γ_m must also be specified, and any value specified for the porous shear modulus G (=SHMOD) will be overwritten with the value implied by the formula $G = G_m e^{-\gamma_m W}$. See page 13 of the main documentation for more details.	60×10^9 Pa

Table G.2: Supplemental (advanced) USER INPUT

keyword	description	typical value(s)
RKM	The bulk modulus K_m of the matrix material. If left unspecified, the value of K_m will be inferred from the porous moduli. If K_m is specified, however, it takes priority, and any value specified for the porous bulk modulus K (=BKMOD) will be overwritten with the value implied by the formula $K = K_m e^{-\gamma_m \psi}$. See page 13 of the main documentation for more details.	80×10^9 Pa
RGAMM	The parameter γ_m that appears in the shear modulus formula $G = G_m e^{-\gamma_m \psi}$. This value is used only if RGM is specified. See page 13 of the main documentation for more details.	1.0 to 3.0
RKAPM	The parameter κ_m that appears in the bulk modulus formula $K = K_m e^{-\kappa_m \psi}$. This value is used only if RKM is specified. See page 13 of the main documentation for more details.	1.0 to 4.0
SC	The parameter s_m^{crush} in Fig. 19.8, equal to the crush pressure divided by YIELDM. Leave this parameter unspecified (or set it to zero) to have the value inferred for you based on the built-in yield function. See page 72 of the main documentation for more details.	0.0 to 10.0
ST	The tensile mean stress (divided by YIELDM) at which the tensile growth curve must be zero. This parameter is the tensile analog of SC. If left unspecified, it will equal SC*YRATIO. See page 72 of the main documentation for more details.	0.0 to 5.0
ALFN	Parameter α^n in Eq. (7.3) controlling rate of nucleation. Must be positive or zero. Default=0.0 The larger ALFN is, the faster pores will nucleate.	0.0 to 0.5
EPSN	The matrix strain ϵ_m^n in Eq. (7.3) at which pore nucleation begins. Must be positive. Default=3.0, (which is basically infinity as far as strains go). The smaller EPSN, the <i>sooner</i> , pores will nucleate.	0.01 to 0.40
PSIMI	The maximum allowable increment in ψ during a single time step. Must be positive. Default=0.1.	0.005 to 0.2

Below we summarize how you can explore the model capabilities listed on page 4 of the main report:

- Porosity dependence of the elastic moduli is determined by the values of κ_m and γ_m given in Eq. (2.4) of the main report. One way to control the porosity dependence is to specify these parameters directly with your inputs **RKAPM** and **RGAMM**; if this is done, then you *must* also provide values for the solid bulk and shear moduli **RKM** and **RGM**, respectively. Most of the time, however, measurements of the porosity dependence of the moduli are not available. In this case, you should leave **RKM**, **RGM**, **RKAPM** and **RGAMM** unspecified. Instead, you provide macroscopic *porous* moduli **BKMOD** and **SHMOD**. In this case, your specified value for the **POROSITY** is then used to automatically *compute* appropriate values of κ_m and γ_m . Keep in mind that values of **BKMOD** and **SHMOD** are used only if solid data (**RKM**, **RGM**, **RKAPM** and **RGAMM**) are *not* specified. If specified, solid data always take precedence and any porous data are overwritten with the values implied by the solid data.
- Porosity dependence of the onset of yield is controlled via ψ -dependence of the yield function $F(\sigma_m, \sigma_s, \psi, \zeta)$ defined in Eq. (4.1) of the main text. Porosity dependence of yield can be controlled by changing the yield function coded in the subroutines contained in **hcrush.F**. When using the default D.O.D. yield function, the porosity dependence of yield can be affected by changing the **smfnt** routine in **hcrush.F**. To accomplish complete crush at a certain pressure, then adjust the **SC** parameter.
- Straining due to phase transformation of the matrix material is accomplished by having the calling routine subtract the transformation strain rate from the total strain rate *before* calling the CKP model.
- Changes in the matrix elastic moduli resulting from phase transformation are modelled by having the calling routine modify the matrix moduli in the user input array. Furthermore, the calling routine *must* also provide a value for the rate of change of the normalized elastic moduli as part of the calling arguments to the CKP model.
- Hardening of the matrix material is controlled through the **HARDMOD** user parameter. The nonhardened matrix yield stress is **YIELDM**.
- Shear dependence of the onset of pore collapse is controlled via the σ_s -dependence of the yield function $F(\sigma_m, \sigma_s, \psi, \zeta)$ defined in Eq. (4.1) of the main text. When using the default D.O.D. yield function, shear dependence can be controlled via the user input **YCURVE**. If **YCURVE** is set to 1.0, then pore collapse will be independent of shear stress, which is the assumption of simple p - α models.
- Shear dependence of the rate of pore collapse is controlled by the isotropic part of the plastic strain rate. This version of the CKP model presumes that the plastic strain rate is directed normal to the yield surface and the shear dependence of the rate of pore collapse is therefore

not directly controllable by the user. It is affected only by changing the yield function.

- Void nucleation is controlled by the parameters **ALFN**, **EPSN**, and **PSI-MI**. Set **ALFN=0.0** and/or **EPSN="∞"** to suppress nucleation.
- True plastic normality is an unchangeable property of the CKP model, though future versions might permit non-normality if users so request.
- Regarding rigorous plastic consistency, the *equilibrium* stress $\underline{\underline{\sigma}}^{\text{eqbm}}$ remains on the evolving yield surface. This is an unchangeable consistency property of the CKP model.
- The overstress model for rate dependence (which permits the *actual* stress to lie transiently outside the yield surface) is controlled by the user-specified **TRELAX** parameter. This feature permits the apparent yield stress to increase under high strain rates. Leave **TRELAX** unspecified (or set it to zero) to ignore rate effects.
- Satisfaction of the principle of material frame indifference (PMFI) is ensured by having the host code call the CKP model using only *unrotated* stress and strain rate inputs.
- Predictor-corrector scheme for numerical integration of rate equations. The iteration convergence can be altered by changing the FORTRAN parameter **KOUNT** in the **ckpore** subroutine.
- You can define your own yield function by changing the subroutines in the **hcrush.F** source code file.
- The flexible D.O.D. default yield function should be used only for preliminary calculations. It is described on page 62 of the main text and is controlled as follows:
 - (xii) Different yield points in tension and compression are achieved by changing the user input **YRATIO**. Set **YRATIO=1.0** to have the same yield in tension and compression.
 - (xiii) Shear-enhanced compaction or dilatation is controlled through the **YSLOPE** parameter.
 - (xiv) Pressure dependence is controlled through the **SC** and **ST** user inputs or by changing the FORTRAN function **smfnt**.
 - (xv) Adjustable porosity dependence of yield is controlled by changing the FORTRAN function **smfnt**.
 - (xvi) Optional Drucker-Prager yield for the matrix is controlled by changing both **YSLOPE** and **ST**.
 - (xvii) Optional yield "cap" type behavior is controlled via **ST**. When using the default D.O.D. yield function, a nominal yield cap is always automatically introduced to ensure positive plastic work in tension.

APPENDIX H.

Nomenclature and Glossary

The following table defines symbols and acronyms that appear throughout the report. The FORTRAN name is the name used for the variable within the numerical source code. The defining equation (or page number) cites the location in this report where the quantity is first defined. Entries preceded with “**(bold parenthetical text)**” are inputs and/or outputs to the main **CKP** physics routine. **Shaded entries** correspond to material parameters available from the **UI** material parameter array within the **ckpore** subroutine. Many of these shaded **UI** values are *derived from* inputs supplied by the user — they are not user inputs *per se*. For example, the user supplies void volume fraction f_v which is then converted to pore ratio ψ and stored in the **UI** array; therefore only ψ is shaded in the following table whereas f_v is not. Similarly, the user provides the conventional yield in shear τ_y for the matrix material, which is converted into the *isomorphic* yield in shear $\bar{\sigma}_s^o$ before it is saved in the **UI** array. Likewise, the user provides macroscopic moduli K and G from which the *matrix* moduli K_m and G_m are *inferred* and stored in the **UI** array.

Symbol or Acronym	FORTRAN Name	Name and meaning	SI units	defining equation (or page)
$\underline{\underline{\mathbf{B}}}$		Gradient of the yield function with respect to stress.		11.2
CKP		Acronym for “Consistent Kinetics Porosity” model.		page 1
D.O.D.		The “dearth of data” default yield function.		page 62
$\underline{\underline{\mathbf{D}}}$	ROD	The small distortion strain rate given by the symmetric part of the velocity gradient, $d_{ij} = \frac{1}{2} \left(\frac{\partial v_i}{\partial x_j} + \frac{\partial v_j}{\partial x_i} \right)$. For frame indifference, this tensor and all other spatial tensors in the CKP model are understood to be unrotated to the polar reference configuration.	s^{-1}	5.1
$\underline{\underline{\mathbf{d}}}$	D	(input) . The part of the total strain rate that is <i>not</i> due to phase transformation: $\underline{\underline{\mathbf{d}}} \equiv \underline{\underline{\mathbf{D}}} - \underline{\underline{\mathbf{d}}}^t$. Within ckpore.F , this is treated as if it were the total strain rate.	s^{-1}	5.3
	DKK	The trace of $\underline{\underline{\mathbf{d}}}$, which is equal to the volumetric strain rate.	s^{-1}	

APPENDIX H. Nomenclature and Glossary

Symbol or Acronym	FORTTRAN Name	Name and meaning	SI units	defining equation (or page)
$\underline{\underline{d}}^e$		The elastic part of the strain rate. The stress rate is assumed linear with respect to $\underline{\underline{d}}^e$.	s^{-1}	5.2,
$\underline{\underline{d}}^{ep}$		The effective elastic-plastic part of the strain rate: $\underline{\underline{d}}^{ep} = \underline{\underline{d}} - \underline{\underline{d}}^n$, so $\underline{\underline{d}}^{ep}$ is mathematically the same thing as $\underline{\underline{d}}^{e, \text{trial}}$. The only distinction is how it is interpreted.	s^{-1}	14.2,
$\underline{\underline{d}}^{e, \text{trial}}$		The trial “elastic” strain rate obtained by tentatively assuming that $\underline{\underline{d}}^p$ is zero. Namely, $\underline{\underline{d}}^{e, \text{trial}} = \underline{\underline{d}} - \underline{\underline{d}}^n$.	s^{-1}	8.1
$\underline{\underline{d}}^i$		The inelastic part of the strain rate, $\underline{\underline{d}}^i = \underline{\underline{d}}^p + \underline{\underline{d}}^n + \underline{\underline{d}}^t = \underline{\underline{D}} - \underline{\underline{d}}^e$		11.3
$\underline{\underline{d}}^n$		The part of the strain rate due to void nucleation.	s^{-1}	5.2, 7.1
$\underline{\underline{d}}^{e'}$		The deviatoric part of $\underline{\underline{d}}^e$	s^{-1}	
$\underline{\underline{d}}^p$		The part of the inelastic strain rate due to plastic flow of the matrix material. This part of the inelastic strain rate is related in a kinematic way to the rate of change of porosity.	s^{-1}	5.2
$\underline{\underline{d}}^t$		The phase transformation part of the strain rate (computed <i>a priori</i> within the host code to construct an effective strain rate tensor, $\underline{\underline{d}} \equiv \underline{\underline{D}} - \underline{\underline{d}}_t$ that is sent to the <code>ckpore</code> subroutine).	s^{-1}	5.3
$\underline{\underline{E}}$		The fourth-order elastic stiffness tensor.	Pa	11.5, 11.6
E		Young’s modulus of the porous material, $E = 9KG/(3K + G)$	Pa	Fig. B.4
E_m		Young’s modulus of the matrix material	Pa	Fig. B.4
F	FVAL	The yield function defined such that elastic stresses satisfy $F(\sigma_m, \sigma_s, \psi, \zeta) < 0$. Within this nomenclature table, F is assumed dimensionless.	1	4.1

APPENDIX H. Nomenclature and Glossary

Symbol or Acronym	FORTTRAN Name	Name and meaning	SI units	defining equation (or page)
F_m	FM	Partial derivative of the yield function with respect to σ_m : $F_m \equiv \frac{\partial F(\sigma_m, \sigma_s, \psi, \zeta)}{\partial \sigma_m}$	Pa ⁻¹	4.4(a)
F_s	FS	Partial derivative of the yield function with respect to σ_s : $F_s \equiv \frac{\partial F(\sigma_m, \sigma_s, \psi, \zeta)}{\partial \sigma_s}$	Pa ⁻¹	4.4(b)
F_ψ	FPSI	Partial derivative of the yield function with respect to ψ : $F_\psi \equiv \frac{\partial F(\sigma_m, \sigma_s, \psi, \zeta)}{\partial \psi}$	1	4.4(c)
F_ζ	FISV	Partial derivative of the yield function with respect to ζ : $F_\zeta \equiv \frac{\partial F(\sigma_m, \sigma_s, \psi, \zeta)}{\partial \zeta}$	Pa ⁻¹	4.4(d)
f_v	FV	Volume fraction of voids at the unstressed reference state.	1	2.2
G	RG	Shear modulus of the porous material	Pa	2.1(a), 2.4(a)
G_m	RGM	Shear modulus of the matrix material	Pa	2.1(a), 2.4(a)
$\underline{\underline{G}}$		An abstract second-order tensor that is presumed to exist as a constant of proportionality in expressions for the rates of internal state variables so that $\dot{\zeta} = \underline{\underline{G}}:\underline{\underline{d}}^p$	varies	10.2
h	HHHH	Hardening modulus in the scalar expression for the evolution of internal state variables, $\dot{\zeta} = h\xi\dot{\lambda}$.	same as ζ	10.2
$\underline{\underline{I}}$		The identity tensor	1	3.1
$\hat{\underline{\underline{I}}}$		A unit tensor in the direction of the identity tensor, $\hat{\underline{\underline{I}}} \equiv \frac{\underline{\underline{I}}}{\ \underline{\underline{I}}\ } = \frac{\underline{\underline{I}}}{\sqrt{3}}$	1	3.5(a)
K	RK	Bulk modulus of the porous material	Pa	2.1(b), 2.4(b)
K_m	RKM	Bulk modulus of the matrix material	Pa	2.1(b), 2.4(b)
$2k$	YLD2K	The exponent that controls the yield surface curvature for the DOD model.	1	19.1, 19.2

APPENDIX H. Nomenclature and Glossary

Symbol or Acronym	FORTTRAN Name	Name and meaning	SI units	defining equation (or page)
$\underline{\underline{\mathbf{M}}}$		Outward <i>unit</i> normal to the yield surface: $\underline{\underline{\mathbf{M}}} = \frac{1}{\xi} [F_m \hat{\underline{\underline{\mathbf{I}}}} + F_s \hat{\underline{\underline{\mathbf{S}}}}].$ Note: $M_{ij}M_{ij} = 1$ The tensor $\underline{\underline{\mathbf{M}}}$ is a unit tensor in the direction of the <i>plastic part</i> $\underline{\underline{\mathbf{d}}}^P$ of the inelastic strain rate. Contrast this with $\underline{\underline{\mathbf{m}}}$.	1	4.11
$\underline{\underline{\mathbf{m}}}$		Unit tensor in the direction of the inelastic strain rate, $\underline{\underline{\mathbf{d}}}^i$. Contrast this with $\underline{\underline{\mathbf{M}}}$.	1	11.4
PMFI		Acronym for the “principle of material frame indifference” that requires the predictions of a constitutive model to be related in a physically sensible manner when comparing two motions that are identical to each other except that one involves a superimposed rigid rotation of the other.		page 4
p	PRES	pressure, $p = -\frac{1}{3}\text{tr}\underline{\underline{\sigma}}$, which is positive in compression.	Pa	3.2(a)
QCKP		The “quasistatic consistent kinetics porosity” model. This model is governed by rate equations that hold only for quasistatic deformations.		page 3
r	YRATIO	The ratio s_m^T/s_m^C of yield in tension to that in compression (used in the DOD model) $0 < r \leq 1$	1	Fig. 19.4
$\underline{\underline{\mathbf{R}}}$		The rotation tensor from the polar decomposition of the deformation gradient.	1	page 39
$\underline{\underline{\mathbf{S}}}$	T1,T2,T3,...	Stress deviator, $\underline{\underline{\mathbf{S}}} = \underline{\underline{\sigma}} - \frac{1}{3}\text{tr}\underline{\underline{\sigma}} = \underline{\underline{\sigma}} + p\underline{\underline{\mathbf{I}}}$. Within the coding, the components are ordered in the standard MIG way: xx,yy,zz,xy,yz,zx.	Pa	3.2(b)
$\hat{\underline{\underline{\mathbf{S}}}}$	SHAT	A unit tensor in the direction of the stress deviator, $\hat{\underline{\underline{\mathbf{S}}}} \equiv \underline{\underline{\mathbf{S}}} / \ \underline{\underline{\mathbf{S}}}\ .$	1	3.5(b)
$\sigma_s \hat{\underline{\underline{\mathbf{S}}}}^{\text{trial}}$	SSSD	The part of the stress rate that is perpendicular to the Rendulic plane, $\sigma_s \hat{\underline{\underline{\mathbf{S}}}}^{\text{trial}} = 2G[\underline{\underline{\mathbf{d}}} - \hat{\underline{\underline{\mathbf{S}}}}(\hat{\underline{\underline{\mathbf{S}}}}:\underline{\underline{\mathbf{d}}})].$	Pa	14.7

APPENDIX H. Nomenclature and Glossary

Symbol or Acronym	FORTTRAN Name	Name and meaning	SI units	defining equation (or page)
S_m^t	ST	The value of $\sigma_m/\bar{\sigma}_m^o$ in tension where the nominal crush curve transitions to a straight line.	1	Fig. 19.8
S_m^c	SC	The value of $\sigma_m/\bar{\sigma}_m^o$ in <i>compression</i> where the nominal crush curve transitions to a straight line.	1	Fig. 19.8
V		The specific volume for a material element (at the zero-transformation reference state).	m^3/kg	6.1
V_o		The initial specific volume (or, if applicable, the specific volume at the zero-transformation reference state).	m^3/kg	
V_Z		The zero-stress reference specific volume for a material element. This specific volume begins equal to the initial volume V_o but it changes whenever there is permanent volume change, as when pores irreversibly collapse.	m^3/kg	6.1
Y		The von Mises yield stress of the solid matrix material, related to the isomorphic solid yield stress by $Y = \sqrt{\frac{3}{2}}\bar{\sigma}_s$.		

GREEK SYMBOLS

α		Distention parameter, equal to the ratio of the mass density of the solid matrix material divided by the mass density of the porous material: $\alpha = \rho_s/\rho$. The distention α is related to the pore volume fraction by $\alpha = \frac{1}{1 - f_v}$; it is related to the pore ratio by $\alpha = \psi + 1$.	1	2.3
α_N	ALFN	Coefficient used in the nucleation model.	1/s	7.3
β	YSLOPE	The shear-enhanced compaction/dilatation slope for the DOD model.	1	19.3
γ	YCURVE	The yield surface curvature parameter = 0 for ellipsoidal, =1 for the rectangular p- ψ description. $0 \leq \gamma < 1$	1	19.2
γ_m	RGAMM	Shear modulus reduction coefficient	1	2.1(a), 2.4(a)

APPENDIX H. Nomenclature and Glossary

Symbol or Acronym	FORTTRAN Name	Name and meaning	SI units	defining equation (or page)
Δt	DT	(input) Time step	s	
$\dot{\delta}^n$		The magnitude of the nucleation part of the strain rate $\underline{\underline{d}}^n$		7.1, 7.3
ε_m		A crude estimate for the volumetric strain in the matrix material	1	7.2
ε_m	EPSN	The volumetric strain in the matrix material at the onset of void nucleation.	1	7.3
$\varepsilon_p^{\text{equiv}}$		Equivalent plastic strain $\varepsilon_p^{\text{equiv}} \equiv \int_0^t \sqrt{\frac{2}{3} \underline{\underline{d}}_p : \underline{\underline{d}}_p} dt = \sqrt{\frac{2}{3}} \int_0^t \dot{\lambda} \xi dt$		10.1
κ_m	RKAPM	Bulk modulus reduction coefficient	1	2.1(b), 2.4(b)
$\dot{\lambda}$	RLMDOT	The proportionality constant in the normality assumption that $\underline{\underline{d}}^p$ is proportional to the gradient of the yield function. The magnitude of the plastic strain rate is given by $\xi \dot{\lambda}$, where ξ is the magnitude of the yield surface gradient.	Pa/s	9.2, 14.1
μ	RMUEL	The fraction of the time step that is elastic.		D.6
ν		Poisson's ratio	1	B.2
ν_m		Poisson's ratio of the matrix material	Pa	B.3
ξ	YXI	Magnitude of the yield surface gradient: $\xi = \sqrt{F_m^2 + F_s^2}$	Pa ⁻¹	4.13
ρ	RHO	(input) The current mass density of the porous material	kg/m ³	
ρ_o	RHO0	initial mass density of the porous material	kg/m ³	
$\underline{\underline{\sigma}}$		(input and output) Cauchy stress	Pa	3.1
$\underline{\underline{\dot{\sigma}}}^{\text{trial}}$		The trial "elastic" stress rate obtained by tentatively assuming that $\underline{\underline{d}}^p$ is zero.	S ⁻¹	8.2

Symbol or Acronym	FORTTRAN Name	Name and meaning	SI units	defining equation (or page)
$\underline{\underline{\sigma}}^{\text{eqbm}}$	SIG	The equilibrium (rate independent) stress found by solving the QCKP equations. The actual stress is given by $\underline{\underline{\sigma}} = \underline{\underline{\sigma}}^{\text{eqbm}} + \underline{\underline{\sigma}}^{\text{over}}$.	Pa	18.1
$\underline{\underline{\sigma}}^{\text{over}}$	OVER	(input and output) The overstress for the rate-dependent model.	Pa	18.1
σ_m	SIGM	Component of the stress tensor in the direction of the identity tensor: $\sigma_m = \underline{\underline{\sigma}} : \hat{\underline{\underline{I}}} = \frac{1}{\sqrt{3}} \text{tr} \underline{\underline{\sigma}} = -\sqrt{3} p.$	Pa	3.4(a), 3.6
σ_s	SIGS	Component of the stress tensor in the direction of the stress deviator: $\sigma_s = \ \underline{\underline{S}}\ = \sqrt{S_{ij} S_{ij}} = \underline{\underline{\sigma}} : \hat{\underline{\underline{S}}}$ $= \sqrt{\frac{2}{3}} \sigma^{VM} = \sqrt{2} \tau^{\text{equiv}}$	Pa	3.4(b), 3.6, 3.12
$\bar{\sigma}_s$	RSV	The isomorphic yield stress of the matrix material used as a material parameter in the Gurson and DOD yield functions. SBY is the initial value, and RSV is the hardened value. The isomorphic yield stress is related to the more conventional von Mises yield stress by $\bar{\sigma}_s \equiv \sqrt{\frac{2}{3}} Y$.	Pa	16.3
$\bar{\sigma}_s^o$	SBY	The initial value of $\bar{\sigma}_s$.	Pa	16.3
σ^{VM}		Von Mises equivalent stress, $\sigma^{VM} \equiv \sqrt{\frac{3}{2} S_{ij} S_{ij}} = \sqrt{\frac{3}{2}} \sigma_s$	Pa	3.12
τ	TRELAX	The overstress relaxation time.	s	18.2
τ^{equiv}		Equivalent shear stress $\tau^{\text{equiv}} \equiv \sqrt{\frac{1}{2} S_{ij} S_{ij}} = \sqrt{\frac{1}{2}} \sigma_s$	Pa	3.13
\dot{Y}	UPSDOT	(input) The ratio of the matrix modulus rate divided by the matrix modulus, which is permissibly nonzero for a matrix material that is transforming. The CKPore model assumes that phase transformation does not change the matrix Poisson's ratio.	1/s	2.6

APPENDIX H. Nomenclature and Glossary

Symbol or Acronym	FORTTRAN Name	Name and meaning	SI units	defining equation (or page)
ψ	PSI or PSIO for initial value	(input and output) Porosity ratio, equal to the volume fraction of voids divided by the volume fraction of matrix material. Related to the volume fraction f_v by $\psi = \frac{f_v}{1 - f_v}$. Related to the distention ($\alpha = \rho_s/\rho$) by $\psi = \alpha - 1$.	1	2.2
$\dot{\psi}^n$	PSIDN	The rate of the pore ratio due to void nucleation	s^{-1}	8.3,
ψ^t_t	PSITT	The value of ψ in tension where the nominal crush curve transitions to a straight line.	1	Fig. 19.8
ψ^t_c	PSITC	The value of ψ in <i>compression</i> where the nominal crush curve transitions to a straight line.	1	Fig. 19.8
ζ	RSV	(input and output) A symbolic representation for the internal state variable(s) used in the yield function. In most of our implementations, ζ is the yield stress of the matrix material (which is an internal state variable because it is permitted to change as a result of matrix hardening).	Varies	4.1

External Distribution

Frank Addressio, Group T-3, MS B216
Los Alamos National Laboratory
Los Alamos, NM 87545

Dr. Thomas J. Ahrens
Seismological Laboratory 252-21
California Institute of Technology
Pasadena, CA 91125

Charles E. Anderson
Southwest Research Institute
6220 Culebra Rd.
P.O. Drawer 28510
San Antonio, TX 78228
Attn: C. Anderson, D. Littlefield, J.D. Walker

M. C. Boyce
Mass. Inst. of Technology
Room 1-304
Cambridg, MA 02139

W. Bruchey
Army Research Laboratory, AMSRL-WM-TA
Aberdeen Proving Ground, MD 21005-5066

John B. Bdzil, Group DX-1, Mail Stop P952
Los Alamos National Laboratory
Los Alamos, NM 87545

Datta Dandekar
Army Research Laboratory, AMSRL-WM-TD
Aberdeen Proving Ground, MD 21005-5066

F. W. Davies
Manager, Applied Physics & Testing
2201 Buena Vista SE, Suite 400
Albuquerque, NM 87106-4265

John K. Dienes, Mail Stop B214
Los Alamos National Laboratory
Los Alamos, NM 87545

Walter J. Drugan
Nuclear Engineering and Engineering Physics
University of Wisconsin — Madison
Madison, WI 53706-1687

G. Filbey
Army Research Laboratory, AMSRL-WM-TA
Aberdeen Proving Ground, MD 21005-5066

Dr. Robert Frey
Army Research Laboratory, WMSRL-WM-TB
Aberdeen Proving Ground, MD 21005-5066

Robert K. Garrett, Jr.
Naval Surface Warfare Center, Dahlgren Div.
Code G22, Bldg. 221, Warheads Branch
17320 Dahlgren Rd.
Dahlgren, VA 22448-5100

George A. Gazonas
Army Research Laboratory, AMSRL-WM-MB
APG, MD 21005-5069

Aaron D. Gupta
Army Research Laboratory, AMSRL-WM-TD
Rm 226, B309, WMRD
ARL, APG, MD 21005-5066.

Y. Horie
X-7 Applied Physics Division, MS D413
Los Alamos National Laboratory
Los Alamos, NM 87545

Y. Huang
Army Research Laboratory, AMSRL-WM-TA
Aberdeen Proving Ground, MD 21005-5066

Gordon R. Johnson
Alliant Techsystems, Inc. (MN11-1614)
600 2nd St. NE
Hopkins, MN 55343

Kent Kimsey
Army Research Laboratory, AMSRL-WT-TC
Aberdeen Proving Ground, MD 21005-5066

P. Kingman
Army Research Laboratory, AMSRL-WM-TA
Aberdeen Proving Ground, MD 21005-5066

Mathew Lewis, MS P946
Los Alamos National Laboratory
Los Alamos, NM 87545

External Distribution (cont'd)

P.J. Maudlin, MS B216
Los Alamos National Laboratory
Los Alamos, NM 87545

A.M. Rajendren
Army Research Office
Research Triangle Park, NC 27709-2211

Glenn Randers-Pehrson (LLNL)
Army Research Laboratory, AMSRL-WM-TD
Aberdeen Proving Ground MD 21005-5066

Edward J. Rapacki, Jr.
Army Research Laboratory, AMSRL-WM-TD
Aberdeen Proving Ground, MD 21005-5066

S. Schraml
Army Research Laboratory, AMSRL-WM-TC
Aberdeen Proving Ground, MD 21005-5066

H. L. Schreyer
Department of Mechanical Engineering
University of New Mexico
Albuquerque, NM 87131

Steven Segletes
Army Research Laboratory, AMSRL-WM-TD
Aberdeen Proving Ground, MD 21005-5066

Dr. John Starkenberg
Army Research Laboratory, AMSRL-WM-TB
Aberdeen Proving Ground, MD 21005-5066

Deborah Sulsky
Department of Mechanical Engineering
University of New Mexico
Albuquerque, NM 87131

T.W. Wright
Army Research Laboratory, AMSRL-WM-T
Aberdeen Proving Ground, MD 21005

Sandia Internal Distribution

MS-0303	M. J. Forrestal, 15414	MS-0836	E.S. Hertel, Jr., 9116
MS-0310	P. Yarrington, 9230	MS-0841	T. C. Bickel, 9100
MS-0316	G. S. Heffelfinger, 9235	MS-0847	J.B. Aidun, 9123
MS-0316	M. D. Rintoul, 9235	MS-0847	S. W. Attaway, 9121
MS-0321	W.J. Camp, 9200	MS-0847	M. L. Blanford, 9121
MS-0367	L. W. Carlson, 1843	MS-0847	S. N. Burchett, 9132
MS-0439	M. Shahinpoor	MS-0847	C. R. Dohrmann, 9226
MS-0515	J. D. Keck, 2561	MS-0847	A.F. Fossum, 9123
MS-0515	S. G. Barnhart, 2561	MS-0847	C.S. Lo, 9123
MS-0521	F. M. Bacon, 2502	MS-0847	H. S. Morgan, 9123
MS-0521	S. T. Montgomery, 2561	MS-0847	M. K. Neilsen, 9123
MS-0525	T. V. Russo, 1734	MS-0847	E. D. Reedy, Jr., 9123
MS-0603	I. J. Fritz, 1742	MS-0847	W. M. Scherzinger, 9123
MS-0615	J. H. Gieske, 9122	MS-0847	D. J. Segalman, 9124
MS-0751	L. S. Costin, 6117	MS-0889	R. A. Anderson, 1846
MS-0751	J. M. Grazier, 6117	MS-0959	P. Yang, 14192
MS-0751	D. H. Zeuch, 6117	MS-1033	D. S. Drumheller, 6211
MS-0819	E. A. Boucheron, 9231	MS-1111	H. P. Hjalmarson, 9235
MS-0819	K. H. Brown, 9231	MS-1159	W. M. Barrett, 15344
MS-0819	D. E. Carrol, 9231	MS-1168	M. D. Furnish, 1612
MS-0819	C. J. Garasi, 9231	MS-1181	J. R. Asay, 1610
MS-0819	J. Robbins, 9231	MS-1181	L. C. Chhabildas, 1610
MS-0819	A. C. Robinson, 9231	MS-1181	D. B. Hayes, 1610
MS-0819	T.G. Trucano, 9231	MS-1181	D. E. Grady, 1610
MS-0819	J. R. Weatherby, 9231	MS-1181	M.D. Knudson, 1610
MS-0819	M. K. Wong, 9231	MS-1186	R. J. Lawrence, 1674
MS-0820	R.M. Brannon, 9232 (5)	MS-1349	A. J. Hurd, 1841
MS-0820	P. F. Chavez, 9232	MS-1407	R. R. Lagasse, 1811
MS-0820	R. A. Cole, 9232	MS-1411	D. B. Dimos
MS-0820	D. A. Crawford, 9232	MS-1411	V. Tikare, 1834
MS-0820	A. V. Farnsworth, Jr., 9232	MS-1411	B. A. Tuttle
MS-0820	S. P. Goudy, 9232	MS-1421	G. A. Samara, 1120
MS-0820	G. I. Kerley, 9232	MS-1421	R. E. Setchell, 1120
MS-0820	M. E. Kipp, 9232	MS-1843	S. J. Glass, 1843
MS-0820	S. A. Silling, 9232		
MS-0820	P. A. Taylor, 9232		
MS-0826	W. L. Hermina, 9113		
MS-0834	A.M. Kravnik, 9114	MS-0612	Review & Approval, 9612 for DOE/OSTI
MS-0834	A.C. Ratzel, 9112		
MS-0835	J. S. Peery, 9121	MS-0899	Technical Library, 9616 (2)
MS-0836	M.R. Baer, 9100	MS-9018	Central Technical Files, 8945-2

This page intentionally left blank.